Modeling the Venus middle atmosphere

Manuraj Shunmuga Sundaram

A thesis submitted for the degree of
Master of Philosophy in Physics at
The Australian National University

July, 2007

Declaration

This thesis is an account of research undertaken between August 2005 and July 2007 at The Atomic and Molecular Physics Laboratories, Research School of Physical Sciences and Engineering, The Australian National University, Canberra, Australia.

Except where acknowledged in the customary manner, the material presented in this thesis is, to the best of my knowledge, original and has not been submitted in whole or part for a degree in any university.

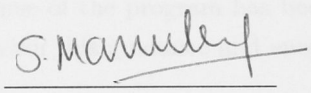

Manuraj Shunmuga Sundaram

Student Number : 3316155

July, 2007

Acknowledgements

I would like to acknowledge the support of the Australian National University and Research School of Physical Sciences and Engineering, Canberra. The staff at the Research School of Physical Sciences have been helpful in all administrative matters and in creating a supportive base for study. I am thankful to colleagues at Atomic and Molecular Physics Laboratories who have helped me get through numerous hurdles along the way. Alan Heays, Steve Gibson and Brenton Lewis provided ample support and ambiance in an otherwise cold computer room.

I am grateful to Dr.Frank Mills for all his efforts from conception to completion of both research projects. His support throughout the course of the program has been constant and more than satisfactory. As the primary supervisor, his guidance and encouragement have helped immensely.

I would like to acknowledge the role played by my friends in Canberra and overseas. The supportive environment and enjoyable distractions have always been welcome. Finally, I am thankful for the support and love of my family. They have made my time away easier and made me look forward to holidays. More importantly, family and friends have put my research in perspective and made it more enjoyable a journey.

Abstract

Exisiting knowledge of chemistry and current photochemical modeling of the Venusian middle atmosphere do not convincingly account for observed scarcity of oxygen. Introduction of a heterogeneous pathway to oxidise CO to CO_2, catalysed by cloud aerosols, affords a simple, yet unexplored, means to reduce oxygen abundances. In the first research project, different degrees of heterogeneous chemistry's dominance are investigated for their impact on atmospheric species and reactions. A heterogeneous dominant $\gamma_{rxn} = 10^{-4}$ (γ_{rxn}: reactive uptake coefficient) atmosphere model is the first to agree with the observational upper limit for oxygen column abundance [Trauger and Lunine, 1983]. The most plausible heterogeneous model developed from this research, with low oxygen abundances and reconciliation of differences between modeled and observational CO abundances, is the $\gamma_{rxn} = 3 \times 10^{-5}$ baseline model. The addition of heterogeneous chemistry brought a decline in oxygen and CO abundances below 90 km. In such conditions, a noticable decrease in chlorine compound abundances and increase in sulphur and chlorosulphane compounds is reported.

An extensive chemical scheme of nitrogen compounds is introduced to the heterogeneous dominant, $\gamma_{rxn} = 10^{-5}$, and purely gasphase atmosphere models. Little change in overall atmospheric chemistry is reported from the introduction of a nominal abundance of NO, recommended by observation [Krasnopolsky, 2006a]. Mixing ratios of NO, factor of three to five higher than that prescribed by observation, are capable of producing significant changes to middle atmospheric chemistry. Combined effects of inclusion of heterogeneous and nitrogen chemical schemes provide better agreement between modeled and observed CO abundances near the lower boundary.

It is argued here that participation of strong heterogeneous influence and nitrogen compounds are potentially crucial to Venus middle atmosphere modeling. Confirmation of these results is pending laboratory determination of suitable reactive uptake coefficient (heterogeneous chemistry) and extensive observational measurements of NO and lightning distribution. Validity of both chemical schemes are established by comparison of respective model results with previously published photochemical model results and extant observational information. Results presented here form an integral part of ongoing modeling efforts of the Venus middle atmosphere.

Contents

Chapter 1

General introduction to the Venus middle atmosphere

This research hopes to fill important lacunae in the current understanding of Venus' middle atmosphere and the study of its constituents. This work provides a template for inclusion of new chemistry to the one dimensional Venus middle atmosphere model, keeping in mind the evolutionary nature of this field. This thesis aspires to be a self-contained document of a Venus middle atmosphere model and influential chemical processes. With a detailed presentation of the chemical and physical interactions that are important in the atmosphere, this document endeavours to be a starting point for terrestrial-type planetary atmosphere modeling studies.

The Venus middle atmosphere maintains significant control of the overall chemical composition of the entire atmosphere, mainly by regulation of the carbon dioxide (CO_2) composition. The dominant mechanism for destruction of CO_2 is photolysis - decomposition of molecules by incoming solar ultra-violet radiation. The area of chemistry that deals with photolysis and associated chemical processes is broadly termed photochemistry. Photochemistry is dominant and prevalent in the atmospheric region that is of interest in this study - 58 to 112 km, known as the middle atmosphere. The lower boundary of the middle atmosphere is marked by an ubiquitous and dense cloud cover which reflects nearly 65 % of incoming radiation, resulting in the highest albedo of any of the solar system planets. The existence of such a pervasive cloud cover (strong absorption between 200 – 350 nm wavelength) facilitates unusual chemical processes and resultant phenonmena in this region. In the lower atmosphere, thermal processes hold importance to the chemistry near the surface.

In the middle atmosphere of Venus, as for Earth and Mars, trace (minor) species have a significant impact on the planet's overall chemistry, composition and climatic conditions. Another interesting aspect of this study is the stability of an atmosphere that is composed of 96.5% CO_2. From a chemistry point of view, the extreme pressure and temperature conditions found close to the surface affords a natural laboratory of exciting and exotic

chemical possibilities that may be near impossible to reproduce on Earth. The slow rotational velocity of the planet and the lack of a moon (satellite) are two of the numerous other puzzles that arise from studies of Venus. Furthermore, studies of Venus provide information on the complex and diverse nature of terrestrial planets.

Atmospheric studies combine observations, laboratory measurements and models. A complete study of an atmosphere would begin from its origins. Formation of an atmosphere is due to a complex combination of gas accretion from the vicinity of the growing planetesimal, outgassing from a planet's interior, and collisional events, just to name a few. Atmospheres provide a feedback effect on a planet during its evolution by providing control over its climate and composition. During the later stages of development, an atmosphere acts as a filter for stellar (solar) radiation and for escape of usually light-wieght gas species. Research on planetary atmospheres must be viewed as integral to studies of planetary evolution.

1.1 Key atmospheric processes and parameters

Atmospheric processes that are relevant to this research can be loosely classified under the two categories of photochemistry and chemical transport. Under photochemistry, photolytic processes as well as catalytic cycles/pathways are discussed. Chemical transport deals with transfer of species within the middle atmosphere region as governed by physical laws and principles.

1.1.1 Photochemistry and kinetics

A schematic representation for a generic photochemical reaction is:

$$\mathrm{A} + h\nu \rightarrow \mathrm{A}^* \tag{1.1}$$

where A is any molecule and A^* can simply be understood as its excited molecular state. A^*, depending on the nature of the reaction, could be an excited vibrational or rotational level, excited electronic state, an ionized molecule, or a dissociated molecule.

Molecules present in the atmosphere are not all subjected to similar levels of incoming solar radiation as a consequence of absorption by molecules at higher altitudes. The physical quantity that deals with a molecule's characteristic absorption, defined as a function of frequency (or wavelength) of sunlight, is called the absorption cross section. Absorption cross sections are defined by Beer's Law:

$$\mathrm{I} = \mathrm{I}_o \mathrm{e}^{(-\alpha[\mathrm{A}]\mathrm{l})} \tag{1.2}$$

where I_o and I are incident and transmitted light intensity; α is the absorption cross section (in $cm^2\ mol^{-1}$); [A] is the concentration of the molecule (in cm^{-3}); and l is the pathlength (in cm).

To facilitate a quantitative understanding of photochemical reactions, we specify the rate of formation of the product(s). In the case of Reaction 1.1, given the absorption cross section α_ν at frequency ν, the instantaneous rate of production of A^* is:

$$\frac{d[A^*]}{dt} = [A] \int_{\nu_o}^{\infty} \pi \mathfrak{F}_\nu e^{-\tau_\nu(z)sec(z)} \alpha_\nu d\nu \tag{1.3}$$

$$\frac{d[A^*]}{dt} = [A]J \tag{1.4}$$

where J (in s^{-1}) is the photolysis rate if A^* represents dissociation of molecule A; $h\nu_o$ is the threshold energy for the reaction to take place (h : Planck's constant); $\pi\ \mathfrak{F}_\nu$ is the photon flux per unit frequency interval outside the planet's atmosphere; τ_ν is the vertical optical thickness; z is the solar zenith angle. Given the concentration (N_i) of every species that absorbs at frequency ν, vertical optical thickness can be calculated as:

$$\tau_\nu(z) = \sum_i \alpha_i(\nu) \int_z^{\infty} N_i(z')dz' \tag{1.5}$$

Another important quantity for characterising a photochemical reaction is the quantum yield. The quantum yield of a reaction (say Reaction 1.1) is the number of photolytic-product molecules (in this example, A^*) formed for each absorbed photon that has adequate energy ($h\nu_o$) to produce excited state molecules.

In addition to photolysis, this research is concerned with bimolecular and termolecular reactions. To characterise the kinetic behaviour of reactions, we consider a simple reaction:

$$A \rightarrow \text{products} \tag{1.6}$$

The speed at which the products are formed, or the reactants are consumed, is determined by the rate constant (k) as defined by the differential rate law equation:

$$\frac{-d[A]}{dt} = k\ [A]^n \tag{1.7}$$

The rate constant is the coefficient of the differential rate law equation that determines the rate of consumption (the change in amount per unit time) of A in terms of the concentration of A ([A]). The rate constant is also known as the rate coefficient. The order

of the Reaction 1.6 is the power of the concentration term (n). A zeroth order reaction is independent of reactants' concentration, whereas a second order reaction is dependent on the product of two reactants' (could be same or two different molecules) concentration. The integrated rate law equation helps determine the concentration of reactant species at any given time if the rate constant and initial concentrations are known. For a first order reaction:

$$[\mathrm{A}] = [\mathrm{A}]_0 e^{-kt} \tag{1.8}$$

For a second order reaction (same molecule or same initial concentrations):

$$\frac{1}{[\mathrm{A}]} = \frac{1}{[\mathrm{A}]_0} + kt \tag{1.9}$$

For a second order reaction with two different reactants' concentrations:

$$\frac{[\mathrm{B}]_0[\mathrm{A}]}{[\mathrm{A}]_0[\mathrm{B}]} = kt([\mathrm{A}]_0 - [\mathrm{B}]_0) \tag{1.10}$$

In the course of this research the kinetic data has mostly been obtained from the JPL compilations on Chemical Kinetics and Photochemical Data for Use in Atmospheric Studies [DeMore et al., 1997, Sander et al., 2006]. The bimolecular (simple two-body) reactions' rate constant (k(T)) is generally expressed in the form of the Arrhenius equation:

$$k(T) = \mathrm{A}_f e^{(\frac{E_a}{RT})} \tag{1.11}$$

where A_f is the Arrhenius factor; E_a is the activation energy for the reaction; R is the gas constant and T is the absolute temperature. Termolecular (three-body) reactions' rate constant is expressed differently due to their explicit dependence on pressure conditions. For low pressure reactions:

$$k_o(T) = {k_o}^{300}(\frac{\mathrm{T}}{300})^{-p} \tag{1.12}$$

For high pressure reactions:

$$k_\infty(T) = {k_\infty}^{300}(\frac{\mathrm{T}}{300})^{-q} \tag{1.13}$$

For a given altitude (temperature) and concentration of third molecule ([M]), effective second-order rate constant is obtained from the following expression:

$$k_f([M], T) = \left(\frac{k_0(T)[M]}{1 + \frac{k_0(T)[M]}{k_\infty(T)}}\right) 0.6^{(1+[log_{10}(\frac{k_0(T)[M]}{k_\infty(T)})]^2)^{-1}} \tag{1.14}$$

1.1.2 Species transport

The model used in this research is one-dimensional in the vertical. The distribution of species along the vertical axis is calculated as net result of various transport mechanisms. For an isothermal, well-mixed atmosphere in hydrostatic equilibrium, the variation in pressure (and thus density) can be calculated as a function of altitude.

Consider three slabs of atmosphere of equal area (A) on top of each other in the vertical axis. Net force on the central slab, in terms of pressure applied by the other slabs:

$$\mathrm{F}_{net} = \mathrm{P_1A} - \mathrm{P_2A} \tag{1.15}$$

where $\mathrm{P_1}$ and $\mathrm{P_2}$ are the downward and upward pressures applied by the two slabs respectively. The weight due to gravity,

$$\mathrm{W}_{grav} = \mathrm{m\ g(r)} = \rho \mathrm{V\ g(r)} = \rho \mathrm{A\ dz\ g} \tag{1.16}$$

where g(r) is the acceleration due to gravity and is constant over small increments in height (dz); and ρ is the mass density. Assuming conditions of hydrostatic equilibrium,

$$\mathrm{P_1A} - \mathrm{P_2A} = \rho \mathrm{A\ dz\ g(r)} \tag{1.17}$$

$$\frac{\mathrm{dP}}{\mathrm{dz}} = -\rho \mathrm{g} \tag{1.18}$$

The equation of state for an ideal gas is:

$$\mathrm{P\ V = n\ R\ T} \tag{1.19}$$

$$\mathrm{P} = \frac{\mathrm{k}}{\mathrm{m}} \rho \mathrm{T} \tag{1.20}$$

where m is the mean mass of the molecules; k is Boltzmann's constant; and T is the absolute temperature. Together, this implies that

$$\frac{\mathrm{dP}}{dz} = -P \frac{\mathrm{m\ g}}{\mathrm{k\ T}} \tag{1.21}$$

$$\mathrm{P} = \mathrm{P}_o e^{-\frac{z}{H}} \tag{1.22}$$

upon integration; and where H is defined as the pressure scale height. The scale height is the distance over which pressure decreases exponentially (e-folding distance for pressure).

The primary transport mechanism considered in this research model is that of eddy diffusion. Given the total number density (N) and mixing ratio of a species (μ_i), the continuity equation determines the rate of change of this mixing ratio:

$$\frac{d\mu_i}{dt} = \frac{1}{N} \frac{d}{dz} (\mathrm{N\ K}_{zz} \frac{d\mu_i}{dz}) \tag{1.23}$$

where K_{zz} is the vertical eddy diffusion coefficient. Above the homosphere (defined as the region where tracers (eg. long-lived chemical species) have constant mixing ratio indicative of rapid mixing process), tracers asymptotically approach gravitational diffusive equilibrium, a situation where there exists a balance between the downward gravitational force and the upward partial pressure gradient force. The resulting height distribution is then based on the tracer's scale height.

$$\frac{d\mu_i}{dt} = \frac{1}{N}\frac{d}{dz}(\mathrm{N}\ \mathrm{K}_{zz}\frac{d\mu_i}{dz}) + \frac{1}{N}\frac{d}{dz}(\mathrm{N}\ \mathrm{D}_i[\frac{d\mu_i}{dz} + (\frac{1}{\mathrm{H}_i} - \frac{1}{\mathrm{H}})\mu_i]) \tag{1.24}$$

where D_i is the diffusion coefficient and H_i is the indiviudal scale height of the specie [Mendillo et al., 2002].

1.2 Venus middle atmosphere - Key species and budgets

The Venus middle atmosphere research considered here, in terms of chemistry and composition, has been limited to understanding and modeling the budgets of four major species as discussed below.

CO_2 is the predominant species with measurements that indicate an abundance of 96.5 ± 0.8 % (by volume) of the total middle atmospheric density [von Zahn et al., 1983]. The early Venus atmosphere is generally believed to have contained as much as 300 times the amount of water vapour as is observed now. Initial atmospheric conditions along with increasing solar luminosity facilitated a growth in the amount of atmospheric CO_2 and water vapour which triggered a positive feedback mechanism that resulted in runaway greenhouse gas effect on the planet. This led to highly elevated temperature conditions that is believed to have evaporated most of the water. Formation of carbonates by reaction with water, as believed to have taken place on Earth, was thus impeded which resulted in an enormous build-up of atmospheric CO_2. The exact reasons that caused this effect are yet unknown, but distance from the early 'faint sun' may have caused water to exist primarily in liquid form on Earth as opposed to that on Venus. The evolution of Earth's atmosphere is significantly different in regard to formation of carbonates (and their deposition in oceans) and in the production of O_2 by cyanobacteria.

Photodissoociation of CO_2 is its most significant loss process. Ideal conditions for CO_2 photolysis are found in the middle atmosphere, with the photolysis peak close to the lower boundary. On absorption of photons of wavelength shortward of 200 nm, CO_2 undergoes photodissociation:

$$CO_2 + h\nu \rightarrow CO{+}O \tag{1.25}$$

Molecular oxygen (O_2) and carbon monoxide (CO): Atomic oxygen produced from photolysis of CO_2 is reactive and combines with other atomic oxygen to form oxygen

molecules.

$$O+O+M \rightarrow O_2 + M \tag{1.26}$$

The spin-forbidden three-body reaction (Reaction 1.26) is five orders of magnitude faster than the spin-forbidden CO_2 recombination reaction (Reaction 1.27) at temperatures typically found in Venus' atmosphere

$$CO+O+M \rightarrow CO_2 + M \tag{1.27}$$

M is a third molecule which removes energy and momentum from the intermediate complex formed by the two reactants thereby facilitating formation of a stable end product. In the Venus middle atmosphere, M is usually CO_2, as it is the most abundant molecule. Multiplication of Reaction 1.25 by 2 and subtraction of Reaction 1.26:

$$2\ CO_2 \rightarrow 2\ CO+O_2 \tag{1.28}$$

Simple stoichiometric analysis of Reaction 1.28 in the Venus atmosphere suggests a 2 : 1 ratio for CO : O_2 abundance. Observations [Clancy and Muhleman, 1991, Trauger and Lunine, 1983] indicate that the ratio is closer to 150, suggestive of mechanisms that convert O_2 to other species. Also, in an initial atmosphere that consists only of CO_2, the CO and O_2 would be expected to reach a steady-state equilibrium composition of 7 % and 3.5 %, respectively, of the total atmospheric composition [Nair et al., 1994, Mills, 1998]. Observations have indicated that CO is present at a few hundreds parts per million of the CO_2 abundance and O_2 is yet to be positively identified. The investigation of CO and O_2 budgets are thus believed to be of significance for understanding of the overall chemistry.

Sulphur dioxide (SO_2) - Venus' clouds are made up of sulphuric acid (H_2SO_4) and SO_2 is crucial to their formation. SO_2, along with other sulphur oxides, are suspected to play an important role with chlorine coupled chemistry [Mills and Allen, 2007].

In the light of these and other issues that will be discussed in the course of this thesis, the CO_2, CO, O_2 and SO_2 budgets have been identified as key to the understanding of overall chemistry of the atmosphere and thus will be studied in detail.

1.3 Venus middle atmosphere - physical structure and chemical abundances

The advancement of observational technology along with the 'Space Race' of the 1960s and '70s fuelled a great deal of scientific interest in the solar system. Space probes sent by

the USA and erstwhile Soviet Republic along with numerous Earth-based observational campaigns [Connes et al., 1968, 1979] provided the vast majority of observational data on Venus. One of the earlier studies that established the physical structure of the Venus atmosphere (up to 110 km) was that by Seiff et al. [1979]. Data returned by the Pioneer Venus entry probes suggested a temperature range for the middle atmosphere of between 274K and 179 K. The range in pressure was reported to be as broad as 0.1 bar (58 km) to 0.001 mbar (112 km). Considerably harsher conditions are observed closer to the surface. The overall physical make-up of the atmosphere region from 58 to 112 km is described by temperature (Figure 1.1), pressure (Figure 1.2) and total number density profiles (Figure 1.3).

In terms of volume, the atmosphere of Venus is dominated by carbon dioxide (CO_2). The N_2 mixing ratio was measured in the lower atmosphere (< 52 km) to be between 2.5 % ($\pm$ 0.3) and 4.6 % ($\pm$ 0.14) [von Zahn et al., 1983]. A measured abundance of 4.5 % ($\pm$ 1.3) at 140 km suggested a constant mixing ratio of 3.5 % ($\pm$ 0.8) for the middle atmosphere [Krasnopolsky and Parshev, 1981b]. The CO_2 abundance, expected to be constant throughout, is $\sim$ 96.5 % ($\pm$ 0.8). The characteristic diffusion recovery time (which is the time required to restore diffusive equilibrium after some arbitrary disturbance has been introduced into the atmospheric system) is

$$T_D \approx 1 \times 10^{-13} n \tag{1.29}$$

The number density (n) at 0.1 mbar (180 K, $\sim$ 80 km) is 4×10^{21} m^{-3} and thus T_D $\simeq$ 13 years which von Zahn et al. [1983] argue is too long a time scale for eddy diffusion not to prevent diffusive separation of gases. Thus, 96.5% is considered acceptable as a constant CO_2 abundance throughout. Abundances of some other important species in the atmosphere are listed in Table 1.1.

Species	Abundance	Reference
CO_2	96.5 $\pm$ 0.8 %	von Zahn et al. [1983]
N_2	3.5 $\pm$ 0.8 %	von Zahn et al. [1983]
Ar	70 $\pm$ 25 ppm	von Zahn et al. [1983]
CO	45 ppm at 66 km	Connes et al. [1968]
	1000 ppm at 100 km	Wilson et al. [1981], Schloerb et al. [1980]
O_2[a]	$< 3 \times 10^{-7}$ ppm	Trauger and Lunine [1983]
$O_2(^1\Delta)$	1.5 MR [b]	Connes et al. [1979]
	1.2 MR [c]	Connes et al. [1979]

Table 1.1: Compilation of selected measured species and references. [a] : Column abundance; [b] : Dayglow; [c] : Nightglow; MR : mega-Rayleigh (10^{12} photons $cm^{-2}s^{-1}/4\pi sr$);

The complex nature of Venus can be seen from the perplexing questions raised by even the most routine studies of the planet. Our constantly evolving knowledge of our neighbour planet has always played catch up to the observed phenomena. The physical and chemical processes prevalent in the middle atmosphere region have been duly investigated only in

the last 30 years. A detailed study of the state of the known atmospheric chemistry is timely in light of initial results sent back from the Venus Express mission.

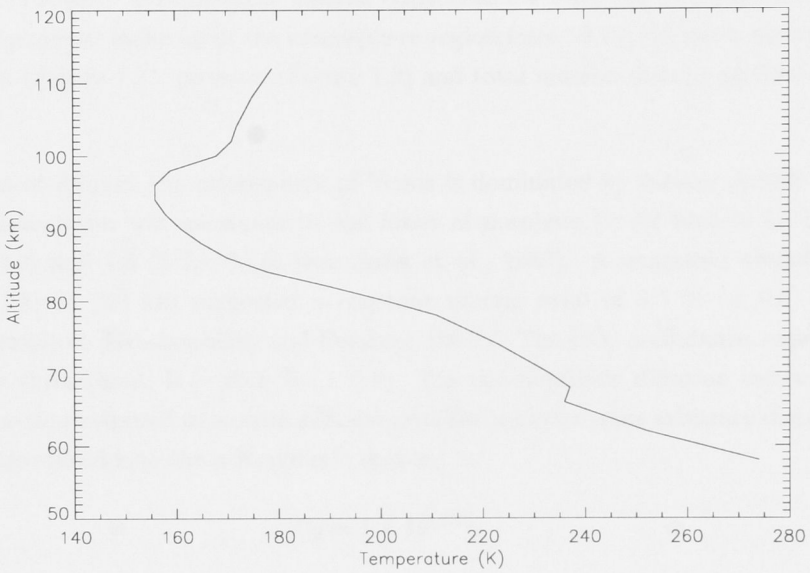

Figure 1.1: Temperature profile from 58 to 112 km

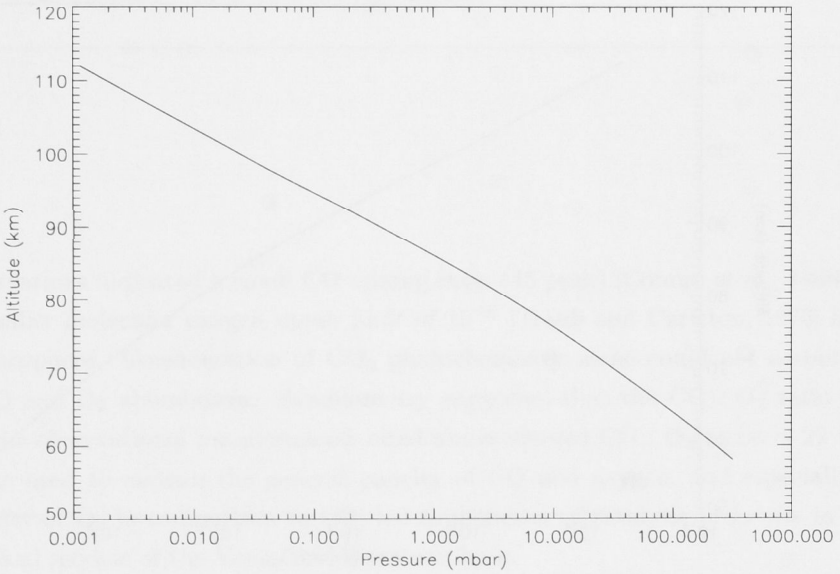

Figure 1.2: Pressure profile from 58 to 112 km

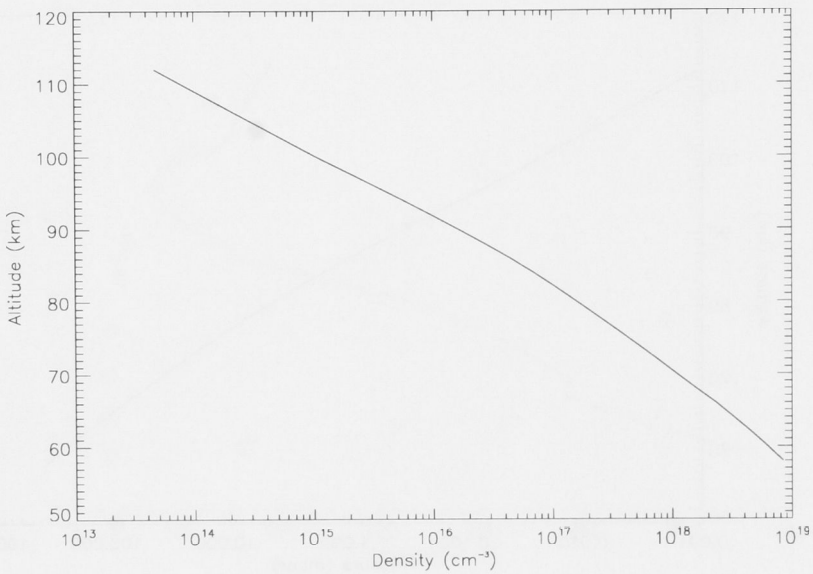

Figure 1.3: Number density profile from 58 to 112 km

Chapter 2

Review of historical modeling of the Venus atmosphere

Early observations indicated a small CO mixing ratio (45 ppm) [Connes et al., 1968] and an even smaller molecular oxygen upper limit of 10^{-6} [Traub and Carleton, 1973] in the middle atmosphere. Consideration of CO_2 photochemistry alone could not account for the low CO and O_2 abundances. Stochiometry suggested that the CO : O_2 ratio must be 2, but the observational measurements cited above showed CO : O_2 to be $\sim$ 22 times larger. The need to explain the general paucity of CO and oxygen, and especially the acute scarcity of O_2 in comparison to CO, led to inclusion of catalytic processes in early photochemical models of the Venus middle atmosphere.

Catalytic processes are reactions activated or aided by means of a substance (called the catalyst) that is itself not directly consumed in the process. Catalysts in atmospheric processes are generally found to be trace species. Often, catalytic processes perform more than one task. In the case of molecular oxygen - a key species and knowledge of whose budget is still deficient - catalytic processes are responsible for reactions that make the O−O chemical bond, ones that inhibit formation of O−O bond, and those that break the O−O bond [DeMore and Yung, 1982]. Of the three tasks mentioned above, chemical catalytic cycles responsible for reactions that break the O−O bond were regarded to be of primary interest. The decomposition of molecular oxygen to atomic oxygen renders the species chemically labile and susceptible to reaction with other species. Catalytic breakage of O-O bond offered an explanation of+ the minute O_2 abundance and provided possible mechanism(s) for oxidation of CO.

Historically, four groups of compounds were considered for catalytic oxidation of CO to CO_2 and/ or destruction of the O-O bond. These groups were hydrogen oxides (HO_x), sulphur oxides (SO_x), chlorine oxides (ClO_x) and nitrogen oxides (NO_x). Hydrogen chemistry, HO_x (H, OH, HO_2 and H_2O_2), had been shown to be important in Martian photochemistry which led early modelers like McElroy et al. [1973] to hypothesize a similar CO

oxidation mechanism

$$CO + OH \rightarrow CO_2 + H \tag{2.1}$$

to produce the carbon dioxide in the atmosphere. Reaction 2.1 has been demonstrated in the laboratory to be a definite sink for CO molecules [Kaufman, 1969, 1979]. Production of atomic hydrogen re-initiates the catalytic cycle in the HO_x model via combination with atomic oxygen and molecular oxygen, Reactions 2.2 and 2.3.

$$H{+}O_2 + M \rightarrow HO_2 + M \tag{2.2a}$$

$$HO_2 + O \rightarrow O_2 + OH \tag{2.2b}$$

$$CO{+}OH \rightarrow CO_2 + H \tag{2.2c}$$

$$\text{Net : } CO{+}O \rightarrow CO_2 \tag{2.2}$$

$$2[H{+}O_2 + M \rightarrow HO_2 + M] \tag{2.3a}$$

$$2HO_2 \rightarrow H_2O_2 + O_2 \tag{2.3b}$$

$$H_2O_2 + h\nu \rightarrow 2OH \tag{2.3c}$$

$$2[CO{+}OH \rightarrow CO_2 + H] \tag{2.3d}$$

$$\text{Net : } 2CO{+}O \rightarrow 2CO_2 \tag{2.3}$$

The initial source for atomic hydrogen in the middle atmosphere is acknowledged to be photolysis of HCl [McElroy et al., 1973]. The McElroy et al. [1973] model used HO_x compounds as part of catalytic process to oxidise CO, and predicted an oxygen column abundance of 10^{-7}, which agreed with the then standard observational upper limit [Traub and Carleton, 1973]. The non-inclusion of catalytic recombination of CO_2 by free chlorine radicals was acknowledged by McElroy et al. [1973] and was justified by the then unavailability of relevant laboratory data for this line of chemistry.

Discovery of sulphuric acid clouds by Hansen and Hovenier [1974] encouraged investigation of SO_x compounds and their role as possible catalysts in CO_2 production. Prinn [1973] suggested the formation of sulphuric acid from oxidation of atomic sulphur and hydrogen mono sulphide (HS); which were products of carbonyl sulphide and hydrogen sulphide photodissociation in the upper atmosphere. Early SO_x models [Prinn, 1975, 1978] were concerned with understanding the principal sulphur compounds and related chemical processes in the middle and lower atmospheres. However, large uncertainties existed

in carbonyl sulphide (OCS) observations and of the vertical mixing rate (eddy diffusion coefficient) which is important for the transport of sulphur compounds in the middle and lower atmosphere. To explain the scarcity of O_2, Prinn [1975] suggested the sequesteration of oxygen in sulphuric acid.

The reliance on OCS as the major sulphur bearing species in the Prinn [1975, 1978] models was rectified by the Winick and Stewart [1980] model, based on observations. SO_2 was deemed to be the primary sulphur bearing species (in the absence of OCS detection) and with adjustments to vertical mixing rates within allowed limits the calculated SO_2 profile and aerosol (H_2SO_4) formation rates were reproduced as observed. However, the predicted CO and oxygen mixing ratios were factors of ~ 6 and ~ 300, respectively, larger than the then accepted observational limits. Despite this, the Winick and Stewart [1980] model was the first comprehensive photochemical model to include HO_x, SO_x, ClO_x and odd-oxygen chemistry.

Detection of HCl in the atmosphere motivated the inclusion of ClO_x chemistry due to the high reactivity of free chlorine radicals (Cl) produced from HCl photolysis. ClO_x compounds were initially thought to influence the CO_2 cycle [Prinn, 1971] via

$$\mathrm{ClOO+CO \rightarrow CO_2 + ClO} \tag{2.4}$$

There is laboratory evidence which shows the rate constant of Reaction 2.4 was overestimated [Cox et al., 1979]. Subsequently, carbonyl chloride (ClCO), which is chemically analogous to ClOO, was hypothesized to play a key role in CO_2 production via direct reaction with atomic or molecular oxygen [Krasnopolsky and Parshev, 1981a,b]. The production and subsequent reactions of ClCO as initially proposed were:

$$\mathrm{Cl+CO+M \rightarrow ClCO+M} \tag{2.5}$$

$$\mathrm{ClCO+O \rightarrow CO_2 + Cl} \tag{2.6}$$

$$\mathrm{ClCO+O_2 \rightarrow CO_2 + ClO} \tag{2.7}$$

However, for this scheme to be feasible, an unrealistically high efficiency is required of Reaction 2.7. Moreover, subsequent laboratory studies have shown that reaction of carbonyl chloride with oxygen occurs as a three-body process via formation of the peroxychloroformyl intermediate radical ($ClCO_3$) [Yung and DeMore, 1982].

$$\mathrm{ClCO+O_2 + M \rightarrow ClCO_3} \tag{2.8}$$

Yung and DeMore [1982] included the intermediate radical $ClCO_3$ in the overall oxi-

dation of CO to CO_2 as shown below:

$$ClCO_3 + O \rightarrow Cl{+}CO_2 + O_2 \tag{2.9}$$

$$ClCO_3 + Cl \rightarrow Cl{+}CO_2 + ClO \tag{2.10}$$

Although all of the Yung and DeMore [1982] models agreed that oxidation of CO, and not SO_2 as previously suspected, was the major O_2 sink, they each subscribed to a different chemical scheme. The three models were each uniquely motivated; Model A was based on a controversially high observation of H_2 by Kumar et al. [1981]; Model B included a challenge to the above-mentioned observation [McElroy et al., 1982] and a hypothesis of lightning-influenced photochemistry via NO_x compounds and ClO_x oxidation scheme; Model C included the ClO_x oxidation scheme and assumed the lowest H_2 mixing ratio of the three. Given the controversial basis for Model A and the absence of confirmed observations for lightning (and thus NO_x compounds) in Model B, Model C was the preferred option. It was the first model to explicitly describe coupling of chlorine and sulphur species in the Venus atmosphere. Observations of an unidentified ultraviolet absorber for the 0.32 – 0.4 μm range [Pollack et al., 1980] could be explained by Model C with gaseous chlorine known to be an excellent absorber at these wavelengths. A more robust test for Model C was that of nightside depletion of CO between 80 km and 90 km observed in 1980 [Schloerb et al., 1980, Wilson et al., 1981]. Models A and B have chemical schemes where most of the CO is destroyed below 70 km, whereas the majority of CO is destroyed in the altitude region between 80 km and 90 km in Model C. A comparison of inputs in the three models is given in Table 2.1.

	Model A	Model B	Model C
μ_{H_2}	2×10^{-5}	5×10^{-7}	1×10^{-13}
μ_{HCl}	4×10^{-7}	4×10^{-7}	8×10^{-7}
μ_{NO_x}	0	3×10^{-8}	0
Chemistry	Base†	Base + NO_x + $ClCO_x$	Base + $ClCO_x$

Table 2.1: Comparison of Yung-DeMore models. †: Basic chemical schemes (see Yung and DeMore [1982, Table IIIA])

Key unresolved questions surrounded the predicted O_2 column abundance (1.8×10^{19} molecules cm^{-2}) which was greater than the Trauger and Lunine [1983] observational upper limit by a factor of 10. Crucial intermediate radicals in the primary CO_2 re-formation pathways have not been positively identified in the atmosphere nor have key reaction rates been measured in the laboratory. Yet, theoretical results from Yung and DeMore [1982] Model C were accepted as standard for Venus middle atmosphere photochemistry.

Subsequent revisions to the model kinetics and photochemistry by Mills [1998] form the framework for the current model. Model results were found to agree with observations

when adjusted within the acceptable uncertainty range for key reaction rates.

The nominal equilibrium constant for ClCO formation and decomposition is given by Sander et al. [2002]:

$$K_{ClCO} = 3.5 \times 10^{-25} e^{3730/T} \tag{2.11}$$

with K_{ClCO} given in $cm^3 molecules^{-1}$.

This is based on work by Nicovich et al. [1990] who measured the rate for M = N_2 and $185 \leq T \leq 260$.

The uncertainty in equilibrium constant is

$$f(T) = 1.2e^{200[(1/T)-(1/298)]} \tag{2.12}$$

The assessed uncertainty reported by Sander et al. [2002] is a about a factor of 2 larger than that quoted in the experimental report [Nicovich et al., 1990] based on the assessment committee's judgement.

Production of $ClCO_3$ (Reaction 2.8) is a crucial intermediate step in the overall CO_2 cycle. Recent laboratory studies have successfully isolated the $ClCO_3$ radical [Pernice et al., 2004]. Infrared spectroscopic studies have revealed that the $ClCO_3$ radical is thermally stable up to 350 C, above which it decomposes. Ultraviolet studies have revealed the photolysis of $ClCO_3$ to produce CO_2 at λ = 255 nm. The O_2 column abundance (abundance of molecular oxygen integrated for the column of air over the entire middle atmosphere) is 3.05×10^{19} molecules cm^{-2} for a model without $ClCO_3$ ([Yung and DeMore, 1982, Model A]) as opposed to 2.14×10^{18} molecules cm^{-2} for a model with $ClCO_3$ chemistry in which the stability of ClCO is enhanced [Pernice et al., 2004], 1-σ model. Validation of the proposed chemical scheme which involves $ClCO_3$ [Yung and DeMore, 1982, Mills, 1998, Pernice et al., 2004] now rests on observation of this radical in the Venus middle atmosphere. However, the absorption line strengths for $ClCO_3$ are still not known. Further characterisation of $ClCO_3$ in laboratory studies is needed to support observational efforts to detect $ClCO_3$.

Chapter 3

Introduction to the Venus middle atmosphere model

3.1 Model - computation and numerical solution finding

The one-dimensional planetary atmosphere model used in this research was developed primarily at Caltech. While the model input data has undergone numerous revisions from the original largely due to laboratory advancements in measurements of kinetic and photolytic data as well as modern observations (remote and near), the code has evolved to handle the improved quality of photochemical data. Details of the initial terrestrial model are discussed in Allen et al. [1981]. Primary, non-nitrogen species (CO_2, CO, O_2, SO_2, H_2O, etc) along with vertical transport by eddy diffusion are included in the model. Solution of the continuity equation for individual species (Equation 3.1) forms the core of the atmosphere model.

$$\frac{\partial n_i}{\partial t} + \frac{\partial \phi_i}{\partial z} = \mathrm{P}_i - \mathrm{L}_i \tag{3.1}$$

where n_i = concentration or number density; z is the altitude. P_i = production rate from chemical reaction i; L_i = loss rate from chemical reaction i; ϕ_i = vertical flux of species i (Equation 3.2).

$$\phi_i = -(\mathrm{K} + \mathrm{D}_i)[\frac{\partial n_i}{\partial z} + \frac{n_i}{\mathrm{T}}(1 + \alpha_i)\frac{\partial \mathrm{T}}{\partial z}] - n_i(\frac{\mathrm{K}}{\mathrm{H}} + \frac{\mathrm{D}_i}{\mathrm{H}_i}) \tag{3.2}$$

where K is eddy mixing coefficient; D_i is the molecular diffusion coefficient; H and H_i are mean atmospheric scale height and the atmospheric scale height of the ith component; T is absolute temperature and α_i is thermal diffusion factor [Allen et al., 1981].

3.2 Model - General Characteristics

The current one-dimensional model is restricted to computations along the vertical (altitude) axis. A facility for inclusion of latitudinal variations exists in the current version of the model but has not been utilized due to lack of sufficient spatial data. In this regard, atmospheric data collected by Venus Express is expected to be extensive and would be handled best by a multi-dimensional model. The model is diurnally averaged - differences in day and night time chemistries are not included. The slow rotational period ($\sim$ Earth 243 days) compared to a revolution around the Sun ($\sim$ 220 Earth days) leaves the "day hemisphere" exposed to continuous irradiation and leads to development of large diurnal variations in physical conditions. Photodissociation (solar-induced chemical reactions) and temperature-dependent reaction rates are influenced by diurnal differences. Photodissociation rates calculated for 45 degrees at local noon are halved to obtain global average conditions. Radiative transfer - the aspects of passage of solar flux (and energy) through the layers of the middle atmosphere, including scattering and absorption phenomena - is included in model calculations. The wavelength range of solar radiation used in the middle atmosphere is from 120 nm to 800 nm. Wavelengths above 8000 A are not expected to be significant for photodissociation. Solar radiation below 1200 A is absorbed in the upper atmosphere (thermosphere or ionosphere) and is of no consequence to this study [Mills, 1998].

There are roughly three distinct atmosphere regimes - the lower, middle and upper atmosphere. The model of the middle atmosphere is a closed physical system with parameters, both constant and variable, that represent in totality the proceses that drive this region. The interaction, chemical and physical, with the lower and upper atmospheres is simulated via boundary conditions imposed on the model.

3.2.1 Model input

Input parameters are needed to put in place constraints on the model calculations. Constraints or boundaries must allow independent computation of other calculable paramaters. Physical conditions are defined from observational profiles of temperature [Seiff, 1983], pressure, number density, scale height (calculated by model) and eddy diffusion [Mills, 1998]. Solar irradiance data from Neckel and Labs [1984] and Woods et al. [1996] have been used, after distance adjustments were made to the original data acquired for Earth. Details of the model are presented elsewhere [Mills, 1998].

Certain chemical parameters such as backgound species' abundances (like CO_2 and N_2) are used to form the model framework within which the other parameters (such as CO and O_2 abundances and consumption) are allowed to vary. Chemical kinetics is constrained by reaction rate constants; these have been obtained from lab studies or extrapolated from

lab measurements of similar reactions. The uncertainty from such extrapolations, more so than laboratory based values, could be large and potentially have a big effect on the outcome of the chemistry. Most of the chemical data is derived from DeMore et al. [1997].

Species	Lower boundary (58 km)	Upper boundary (112 km)
CO_2	$\mu = 0.965$	$\phi = 5 \times 10^{11}$
CO	$\mu = 4.5 \times 10^{-5}$	ϕ = -5 $\times 10^{11}$
O_2		$\phi = 9 \times 10^{8}$
H_2		v = -2.7 $\times 10^{6}$
HCl	$\mu = 4 \times 10^{-7}$	$\phi = 1 \times 10^{7}$
SO_2	$\mu = 1 \times 10^{-6}$	$\phi = 0$
O		ϕ = -5.03 $\times 10^{11}$
H		ϕ = -4.5 $\times 10^{6}$
Cl		ϕ = -1 $\times 10^{7}$
Cl_2	v = -1.5 $\times 10^{-2}$	
OCS	$\mu = 1 \times 10^{-9}$	
$O_2(^1\Delta)$		v = 0

Table 3.1: Upper and lower boundary conditions. μ: mixing ratio; ϕ: flux ($cm^{-2}s^{-1}$) and positive value indicates upward flow; v: velocity (cm/s).

The lower boundary is set at 58 km due to reported stability against convection at this height [Seiff, 1983]. Mixing ratios, as a boundary condition, are sufficient to represent species that are produced in the lower atmosphere, destroyed in the upper atmosphere, and have photochemical lifetimes (near 58 km) that are much larger than vertical mixing times. Most species, with exception of OCS and SO_2 fulfill these conditions (details of which are in Mills [1998]). All unspecified species and values not listed in Table 3.1 are set to v = -2 $\times 10^{-2}$ at the lower boundary (for minimum concentration gradient/ maximum downward diffusive flux).

The upper boundary is well below the homopause at 130 km, above which species are not well mixed and approach gravitational diffusive equilibrium asymptotically [Mendillo et al., 2002]. Some CO_2 photodissociation, which along with that of HCl is vital to the overall chemistry, is contained within this region. Photodissociation of HCl is comparable to the escape flux of hydrogen from the Venus atmosphere. At the upper boundary, downward fluxes of CO, O and Cl are set to balance upward fluxes of CO_2, O_2 and HCl respectively. The mixing ratio of N_2 is held constant at 0.034 throughout. The specifications on the mixing ratio of water is discussed below. Fluxes of species not specified in Table 3.1 are set $\phi = 0$ (photochemical equilibrium), as their concentrations are negligible around 112 km [Mills, 1998].

3.2.2 Model computational scheme/ output

The continuity equation (3.1) is an example of a 'parabolic equation', with a schematic representation

$$\frac{\partial U}{\partial t} = \sigma \frac{\partial^2 U}{\partial x^2} \tag{3.3}$$

where U = U(x,t); σ : constant > 0; $0 \leq x \leq \pi$; and $t \geq 0$. For an initial value problem, U(x,0) = ϕ(x); U(0,t) = 0; and U(π,t) = 0. Solution of Equation 3.3, with boundary conditions, is pursued numerically with small increments Δx and Δt.

$$x = j\Delta x \tag{3.4}$$

$$t = n\Delta t \tag{3.5}$$

The difference equation approximation of Equation 3.3, given elsewhere [Richtmyer and Morton, 1967], is

$$\frac{U_j^{n+1} - U_j^n}{\delta t} = \sigma \frac{U_{j+1}^n - 2U_j^n + U_{j-1}^n}{\delta x^2} \tag{3.6}$$

Recursive application of Equation 3.6 offers a numerical approximation for all values of U_j^n which makes it possible to calculate concentrations of all species at any given time. Significant species (defined as those with $\mu \geq 10^{-9}$) whose concentration remain constant with time, converge to a solution which differs by less than 1 in 10^4 when calculated over a geological time scale (of 10^{15} years). A discussion on convergence problems and compuational tricks to overcome these is given in the Appendix.

3.2.3 Model set-up

The model is set-up as a (complex) web of inter-connected species with their respective production and loss reactions. For every 'run' of the model (iteration), the species are subjected to the entire set of photolytic and kinetic reactions as determined by the rates. One iteration of the model is set to a logarithmic increase in timestep of $\sqrt{10}$ seconds. As the model is run, species converge to their steady-state concentrations, in obedience with their production and loss rates at every altitude, and the entire atmosphere evolves starting from 10^{-15} seconds up to 10^{15} seconds over 60 such time steps. 10^{15} seconds is roughly 50 million Venus-years, a long enough timescale for all atmospheric constituent species to be considered to be at their steady-state values.

At this juncture, it is important to discuss the unique relationship between concentration of species and their rates (of production and loss reactions). The concentration of a species is calculated from the net production or loss from all its reactions, based on an initial value that is input in the model. Reaction rates in the model are calculated at every altitude from the respective reaction rate constants and concentrations of species

involved. Thus, the reaction rate - concentration relationship is in nature an 'iterative feedback' set-up, whereby a change in one affects the other. Both, concentration and reaction rate, are calculated for each timestep and at every altitude. Transport between altitudes takes place through molecular and eddy diffusion and is considered important when chemical loss timescales are larger than vertical transport timescales.

Chapter 4

Introduction to Observations

4.1 Observations - CO, O_2 airglow and O_2

Observations of the abundances of critical species serve as input parameters to the middle atmosphere model, and, along with laboratory measurements, set the conditions for model calculations. Observations of species' profiles are used to test the model's accuracy and improve model performance. The model accuracy is strongly influenced by quality of observational input data. In this regard, uncertainties in observational measurements are taken in to account to understand the degree of uncertainty in the model results.

Observations of the Venus atmosphere have been made for a range of wavelengths, and give information on a variety of atmospheric components. The ultraviolet regime (220 – 400 nm) has provided information on sulphur bearing compounds above and below the cloud region, which are crucial for understanding cloud formation processes, precipitation, and surface-atmosphere interactions [Bertaux et al., 1996]. Near-IR radiation was first detected in the 1.74 μm and 2.3 μm regions. These spectral windows indicated cyclic variations in the Venusian cloud structure, and the presence of CO in the nightside lower atmosphere [Allen and Crawford, 1984] which has since been confirmed [Marcq et al., 2005]. Trace atmospheric constituents such as carbonyl sulphide (OCS), water (H_2O), sulphur dioxide (SO_2) and halides (HF and HCl) have been identified and measured using near-IR and IR observational studies. Ground-based millimeter and sub-millimeter observations have been used to estimate CO profiles and distinguish diurnal variations in the middle atmosphere region. Radio occultation measurements have been instrumental in estimation of the vertical distribution of the H_2SO_4 vapour. A review of the state of compositional knowledge of Venus atmosphere below 100 km is given elsewhere [de Bergh et al., 2006].

Observations of CO in the Venus atmosphere were first reported for 2.35 μm, later resolved to be the first overtone band of CO. The abundance and location of CO in the atmosphere of Venus could be deduced from such observations. Connes et al. [1968] reported a CO mixing ratio of 45 parts per million (ppm) at 175 millibars (mb), approximately 66 km above surface. Measurements since have reported variable mixing ratios for CO. Observations of the rotational transition ($J = 0 \rightarrow 1$) at different phase angles indicated CO

mixing ratios in the range of 20 – 100 ppm (at 2.6 mm wavelength) for pressure range of 2 – 100 mb [Schloerb et al., 1980]. Different measurements at phase angles 180 and 120 degrees were suggestive of variations in the CO abundance and implied nightside depletion below the 1 mb level. Wilson et al. [1981] using same band, reported a CO mixing ratio of 6×10^{-6} (upper limit near 62 km); much smaller than the extant model calculations, and a column abundance more than an order of magnitude less than reported 11 years earlier Connes et al. [1968]. Long-term and possibly cyclic ($\sim$ 10 years) variations in abundances have been suggested to account for the observed differences [Clancy and Muhleman, 1991]. Figure 4.1 shows profiles of the CO mixing ratio measured at various times on the nightside, near inferior conjunction, of Venus.

The Clancy and Muhleman [1991] observations shown in Figure 4.1 were from 1986 (3 AM and 9 AM) and 1990 (antisolar and terminator). The CO bulge is reported to be centered at 3 AM. The 1986 observations show an anamolous increase (by factor of $\sim$16) in the CO abundance and temperature over the observed period (1979-1990). Lellouch et al. [1994] reported CO mixing ratio values taken at 15 different points on the Venus nightside. The range of their observations (low and high points) along with the uncertainties are shown in Figure 4.1 for comparison. For the CO mixing ratio below 70 km altitude, we include the Young [1972] interpretation of the observations of Connes et al. [1968].

Terrestrial planets are known to emit luminescence in particular wavelength bands in the form of airglow. Studies of these signature airglow patterns have revealed interesting details about atmospheric chemistry. For purposes of observation, airglow is broadly classified by Fox [1986] as dayglow (emission caused by interaction of solar radiation with atmospheric gas constituents), nightglow (luminosity due to chemical reactions between species that are usually created in the dayside) and aurora (emissions that are due to electron impact on neutral atoms and molecules where the electrons are not produced by photoionization). Most ground-based observations are limited to inferior location of Venus (compared to Earth) and report nightside airglow measurements only. The mechanism behind the $O_2(a^1\Delta_g)$ airglow is not completely understood. Dayside and nightside airglow may be due to either process described by Fox [1986].

Early measurements of the infrared region at 1.27 μm wavelength were done for day and night sides of Venus by Connes et al. [1979]. Intense airglow was identified as spontaneous emission by $O_2(a^1\Delta_g)$ to return to the ground state ($O_2(X^3\Sigma_g^-)$):

$$O_2(a^1\Delta_g) \rightarrow O_2(X^3\Sigma_g^-) + 0.98\text{eV} \tag{4.1}$$

Connes et al. [1979] reported 1.2 MR and 1.5 MR (MR = mega Rayleigh = 10^{12} photons $cm^{-2}s^{-1}$ into 4 π steradians) for the night and sunlit sides respectively. This was interpreted as evidence for the existence of rapid transport of constituents (atomic oxygen) between the day and night sides based on the assumption that the nightside airglow was produced via Reactions 4.1 and 4.2. Mechanisms other than the three body recombination

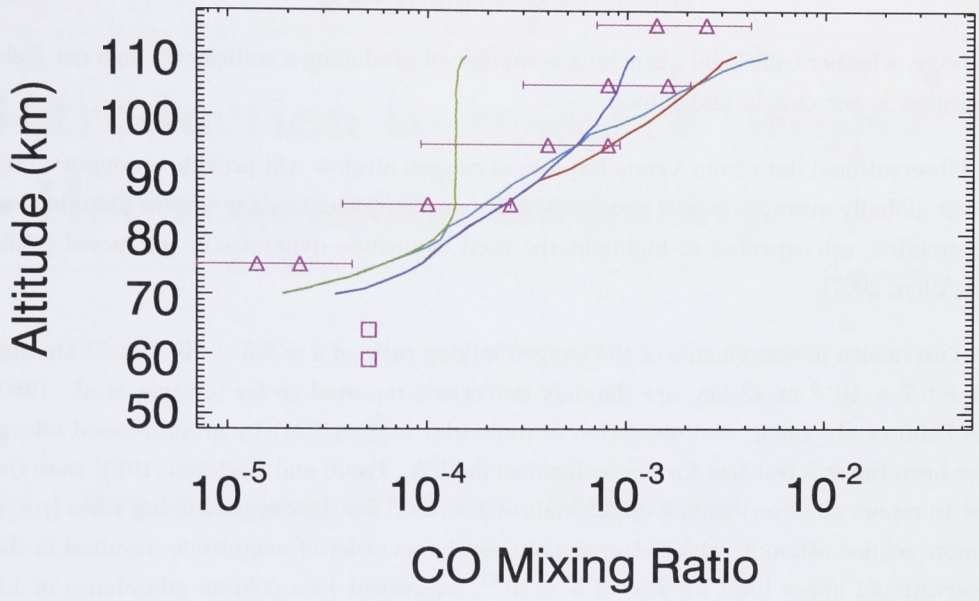

Figure 4.1: Observed CO mixing ratios. Clancy and Muhleman [1991] profiles are shown by the four solid lines - dark-blue, red, light-blue and green representing observations made at terminator (1990), anti-solar (1990), 3 AM (1986) and 9 AM (1986) respectively, with uncertainty bars shown for the 3 AM and 9 AM observations. Lellouch et al. [1994] measurements are shown as magenta coloured triangles with indicated uncertainties. The squares(magenta) represent the Young [1972] interpretation of the Connes et al. [1968] observation.

of oxygen (Reactions 4.3, 4.4 and 4.5) have since been included in the modeling to try to explain the unexpectedly high airglow emission [Yung and DeMore, 1982] but laboratory studies have shown the yields of $O_2(a^1\Delta_g)$ from these reactions are too small [Leu and Yung, 1987].

$$O+O+M \rightarrow O_2(a^1\Delta_g) + M \tag{4.2}$$

$$Cl+O_3 \rightarrow ClO+O_2(a^1\Delta_g) \tag{4.3}$$

$$O+ClO \rightarrow Cl+O_2(a^1\Delta_g) \tag{4.4}$$

$$HO_2 + O \rightarrow OH+O_2(a^1\Delta_g) \tag{4.5}$$

The direct yield of $O_2(a^1\Delta_g)$ from Reaction 4.2 in laboratory studies is smaler than what is needed to explain the absorbed nighside airglow on Venus. Consequently, collisional quenching of higer excited states of O_2 has been suggested to account for the high intensity of the $O_2(a^1\Delta_g)$ airglow [Crisp et al., 1996]. Collisional quenching is the process of transition of a molecule from a more excited state to a less excited state via inter-particle collision. Collisional quenching was implicitly included in Yung and DeMore [1982] models i.e, Reaction 4.6:

$$O_2(c^1\Sigma_u^-) + \mathrm{M} \rightarrow O_2(a^1\Delta_g) + M \tag{4.6}$$

However, whether collisional quenching is capable of producing a sufficiently high net yield of airglow is not clearly understood.

Observational data from Venus Express of oxygen airglow will provide an opportunity to test globally averaged model results. Variations in CO and oxygen airglow abundances, if correlated, are expected to highlight the need to include dynamics in the model [Mills and Allen, 2007].

Two in situ measurements of the oxygen mixing ratio, $4.4 \pm 2.5 \times 10^{-5}$ at 52 km and $1.6 \pm 0.7 \times 10^{-5}$ at 42 km, are the only detections reported so far [Oyama et al., 1980, von Zahn et al., 1983]. Non-detection of molecular oxygen (O_2) by ground-based efforts have been the strictest test for photochemical models. Traub and Carleton [1974] were the first to report an observational upper limit of 1×10^{-6} for the oxygen mixing ratio (μ_{O_2}). A more refined attempt, with better signal:noise by an order of magnitude, resulted in the observational upper limit for μ_{O_2} of 3×10^{-7}, equivalent to a column adundance of 1.5×10^{18} cm^{-2} [Trauger and Lunine, 1983]. Recent spectroscopic measurement [Mills, 1999] has highlighted problems with the marginal detection by Oyama et al. [1980]. More recent interpretation of Trauger and Lunine [1983] observational data has indicated that the O_2 column abundance could be smaller still. With a simple reflection model, Krasnopolsky [2006b] has suggested that the upper limit on the O_2 column abundance is 8×10^{17} cm^{-2}. Though long-term variations have been suspected in the O_2 abundance [Trauger and Lunine, 1983] similar to that observed for CO, there has been no conclusive evidence supporting this argument.

Chapter 5

Introduction to research project 1 - Heterogeneous chemistry

5.1 Heterogeneous chemistry - Background

Heterogeneous chemistry, defined broadly, refers to chemical reactions that occur between reactants that exist in different phases (states of matter). In this research, it is reactions amongst Venus middle atmosphere constituents in gas phase and condensed (liquid or solid) aerosols that are of interest. By nature, heterogeneity of reactants make them sensitive to surface properties. It is on the surfaces of or within suspended aerosols that the chemistry is contained and determined. In addition to chemical (kinetics, reactivity) and physical (temperature, pressure, abundances) factors that are present in homogeneous chemistry, heterogeneous reactions depend upon other parameters.

Analogous to the reaction rate constant for homogeneous reactions, the reactive uptake coefficient, γ, is representative of the probability of a reaction occuring. It is defined as the ratio of the rate of reactive uptake or removal of the gas molecules by reactions in/ on the condensed phase to the gas collision rate at the interface.

The reactive uptake coefficient is the best means available to quantify the rate of heterogeneous mechanisms. Laboratory scientists routinely study various elements of heterogeneous chemistry to measure γ:

$$\frac{1}{\gamma} = \frac{1}{\alpha} + \frac{1}{\gamma_{dif}} + \frac{1}{\gamma_{chm} + \gamma_{sol}} \tag{5.1}$$

where the mass accommodation coefficient or sticking coefficient, α, is the ratio of the rate at which molecules cross the interface region (between condensed and gas phases) to the gas collision rate at the interface:

$$\alpha = \frac{\text{number of gas molecules entering the condensed phase in unit time}}{\text{number of gas molecules striking at the interface in unit time}} \tag{5.2}$$

γ_{dif} : gas-phase diffusion coefficient and is given by:

$$\frac{1}{\gamma_{dif}} = \frac{cd_f}{8D_g} - \frac{1}{2} \tag{5.3}$$

γ_{sol} : solubility coefficient and is given by:

$$\frac{1}{\gamma_{sol}} = \frac{\pi^{1/2}}{2} \frac{c}{4RT\mathrm{H}} \frac{1}{D_l{}^{1/2}} \tag{5.4}$$

γ_{chm} : chemical reaction coefficient and is given by:

$$\frac{1}{\gamma_{chm}} = \frac{c}{4RT\mathrm{H}} \frac{1}{D_l k^{1/2}} \tag{5.5}$$

where: H : Henry's law coefficient; d_f : effective diameter; D_g : gas-phase diffusion coefficient; D_l : liquid phase coefficient; k : pseudo first-order rate constant; R : gas constant; c: trace gas average thermal velocity ; T : temperature [Hu et al., 1995].

5.2 Heterogeneous chemistry - motivation and modeling

Heterogeneous chemistry has been included in Earth stratosphere models to explain drastic decrease in O_3 levels over the Antarctic (Halley Bay) in observations made in the southern hemisphere spring season [Solomon et al., 1986]. This study identified Polar Stratospheric Clouds as a site for heterogeneous reactions. Detailed studies have since confirmed major perturbances in atmosphere chemistry due to heterogeneous chlorine chemistry [Solomon et al., 1997]. The formulation of heterogeneous chemistry in the Earth's atmosphere [Borrmann et al., 1996] is mathematically similar to that used in this research.

In the case of the Mars atmosphere, heterogeneous chemistry was included as an additional mechanism to facilitate adsorption and subsequent destruction of HO_x radicals, thereby reducing the CO sink [Nair et al., 1994]. Dust grains, suspended in the air, play the role of catalysts. Though heterogeneous chemistry provides favourable results in regard to observed CO mixing ratio, modelled O_3 abundances are still higher by a factor of 4 for the preferred model. Consequently, Nair et al. [1994] preferred to manipulate gas-phase chemical parameters within their accepted limits than pursue heterogeneous chemistry.

Clouds on Venus extend from 45 km to 70 km, with 15 km of haze on both sides. They are thicker and more ubiquitous than those on Earth and Mars. As in the case of Earth's stratosphere, the extensive Venus cloud layer may facilitate occurrence of heterogeneous processes. The primary constituent of the Venus cloud and haze layers is concentrated ($\sim 70 - 85$ wt% H_2SO_4) sulphuric acid, present in a condensed aerosol state [Hansen and Hovenier, 1974, Esposito et al., 1983]. Chlorine activation via heterogeneous chemistry, as occurs in the Earth's polar stratosphere, is strongly inhibited on Venus due to the

weak solubility of HCl in such highly concentrated sulphuric acid [Mills, 1998]. However, laboratory work suggests that CO_2 may be produced via heterogeneous processes in the Venus atmosphere, as shown schematically in Reaction 5.6.

$$CO + O + \text{aerosol} \rightarrow CO_2 + \text{aerosol} \tag{5.6}$$

The detailed mechanism underlying Reaction 5.6 is unknown at present. One proposed mechanism is that single- or multi-photon absorption in sulphuric acid aerosols may dissociate H_2SO_4 to form OH or O which can react with dissolved CO to form CO_2 [Mills and Phillips, 1993, Mills et al., 1996, Wrenn et al., 1999]. A second possibility is that photo-excitation of CO may be followed by either Reaction 5.7 [Roussel and Back, 1989] or Reaction 5.8 [Raper and DeMore, 1964, Roussel and Back, 1989]

$$CO^* + CO \rightarrow CO_2 + C \tag{5.7}$$

$$CO^* + O_2 + M \rightarrow CO_3 + M \tag{5.8a}$$

$$CO_3 + O_2 \rightarrow CO_2 + O_3 \tag{5.8b}$$

$$net : CO^* + 2O_2 \rightarrow CO_2 + O_3 \tag{5.8}$$

A third proposed mechanism [Wrenn et al., 1999, Rowland and Phillips, 2000, Rowland et al., 2002] is that photo-excitation of sulphuric acid with trace amounts of dissolved Fe and/or SO_2 can produce SO_3^-, SO_4^-, and HSO_5^- which can oxidize dissolved CO to CO_2 (Reaction 5.9) and provide an effective sink for oxygen (Reaction 5.10).

$$CO + HSO_5^- \rightarrow CO_2 + HSO_4^- \tag{5.9}$$

$$SO_3^- + O_2 \rightarrow SO_5^- \tag{5.10}$$

Given the uncertainties associated with Reaction 5.6, this research postulates the existence of Reaction 5.6, identifies effective rate at which this reaction would be important for the atmospheric chemistry and assesses the potential impact of heterogeneous chemsitry on photochemical modelling. Follow-up laboratory studies are required to confirm the occurrence of reaction and its rate. The process of adaptation of heterogeneous chemistry to the model provides a template for inclusion of other such mechanisms for future modelling work.

5.3 Atmospheric aerosols

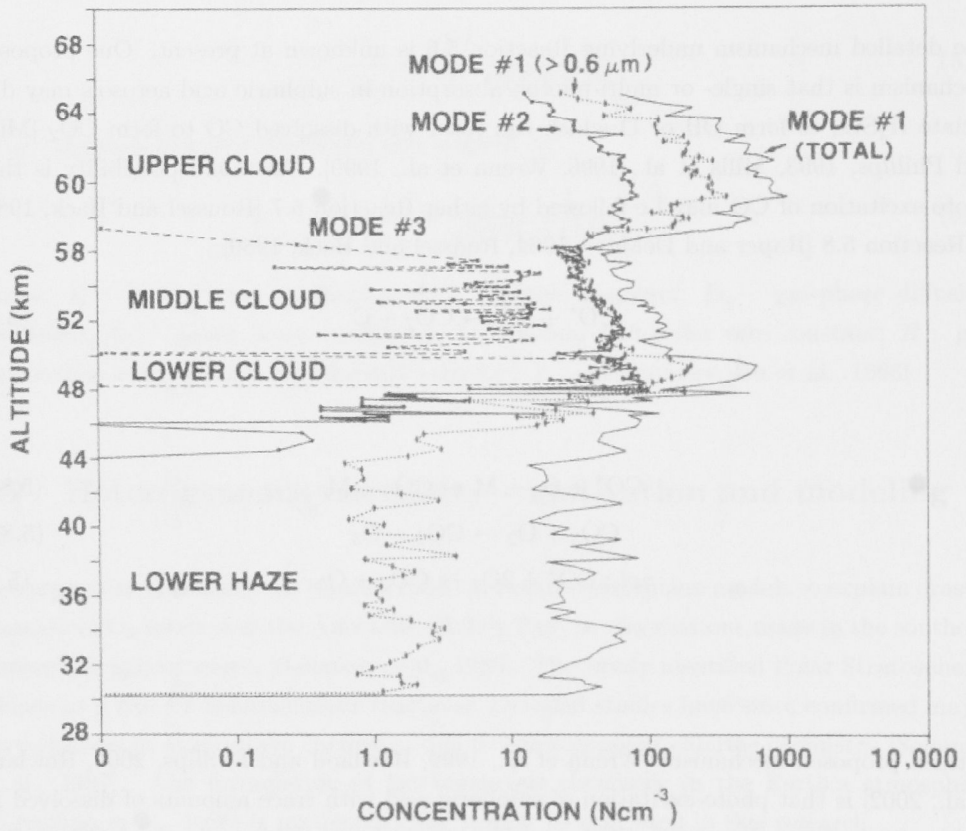

Figure 5.1: Aerosol modes in the Venus cloud region from Knollenberg and Hunten [1980]. (Upper haze layer, from 70 km to 90km, is not pictured)

Mode 1 and mode 2 aerosols in the Venus upper cloud and upper haze layers are assumed to have a radius of 0.25 μm and 1.0 μm, respectively. To calculate the aerosols' effective number density the aerosol surface area was integrated over the best-fit size distributions inferred from observations [Knollenberg and Hunten, 1980] as discussed below. The rate-limiting gas for Reaction 5.6 was assumed to be CO because of the oxygen available from SO_3 and HSO_3^- dissolved in sulphuric acid aerosols.

The aerosol concentrations observed by the Pioneer Venus descent probes were parameterized in terms of three modes, only two of which (mode 1 and mode 2) were identified above 58km altitude [Knollenberg and Hunten, 1980]. For the mode 1 aerosols, the distribution with respect to size was best fit with a log-normal function, Equation 5.11,

$$n_o(D) = \frac{N_T}{\sqrt{2\pi} D \ln(\sigma_g)} e^{(-1/2)\left[\frac{\ln(D/\bar{D}_g)}{\ln(\sigma_g)}\right]^2} \tag{5.11}$$

where n_o = observed aerosol number density distribution function (cm^{-3} μm^{-1}), N_T = total aerosol number density (cm^{-3}), D = aerosol diameter (μm), $\bar{D}_g$ = geometric mean aerosol diameter (μm), and σ_g = geometric standard deviation. The parameters needed to describe the mode 1 log-normal functions throughout the 58 – 90 km altitude range were taken from Table 4 and Figure 10 of Knollenberg and Hunten [1980]. For the mode 2 aerosols, the distribution with respect to size was best fit with a Gaussian function, Equation 5.12,

$$n_o(D) = \frac{67.7}{\sqrt{2\pi}\sigma} e^{\frac{-(D-D_m)^2}{2\sigma^2}} \tag{5.12}$$

where D = aerosol diameter (μm), D_m = aerosol modal diameter (μm), σ = standard deviation (μm). The parameters needed to describe the mode 2 Gaussian functions throughout the 58 – 90 km altitude range were taken from Figure 3 of Knollenberg and Hunten [1979].

It is reported here that a typographical error (presumably) in Figure 3 of Knollenberg and Hunten [1979] has resulted in the omission of a 'squared' term in the exponential. As a result the expression, as given in their Figure 3, has incorrect dimensions for the exponential term. The corrected expression is used here (Equation 5.12). The formulation for the Gaussian distribution function is adopted from Figure 3 Knollenberg and Hunten [1979], where the authors have used it to represent mode 2 aerosols between 53km and 57km. This research has extended the application of this formulation to the upper cloud layer (58km to 66km). The standard deviation and modal diameter values are, however, taken from Table 4 of Knollenberg and Hunten [1980] to solve for the modeled aerosol density.

The modelled total surface area is matched to the the observations, using Equation 5.13, to determine the effective aerosol number density, n_{aer} (cm^{-3}):

$$\frac{A_{aer}}{V_{atm}} = n_{aer} 4\pi r_{aer}^2 = \frac{A_o}{V_{atm}} = \int_0^\infty n_o(D)\pi D^2 \mathrm{d}D \tag{5.13}$$

where A_{aer} = modelled aerosol total surface area (μm^2), n_{aer} = modelled aerosol number density (cm^{-3}), r_{aer} = modelled aerosol radius (μm), V_{atm} = volume of atmosphere (cm^3) and A_o = observed aerosol total surface area (μm^2). For the log-normal distribution used to describe the mode 1 aerosols, Equation 5.13 can be rearranged to solve for n_{aer} as in Equation 5.14.

$$n_{aer} = \frac{N_T}{4r_{aer}^2\sqrt{2\pi}\ln\sigma_g}\int_0^\infty De^{(-1/2)(\ln(D/D_g)/\ln\sigma_g)^2}\mathrm{d}D = \frac{N_T D_g^2}{4r_{aer}^2}e^{2(\ln\sigma_g)^2} \tag{5.14}$$

For the Gaussian distribution used to describe the mode 2 aerosols, Equation 5.13 can be rearranged to solve for n_{aer} as in Equation 5.15.

$$n_{aer} = \frac{16.81}{\sqrt{2\pi}\sigma {r_m}^2}\int_0^\infty D^2 e^{\frac{-(D-D_m)^2}{2\sigma^2}}\mathrm{d}D = 6.75[{D_m}^2\sqrt{\frac{\pi}{2}} + \sigma^2\sqrt{\frac{\pi}{2}} + 2\sigma D_m] \tag{5.15}$$

The effective number densities, calculated in the course of this research and subsequently used for the mode 1 and 2 particles in the model are shown in Table 5.1. Previous values, adapted from Esposito et al. [1983] and Knollenberg and Hunten [1980, Figure 16], were subsequently discarded. Additional information on integration and model code are provided in the Appendix.

Altitude (km)	n_{aer} mode 1 (cm^{-3})	n_{aer} mode 2 (cm^{-3})
58	316	69
60	975	76
62	835	70
64	338	73
66	290	26
68	200	30
70	200	30
72	500	
74	500	
76	500	
78	500	
80	500	
82	500	
84	500	
86	500	
88	500	
90	500	

Table 5.1: Number densities for mode 1 and 2 aerosol particles

5.4 Reactive Uptake Coefficient

There may potentially be numerous heterogeneous mechanisms that may each function at different degrees of efficiency. To study heterogeneous chemistry in its entirety, it is

necessary to study all possible heterogeneous mechanisms; however, our aim is to develop a non-complex understanding of the significance of heterogeneous chemistry, for which it is sufficient to model one reaction - Reaction 5.6.

In the model, Reaction 5.6 had to be included as two separate reactions representative of the two aerosol modes. This was done so that aerosols could be modeled as closely (and accurately) to the observational data as possible (for details refer to Section 5.3).

$$CO + O + aer1 \rightarrow CO_2 + aer1 \tag{5.16}$$

$$CO + O + aer2 \rightarrow CO_2 + aer2 \tag{5.17}$$

A simple assessment of Reactions 5.16 and 5.17 reveals that their addition to the model provides an extra pathway for production of CO_2 (and simultaneous destruction of CO and O). If production of CO_2 via heterogeneous processes is much smaller than that by gas-phase processes, then heterogeneous chemistry is a small perturbation on the gas-phase chemistry that is already included in the Venus chemistry model [Pernice et al., 2004]. However, if production of CO_2 via heterogenous chemistry is comparable to or greater than that via gas-phase processes, then the modelled chemistry is expected to differ significantly from previous results. It is this deviation from the standard, gas-phase-only Venus atmosphere model that is of interest to this research.

Reactions 5.16 and 5.17 were incorporated into the photochemical model with assigned heterogeneous reaction rates, K, in terms of the reactive uptake coefficient [Jayne et al., 1996, Hu et al., 1995, Golden and Williams, 1994], as shown in Equation 5.18.

$$K = \frac{\gamma_{rxn} J_i A_{aer}}{V_{atm}} \approx \gamma_{rxn} n_i \sqrt{\frac{3kT}{m_i}} n_{aer} \pi r_{aer}^2 \tag{5.18}$$

where γ_{rxn} = the reactive uptake coefficient, J_i = flux of the rate-limiting gas species i onto the aerosols, A_{aer} = total surface area of the aerosols, V_{atm} = atmospheric volume containing the aerosols, n_i = concentration of the rate-limiting gas species i in the atmosphere, k = Boltzmann's constant, T = temperature, m_i = atomic/molecular weight of the rate-limiting gas species i, n_{aer} = effective number density of the aerosols, and r_{aer} = effective radius of the aerosols. In deriving Equation 5.18, it was assumed the heterogeneous reaction is not limited by diffusion of the rate-limiting gas through the atmosphere, the gas molecules are in local thermodynamic equilibrium for their translational motion, and the aerosols are uniform in size.

The rate of heterogeneous production of CO_2 (and loss of CO and O) is dictated by the value of γ_{rxn} (reactive uptake coefficient) chosen. Thus, to understand the potential role played by heterogeneous reactions in the Venusian atmosphere, it is imperative to know the value of γ_{rxn} (as evident from Equation 5.18) but there are no existing measurements

as to what γ_{rxn} might be. If we assume the production rate of CO_2 via heterogeneous processes is equal to that by gas-phase processes, then we may calculate the "minimum threshold γ_{rxn}", γ_t:

$$\gamma_{tj} = (\frac{m_{CO}}{3kT})^{1/2} \frac{R_{CO_2}}{\pi r_{aer}^2 n_{aer} n_{CO}} \tag{5.19}$$

where γ_{tj} = threshold γ_{rxn} at altitude j; m_{CO} = mass of CO; R_{CO_2} = rate of CO_2 production via gas-phase processes; n_{CO} = CO gas concentration.

Altitude (km)	γ_t
58	2×10^{-8}
60	6×10^{-8}
62	8×10^{-7}
64	4×10^{-5}
66	6×10^{-4}
68	1×10^{-3}
70	2×10^{-3}
72	1×10^{-3}
74	1×10^{-3}
76	2×10^{-3}
78	2×10^{-3}
80	3×10^{-3}
82	6×10^{-3}
84	7×10^{-3}
86	5×10^{-3}
88	3×10^{-3}
90	2×10^{-3}

Table 5.2: Threshold gamma values (γ_t) in the upper cloud and upper haze layer.

The range of γ_{tj} values thus calculated is shown in Table 5.2. Predictably, in accordance with the trend of aerosol number density, γ_t increases with altitude with maximum at 84 km at which altitude gasphase CO_2 production is maximum. From Table 5.2, it is evident that at lower altitudes, a small γ_{rxn} is sufficient to produce CO_2 at the requisite rate. Thus, $\gamma_{rxn} \geq \gamma_t$ at each altitude defines the range of γ_{rxn} that is of interest to the present study. So, we will examine the range $10^{-10} \leq \gamma_{rxn} \leq 10^{-4}$ in this study, disregarding any variations in altitude. Our assumption that γ_{rxn} is constant, irrespective of atmospheric conditions, is a simplification. In reality, γ_{rxn} is likely to be dependent on temperature, sulphuric acid concentration, availability of solar photons and other factors. Laboratory measurements and/ or observations will be needed to refine our simplified treatment of γ_{rxn}.

Chapter 6

Introduction to research project 2 - Nitrogen oxides chemistry

6.1 Nitrogen oxides chemistry - background and motivation

Oxides of nitrogen (NO, NO_2, HNO, HNO_2, HNO_3 - broadly referred to as NO_x) have long been suspected to play a chemical role in Venus' middle atmosphere. Observations of lightning in the cloud region [Taylor et al., 1979] provided motivation for inclusion of NO_x chemistry in early atmosphere modeling [Watson et al., 1979, Chameides et al., 1979]. However, claims of lightning occurrence have been dogged by controversy, in the form of observations to the contrary, and continue to be tested to this day by Venus Express [Russell et al., 2007]. If proven conclusively, the impact of lightning on Venus atmosphere photochemistry may be significant. Lightning, where it occurs, provides a unique environment for atmospheric chemistry. Build up of charges and subsequent discharge of ions along with significant amount of energy release with each stroke disrupts existent equilibrium in the local atmospheric region. The resultant conditions created by lightning process in the middle atmosphere have the potential to drive chemical reations that might otherwise not be possible. A detailed study of lightning process was not possible in this research, nor was it the intention. Focus of the research here was on the primary product of lightning - nitric oxide (NO) and the impact of inclusion of NO_x chemistry in the Venus middle atmosphere photochemistry.

Recent positive confirmation of NO mixing ratio ($\sim$ 5.5 $\pm$ 1.5 ppb near 60 km) [Krasnopolsky, 2006a] has added considerable strength to the plausibility of lightning. Krasnopolsky [2006a] used a simplified photochemical model (with only 4 NO_x reactions) to demonstrate that the presence of NO near the lower boundary of middle atmosphere may affect SO_2 and O_2 abundances.

Early studies of the impact on the major photochemical components in the Venus middle atmosphere (CO, O_2 and O) by NO_x chemistry, assuming Earth-like lightning, indicated significant perturbances in their relative abundances [Chameides et al., 1979].

The effect on cloud chemistry and SO_2 abundances, due to the generation of NO_x and related chemical species, was significant. Unidentified large particles observed by Pioneer Venus could be $NOHSO_4$, by-product of NO_x compounds reacting with cloud aerosols [Watson et al., 1979].

A comprehensive study of NO_x chemistry, against the backdrop of a thorough photochemical model was carried out by Yung and DeMore [1982]. In their Model B, they used less H_2 ($\sim \mu_{H_2} = 5 \times 10^{-7}$) than Model A and invoked NO_x chemistry to facilitate breakage of O-O bonds. With a scheme of 29 NO_x reactions, the important oxygen sinks in Model B were

$$CO + OH \rightarrow CO_2 + H \tag{6.1}$$

$$SO_2 + O + M \rightarrow SO_3 + M \tag{6.2}$$

Yung and DeMore [1982] used extant observations of lightning-like impulses to estimate $\mu_{NO} = 30$ ppb at the lower boundary of their atmosphere model, which was acknowledged as the upper limit. Other modeling work has set the NO mixing ratio value between 0.8 ppb and 40 ppb depending on the nature of NO sink in the model [Krasnopolsky, 1983].

Subsequent Venus photochemical modeling work has neglected NO_x chemistry with ClO_x radicals preferred and proven efficient in O-O bond breakage. Recent interpretation of observational work has suggested a more accurate derivation of NO abundance and flux ($\sim (6\pm2)\times 10^7$ cm^{-2}s^{-1}) values [Krasnopolsky, 2006a]. These calculations have presented a strong case for investigation of NO_x chemistry in the context of a complete and fully functional photochemical model and the study of its impact on overall photochemistry.

6.2 Nitrogen oxides chemistry - modeling

Primarily proposed as a model with intermediate H_2 abundances, as the high H_2 mixing ratio in Model A [Yung and DeMore, 1982] was challenged [McElroy et al., 1982], Model B [Yung and DeMore, 1982] contained ClO_x and NO_x chemistry to faciliate catalytic oxidation of CO to CO_2 [Yung and DeMore, 1982]. NO_x chemistry has been omitted from what has now become the standard photochemical model of Venus middle atmosphere [Mills, 1998, Pernice et al., 2004]. However, the positive confirmation of NO in the middle atmosphere [Krasnopolsky, 2006a] warrants re-introduction of NO_x chemistry in the standard model along with revisions of updated chemistry and new observations.

Introduction of new chemistry into the model necessitates simultaneous inclusion of new species that are generated as a result. There are multiple temperature-dependent reactions, but only those for each species whose temperature is best representative of

Venus middle atmosphere temperature are activated for final modeling calculations. The total number of new species introduced in the model is 12 [Sander et al., 2006]. The current model [Mills, 1998] derives the majority of chemical data from DeMore et al. [1997], with the latest compilation of laboratory measurements [Sander et al., 2006] used to update kinetic/ photolytic data where revisions to exisiting values were significant (greater than 10%). For detailed step-by-step information on addition of a new chemistry regime, with cross sectional and kinetic data, and justification of usage of specific input information the reader is referred to the Appendix.

The scheme of NO_x chemistry in Model B [Yung and DeMore, 1982] contained 29 reactions, as listed in Table 6.1. The aim of this project was to incorporate this set of 29 reactions, along with relevant kinetic and photochemical laboratory revisions that may be significant, into the standard photochemical model [Pernice et al., 2004] in combination with our model which includes heterogeneous chemistry (Section 5.1). Once included, NO_x chemistry would be activated by specifying a NO mixing ratio of 5.5 ppb at the lower boundary of middle atmosphere (which is the only addition to boundary conditions that are listed in Table 3.1). The lower boundary condition for all other new species was set to v = -2 $\times$ 10^{-2} and the fluxes for all new species were set to $\phi = 0$ at the upper boundary. In the 29 reactions used from Yung and DeMore [1982], 4 reactions are treated separately for M = CO_2 and N_2 and an additional reaction is included to simulate lightning.

No.	Reaction	Rate constant	Reference
1	$NO + h\nu \rightarrow N + O$	see Appendix	[Krasnopolsky, 2006a]
2	$NO_2 + h\nu \rightarrow NO + O$	see Appendix	[Sander et al., 2006]
3	$NO_3 + h\nu \rightarrow NO_2 + O$	see Appendix	[Sander et al., 2006]
4	$NO_3 + h\nu \rightarrow NO + O_2$	see Appendix	[Sander et al., 2006]
5	$HNO + h\nu \rightarrow H + NO$	$J = 10^{-3}$	[Yung and DeMore, 1982]
6	$HNO_2 + h\nu \rightarrow OH + NO$	see Appendix	[Sander et al., 2006]
7	$HNO_3 + h\nu \rightarrow OH + NO_2$	see Appendix	[Sander et al., 2006]
8	$N + O \rightarrow NO + h\nu$	$k = 1.8 \times 10^{-17}\ (300/T)^{0.5}$	[Dalgarno et al., 1992]
9	$N + O + CO_2 \rightarrow NO + CO_2$	$k = 1.9 \times 10^{-31}$	[Stewart et al., 1980]
10	$N + O_2 \rightarrow NO + O$	$k = 1.5 \times 10^{-11}\ e^{3600/T}$	[Sander et al., 2006]
11	$N + O_3 \rightarrow NO + O_2$	$k = 2 \times 10^{-16}$	[Sander et al., 2006]
12	$N + OH \rightarrow NO + H$	$k = 5.3 \times 10^{-11}$	[DeMore et al., 1997]
13	$N + NO \rightarrow N_2 + O$	$k = 2.1 \times 10^{-11}$	[Sander et al., 2006]
14	$NO + O + N_2 \rightarrow NO_2 + N_2$	$k = 9 \times 10^{-32}\ (T/300)^{-1.5}$	[Sander et al., 2006]
15	$NO + O + CO_2 \rightarrow NO_2 + CO_2$	$k = 2.3 \times 10^{-31}\ (T/300)^{-1.5}$	[Sander et al., 2006]
16	$NO + O_3 \rightarrow NO_2 + O_2$	$k = 3 \times 10^{-12}\ e^{-1500/T}$	[Sander et al., 2006]
17	$NO + H + CO_2 \rightarrow HNO + CO_2$	$k = 1.5 \times 10^{-32}\ e^{300/T}$	[Hampson and Garvin, 1978]
18	$NO + OH + N_2 \rightarrow HNO_2 + N_2$	$k = 7 \times 10^{-31}\ (T/300)^{-2.6}$	[Sander et al., 2006]
19	$NO + OH + CO_2 \rightarrow HNO_2 + CO_2$	$k = 2.3 \times 10^{-30}\ (T/300)^{-2.6}$	[Sander et al., 2006]
20	$NO + HO_2 \rightarrow NO_2 + OH$	$k = 3.5 \times 10^{-12}\ e^{250/T}$	[Sander et al., 2006]
21	$NO + ClO \rightarrow NO_2 + Cl$	$k = 6.4 \times 10^{-12}\ e^{290/T}$	[Sander et al., 2006]
22	$NO_2 + O \rightarrow NO + O_2$	$k = 5.1 \times 10^{-12}\ e^{210/T}$	[Sander et al., 2006]
23	$NO_2 + O + N_2 \rightarrow NO_3 + N_2$	$k = 2.5 \times 10^{-31}\ (T/300)^{-1.8}$	[Sander et al., 2006]
24	$NO_2 + O + CO_2 \rightarrow NO_3 + CO_2$	$k = 8.3 \times 10^{-31}\ (T/300)^{-1.8}$	[Sander et al., 2006]
25	$NO_2 + OH + N_2 \rightarrow HNO_3 + N_2$	$k = 1.8 \times 10^{-30}\ (T/300)^{-3}$	[Sander et al., 2006]
26	$NO_2 + OH + CO_2 \rightarrow HNO_3 + CO_2$	$k = 5.9 \times 10^{-30}\ (T/300)^{-3}$	[Sander et al., 2006]
27	$NO_2 + SO \rightarrow NO + SO_2$	$k = 1.4 \times 10^{-11}$	[Sander et al., 2006]
28	$HNO + O \rightarrow OH + NO$	$k = 10^{-13}$	[Yung and DeMore, 1982]
29	$HNO + H \rightarrow H_2 + NO$	$k = 10^{-13}$	[Hampson, 1980]
30	$HNO + Cl \rightarrow HCl + NO$	$k = 10^{-13}$	[Yung and DeMore, 1982]
31	$2HNO \rightarrow N_2O + H_2O$	$k = 4 \times 10^{-15}$	[Hampson and Garvin, 1978]
32	$HNO_2 + OH \rightarrow H_2O + NO_2$	$k = 6.6 \times 10^{-12}$	[Sander et al., 2006]
33	$HNO_3 + OH \rightarrow H_2O + NO_3$	$k = 2.4 \times 10^{-14}$	[Sander et al., 2006]
34	$N_2 + O \rightarrow NO + N$	see Appendix	*lightning*

Table 6.1: Table of NO_x reactions, reaction rate constants and references. Units for photodissociation rates are s^{-1}. Units for rate constants are cm^3s^{-1} for two-body (bimolecular) reactions and cm^6s^{-1} for three-body (termolecular) reactions. Values for reactions with CO_2 as third body (i.e, M) were calculated from existent values for N_2 as third body (and multiplying by 3.3) [Mills, 1998].

Chapter 7

Results and Discussion - Heterogeneous chemistry project

7.1 CO_2 production via heterogeneous chemistry

Before the discussion of results, it is necessary to understand what constitutes 'heterogeneous chemistry' in this study. Range of γ_{rxn} values of interest to this research vary between 2×10^{-8} to 10^{-3}, which are the 'threshold γ_{rxn}' values for altitudes 58 – 90 km (see Table 5.2). γ_{rxn} is regarded as the simplified determinant of the strength of heterogeneous involvement in the modeling process. Threshold γ_{rxn} values indicate what rate of heterogeneous chemistry is required at each altitude between 58 km and 90 km for heterogeneous pathways to match gas-phase reactions in the rate of CO_2 production.

γ_{rxn}	CO_2 produced via heter. processes
10^{-10}	2.1%
10^{-9}	5.8%
10^{-8}	9.3%
10^{-7}	11.9%
10^{-6}	16%
10^{-5}	29.9%
10^{-4}	51.1%

Table 7.1: Column total CO_2 production (%) by heterogeneous processes (Reactions 5.16 and 5.17).

To this effect, the percentage fractions of column total atmospheric CO_2 produced via heterogeneous (aerosol catalysis) processes are listed for selected γ_{rxn} values in Table 7.1. With increasing γ_{rxn} values, Venus middle atmosphere model changes behaviour from one that is dependent primarily on gasphase processes for CO_2 production, to one strongly influenced by heterogeneous processes. For $\gamma_{rxn} = 10^{-10}$, the fraction of total CO_2 produced by heterogeneous reactions is 2.1%, which may be regarded as a minor perturbation in overall chemisry and thus absorbed into the overall scheme of gas-phase reactions. For our

research purposes, we may consider $\gamma_{rxn} = 10^{-10}$ as a valid representation of gas-phase chemistry and the previous standard photochemical model [Pernice et al., 2004].

For $\gamma_{rxn} = 10^{-5}$, a third of total atmospheric CO_2 is produced heterogeneously and this is regarded as the first major shift in the nature of overall chemistry. With over 51% of CO_2 produced via heterogeneous processes, $\gamma_{rxn} = 10^{-4}$ represents a heterogeneous chemistry dominant atmosphere model. Table 7.2 compares percentage production of CO_2 by heterogeneous processes - Reaction 5.16 & Reaction 5.17 and gas-phase reactions (grouped together) for $\gamma_{rxn} = 10^{-4}$. The cloud and haze layers where aerosols are present extend up to 90 km, above which heterogeneous chemistry is not modeled.

Altitude (km)	Reaction 5.16	Reaction 5.17	Gasphase reactions
58	22	78	0
60	45	55	0
62	43	57	0
64	22	78	0
66	41	59	0
68	29	70	0
70	29	70	0
72	98	0	2
74	96	0	4
76	94	0	5
78	90	0	9
80	82	0	17
82	68	0	30
84	46	0	53
86	45	0	51
88	51	0	46
90	63	0	36

Table 7.2: Percentage CO_2 production by Reactions 5.16 and 5.17, and gasphase reactions for $\gamma_{rxn} = 10^{-4}$ model

For $\gamma_{rxn} = 10^{-4}$, heterogeneous mechanisms account from 45 % to 100 % of all CO_2 produced in the atmosphere between 58 and 90 km altitudes.

Though gasphase processes assume greater significance in the gasphase dominated atmospheres ($\gamma_{rxn} \leq 10^{-6}$), an investigation of altitude dependent production of CO_2 reveals that, heterogeneous processes account for all CO_2 produced below 64km across all γ_{rxn} cases including gasphase dominant atmospheres. This is a clear indication that heterogeneous processes may make a significant impact on the chemistry at lower altitudes of the middle atmosphere, where the concentration of aerosol particles is high and a greater fraction are large size particles (discussed in Section 5.3).

In this research, "gasphase atmospheres" will refer to atmosphere models where gas-phase chemistry is the predominant nature of the atmosphere model, which for our purposes is accurately represented be $\gamma_{rxn} = 10^{-10}$. "Heterogeneous atmospheres" will refer

to atmosphere models in which heterogeneous chemistry is comparable to or dominant over gasphase chemistry ie $\gamma_{rxn} \geq 10^{-5}$.

From a laboratory viewpoint, $\gamma_{rxn} = 10^{-5}$ is considered a plausible value for heterogeneous reactions in the Venus middle atmosphere *[L.Phillips, personal communication via F.Mills, 2005]*. With this laboratory assessment as a basis, plausible values for γ_{rxn} could be in the range of 10^{-6} to 10^{-4}. Calculations of total column CO_2 produced in Table 7.1 has indicated that nearly 30% or more CO_2 is produced by heterogeneous processes for $\gamma_{rxn} > 10^{-5}$. For purposes of this research analysis, we regard 30% as the threshold and will consider $\gamma_{rxn} = 10^{-4}$ and $\gamma_{rxn} = 10^{-5}$ as atmosphere models where heterogeneous chemistry is likely to play a dominant and influential role in overall chemistry. γ_{rxn} values greater than $\gamma_{rxn} = 10^{-4}$ are not considered in this research.

7.2 Key species' abundances - Baseline chemistry

The most direct impact from the inclusion of Reactions 5.16 and 5.17 is expected to be on CO, O and CO_2. However, in the Venus atmosphere model, altitude dependent abundances of CO_2 are invariant for all cases studied in this research. The overall total column abundance of CO_2 is unchanged regardless of other variations in model. Consequently, any changes in CO and O abundances assume importance and require investigation. Given the chemical relationships between all species in the model, a 'trickle-down-effect' is expected from changes to any one species. However, for purposes of structure and comprehension, it is necessary that we limit our discussions to some of the key atmospheric constituent-species. The analytical aspects on this research are in understanding changes, if any, to the atmospheric chemistry arising from the addition of heterogeneous CO_2 production pathways. Their addition to the baseline atmosphere model [Mills, 1998, Pernice et al., 2004] is investigated in this section.

7.3 CO abundances

Carbon monoxide consumption is expected to increase from the addition of heterogeneous reactions to the model. A comparison of total column abundances (concentrations integrated for a column of air above 58 km) of CO for $\gamma_{rxn} = 10^{-10}$ and $\gamma_{rxn} = 10^{-4}$ reveals a reduction of 72 % in the latter. Figure 7.1 facilitates a more detailed comparison of CO abundances, at all altitudes (58 to 112 km), for varying values of γ_{rxn}.

Abundances for all model atmospheres are indistinguishable above 95 km with all chemistry dictated by gasphase processes above this altitude. There exists little dissimilarity ($\sim$ factor of 2 near lower boundary) between the different gasphase cases ($\gamma_{rxn} =$

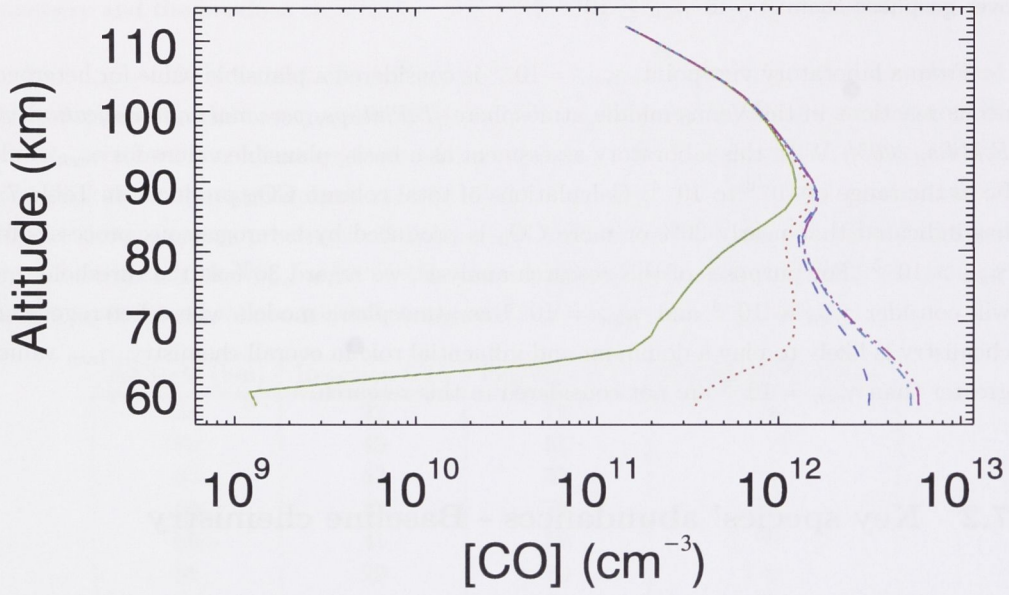

Figure 7.1: CO concentration profiles for different γ_{rxn} values. Green solid line and red dotted line represent heterogeneous dominant cases $\gamma_{rxn} = 10^{-4}$ and $\gamma_{rxn} = 10^{-5}$ respectively. Dark blue (small dashes), light blue (dash and single dot) and magenta lines (dash and triple dots) represent gasphase dominant cases of $\gamma_{rxn} = 10^{-6}$, $\gamma_{rxn} = 10^{-7}$ and $\gamma_{rxn} = 10^{-10}$ respectively. Horizontal axis is plotted logarithmically.

10^{-6}, $\gamma_{rxn} = 10^{-7}$ and $\gamma_{rxn} = 10^{-10}$) at all altitudes. At altitudes below 70 km, the difference in CO concentration (Figure 7.1) and production and loss rates (Table 7.3) can be as large as four orders of magnitude between gasphase and heterogeneous atmospheres.

	Gasphase	Heterogeneous
Production (60)	1.1×10^8	8.3×10^3
Loss (60)	1.1×10^8	1.2×10^4
Conc (60)	5.9×10^{12}	4.9×10^8

Table 7.3: CO concentration (cm^{-3}), production and loss rates ($cm^{-3}s^{-1}$) at 60 km for gasphase ($\gamma_{rxn} = 10^{-10}$) and heterogeneous ($\gamma_{rxn} = 10^{-4}$) scenarios

$$ClCO + CO_2 \rightarrow Cl + CO + CO_2 \tag{7.1}$$

$$ClCO + N_2 \rightarrow Cl + CO + N_2 \tag{7.2}$$

$$OCS + h\nu \rightarrow CO + S \tag{7.3}$$

The primary sources for CO are Reactions 1.25, 7.1, 7.2 and 7.3. Photodissociation of CO_2 peaks near 85 km and has become smaller than the other sources at 60 km (Table 7.4). In the $\gamma_{rxn} = 10^{-4}$ model, production of CO via Reactions 1.25, 7.1 and 7.2 has become small enough so that Reaction 7.3 is a significant source for CO. Similarly, the reduced concentration of CO in the $\gamma_{rxn} = 10^{-4}$ model changes the primary loss pathway from Reaction 7.4 to Reaction 5.17.

Primary CO loss processes at 60 km are:

$$Cl + CO + M \rightarrow ClCO + M \tag{7.4}$$

$$CO + O + aer1 \rightarrow CO_2 + aer1 \tag{5.16}$$

$$CO + O + aer2 \rightarrow CO_2 + aer2 \tag{5.17}$$

Reaction	Gasphase	Heterogeneous
Reaction 7.1	99%	58%
Reaction 7.2	1%	1%
Reaction 7.3	0%	41%

Table 7.4: Reactions' percentage contribution to CO production at 60 km in gasphase ($\gamma_{rxn} = 10^{-10}$) and heterogeneous ($\gamma_{rxn} = 10^{-4}$) scenarios

OCS, a major source of CO at very low altitudes (around 58 km) in the heterogeneous atmosphere model, is loosely constrained. The lower boundary condition of the OCS mixing ratio is set from modeled interpretation of observation of that species [Bézard et al., 1990]. Other observations have proved inconclusive in detection of OCS, leaving significant uncertainty of the appropriate value to be used in our model. Abundance of OCS in our model is sensitive to the lower boundary condition and eddy mixing values, given that its vertical mixing time and photochemical lifetimes are comparable. As a result, of which the deviation in CO abundance around 60 km was not completely resolved during the course of this research, but has raised the need for investigation into observational confirmation of OCS and a better understanding of eddy diffusion rates. An atmospheric model with higher OCS mixing ratio at the lower boundary is considered and resulting model predictions are discussed in Section 7.10.

Reaction	Gasphase	Heterogeneous
Reaction 7.4	99%	35%
Reaction 5.16	0%	33%
Reaction 5.17	0%	27%

Table 7.5: Reactions' percentage contribution to CO loss at 60 km in gasphase ($\gamma_{rxn} = 10^{-10}$) and heterogeneous ($\gamma_{rxn} = 10^{-4}$) scenarios

7.4 Oxygen abundances

Atomic oxygen is directly affected by inclusion of heterogeneous chemistry. Atomic oxygen is highly reactive and contributes to the formation of many species like SO_2, O_2, CO_2, $O_2(a^1\Delta_g)$, ClO and O_3. Important loss reactions for O are:

$$SO + O + CO_2 \rightarrow SO_2 + CO_2 \tag{7.5}$$

$$ClSO_2 + O \rightarrow ClO + SO_2 \tag{7.6}$$

$$CO + O + aer1 \rightarrow CO_2 + aer1 \tag{5.16}$$

$$ClO + O \rightarrow O_2 + Cl \tag{7.7}$$

$$2O + CO_2 \rightarrow O_2(a^1\Delta_g) + CO_2 \tag{7.8}$$

$$2O + CO_2 \rightarrow O_2 + CO_2 \tag{7.9}$$

$$O + O_2 + CO_2 \rightarrow O_3 + CO_2 \tag{7.10}$$

All the above reactions are important loss pathways for both heterogeneous and gasphase atmospheres. There is no major difference in the total atomic oxygen concentration for both cases. Given its reactive nature and scarcity in the atmosphere, there have been no measurements of atomic oxygen. However, previous attempts to measure O_2 (discussed in Section 4.1) have raised interesting questions about our understanding of the extant atmospheric chemistry. Analysis of O_2 behaviour in response to addition of

heterogeneous chemistry is expected to help us better understand the vital processes that link oxygen with other species.

One of the key unresolved issues from three decades of photochemical modeling of Venus middle atmosphere is the total column abundance of molecular oxygen. Yung and DeMore [1982, Model A] assumed nominal rate values for crucial reactions unconfirmed by laboratory studies and proposed total column abundance of 3.05×10^{19} cm^{-2}. Yung and DeMore [1982, Model C], contains chlorine catalytic schemes, estimated 1.5×10^{19} cm^{-2} and was consistent with the then extant observational measurements of [Traub and Carleton, 1973]. A more stringent upper limit for oxygen column abundance, established from observations by Trauger and Lunine [1983], is 1.5×10^{18} cm^{-2}. Interpretation of this measurement has since been revised to 8×10^{17} cm^{-2} [Krasnopolsky, 2006b]. Inclusion of $ClCO_3$ (peroxy chloroformyl radical) and adjustments to the modeled nominal reaction rates alters the O_2 column abundance to 2.13×10^{18} cm^{-2} [Pernice et al., 2004], which is still larger than the observational upper limits [Trauger and Lunine, 1983, Krasnopolsky, 2006b].

Inclusion of heterogeneous chemistry is expected to affect the O_2 abundance, via trickle-down-effect from atomic oxygen, but the magnitude of the impact is difficult to predict. This difficulty arises largely from the complex network of reactions that link all species and the "iterative feedback" mechanism (discussed in Section 3.2.3) that exists in the model. Our immediate task is to study the O_2 total column abundances to assess variations, if any, and analyse the influence of heterogeneous chemistry. Table 7.6 lists the spectrum of chemistries studied in this research and respective oxygen column abundances.

Number	γ value	oxygen column abundance (molecules cm^{-2})
1	10^{-10}	2.1×10^{18}
2	10^{-9}	2.1×10^{18}
3	10^{-8}	2.1×10^{18}
4	10^{-7}	2.1×10^{18}
5	10^{-6}	2.1×10^{18}
6	10^{-5}	1.9×10^{18}
7	10^{-4}	1.2×10^{18}
Obs.	Trauger and Lunine [1983]	$<1.5 \times 10^{18}$
Obs.	Krasnopolsky [2006b]	$<0.8 \times 10^{18}$

Table 7.6: Oxygen column abundances for different γ_{rxn} values

Studies of profiles and abundances of trace species is an important means to test the performance and accuracy of an atmosphere model. Of all the models studied here and elsewhere [Yung and DeMore, 1982, Mills, 1998, Pernice et al., 2004], $\gamma_{rxn} = 10^{-4}$ (heterogeneous) atmosphere is the first to satisfy Trauger and Lunine [1983] observational

upper limit for O_2 column abundance. These results indicate that heterogeneous chemistry may be able to explain the observed low O_2 column abundances on Venus. Table 7.6 compares O_2 column abundances and any subtle changes in concentration over different altitudes are effectively hidden. In order to understand any inherent variations and model behaviour, it is necessary to study the O_2 concentration profiled over all altitudes and different γ_{rxn} values, as shown in Figure 7.2.

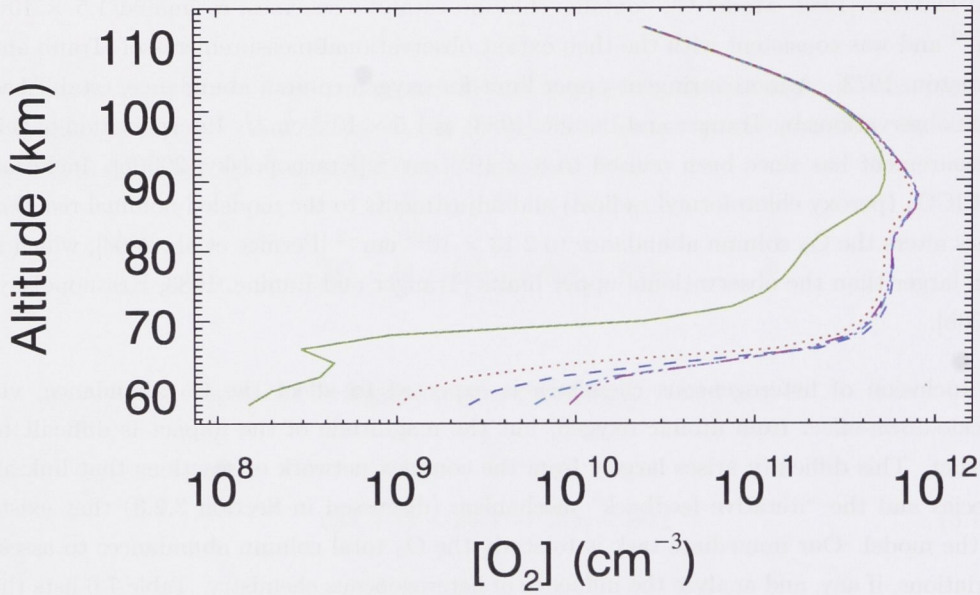

Figure 7.2: Oxygen concentration profiles for different γ_{rxn} values. Green solid line and red dotted line represent heterogeneous dominant cases $\gamma_{rxn} = 10^{-4}$ and $\gamma_{rxn} = 10^{-5}$, respectively. Dark blue (small dashes), light blue (dash and single dot) and magenta lines (dash and triple dots) represent gasphase dominant cases of $\gamma_{rxn} = 10^{-6}$, $\gamma_{rxn} = 10^{-7}$ and $\gamma_{rxn} = 10^{-10}$, respectively. Horizontal axis is plotted logarithmically.

Modeled O_2 abundances for heterogeneous atmospheres are smaller compared to the gasphase atmosphere, below 90 km. The greatest disparity in O_2 concentration, seen around 67 km altitude, is more than three orders of magnitude between $\gamma_{rxn} = 10^{-4}$ and $\gamma_{rxn} = 10^{-10}$ models. Differences between the other heterogeneous ($\gamma_{rxn} = 10^{-5}$) and gasphase atmosphere models are as large as an order of magnitude near the lower boundary. Such large differences in abundances reflect dissimilarities in consumption and production of the species between different atmosphere models.

Figures 7.3 and 7.4 compare rates of the five dominant O_2 loss reactions for heterogeneous ($\gamma_{rxn} = 10^{-4}$) and gasphase ($\gamma_{rxn} = 10^{-10}$) atmospheres. Compared to the gasphase atmosphere, reaction rates for O_2 production and loss, are about two orders of magnitude

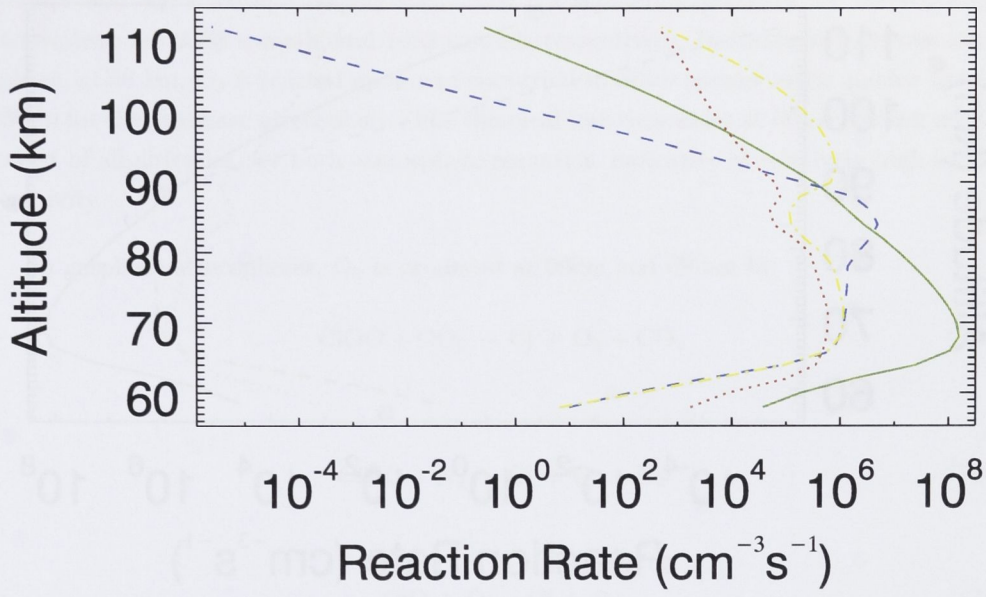

Figure 7.3: Primary O_2 loss reaction rates for $\gamma_{rxn} = 10^{-4}$ atmosphere. Yellow (dash and single dot) line represents Reaction 7.10, dark-blue dashes represents peroxy chloroformyl formation ($ClCO + O_2 + M \rightarrow ClCO_3 + M$) and red dots represent Reaction 7.13. Green (solid) line represents combined Reactions 7.11 and 7.12. The units for reaction rates are mol cm^{-3} s^{-1}.

smaller in the heterogeneous atmosphere model. However, the impact of heterogeneous chemistry on production and consumption of O_2 is best understood from the changes to individual reactions. To study these changes, it is necessary to choose a specific altitude and compare the reactions that are prominent producers and destroyers of O_2. The region with greatest difference in O_2 abundances between gasphase atmosphere and heterogeneous chemistries is around 66km – 68 km. At this region, dissimilarities between the different atmosphere models are expected to be most pronounced. Key O_2 destruction reactions at 66 km and 68 km, for the gasphase case, are

$$Cl + O_2 + CO_2 \rightarrow ClOO + CO_2 \tag{7.11}$$

$$Cl + O_2 + N_2 \rightarrow ClOO + N_2 \tag{7.12}$$

$$O + O_2 + CO_2 \rightarrow O_3 + CO_2 \tag{7.10}$$

In the heterogeneous case ($\gamma_{rxn} = 10^{-4}$), Reactions 7.11 and 7.13 are primary destruc-

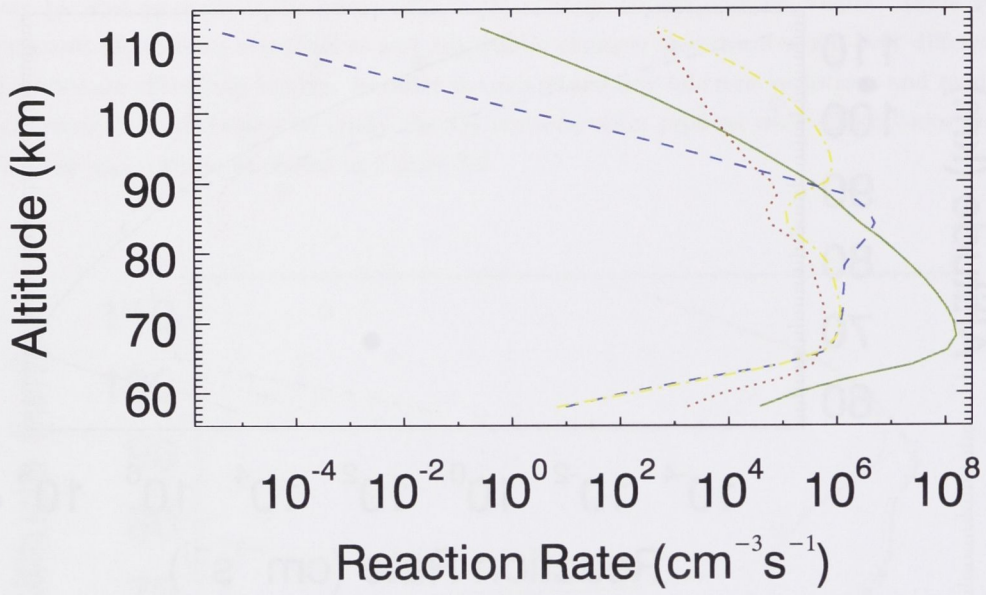

Figure 7.4: Primary O_2 loss reaction rates for $\gamma_{rxn} = 10^{-10}$ atmosphere. Yellow (dash and single dot) line represents Reaction 7.10, dark-blue dashes represents peroxy chloroformyl formation ($ClCO + O_2 + M \rightarrow ClCO_3 + M$) and red dots represent Reaction 7.13. Green (solid) line represents combined Reactions 7.11 and 7.12. The units for reaction rates are mol cm^{-3} s^{-1}.

tion pathways for O_2.

$$S + O_2 \rightarrow SO + O \tag{7.13}$$

The contribution of the reactions to destruction of O_2 for gasphase and heterogeneous atmospheres, at 66km and 68 km, is outlined in Table 7.7.

Reaction	Altitude = 66km		Altitude = 68km	
	Gasphase	Heterogeneous	Gasphase	Heterogeneous
Reaction 7.11	97%	69%	97%	81 %
Reaction 7.12	1%	0%	1%	0%
Reaction 7.10	1%	0%	1%	0%
Reaction 7.13	0%	30%	0%	17%

Table 7.7: Reactions' percentage contribution to O_2 loss at 66km and 68 km in gasphase ($\gamma_{rxn} = 10^{-10}$) and heterogeneous ($\gamma_{rxn} = 10^{-4}$) scenarios

Reaction 7.13 plays a more important role in O_2 loss in the heterogeneous atmosphere model (Table 7.7). Inclusion of heteroegneous chemistry reduces the rate of Reaction 7.11, by two orders of magnitude, at 66km and 68 km (Figures 7.3 and 7.4) due to the factor of 100 decrease in O_2.

The calculated lifetimes of O_2 at 66 and 68 km, in the gasphase atmosphere, are 1976 seconds and 2322 seconds respectively. The corresponding lifetimes for heterogeneous atmosphere are 2363 seconds and 1683 seconds respectively. In the heterogeneous atmosphere, at 68 km, O_2 is reacted upon and converted to other species much quicker than at 66 km for the gasphase atmosphere. The chemical loss timescales at 66 and 68 km are the lowest of all altitudes, for both atmosphere scenarios, indicative of relatively high level of reactivity.

In gasphase atmospheres, O_2 is produced at 66km and 68 km by

$$ClOO + CO_2 \rightarrow Cl + O_2 + CO_2 \tag{7.14}$$

$$ClOO + N_2 \rightarrow Cl + O_2 + N_2 \tag{7.15}$$

$$ClO + O \rightarrow Cl + O_2 \tag{7.7}$$

In the heterogeneous atmosphere Reaction 7.16 in addition to the above mentioned reactions, assume importance in the production of O_2.

$$SO_2 + h\nu \rightarrow S + O_2 \tag{7.16}$$

Table 7.8 lists the dominant reactions that are involved in O_2 production and their percentage contribution.

Reaction	Altitude = 66km		Altitude = 68km	
	Gasphase	Heterogeneous	Gasphase	Heterogeneous
Reaction 7.14	97%	73 %	97%	88%
Reaction 7.15	1%	1%	1%	1%
Reaction 7.7	1%	4%	1%	6%
Reaction 7.16	0%	21%	0%	3%

Table 7.8: Reactions percentage contribution to O_2 production at 66km and 68 km in gasphase ($\gamma_{rxn} = 10^{-10}$) and heterogeneous ($\gamma_{rxn} = 10^{-4}$) scenarios

Tables 7.7 and 7.8 list percentage (%) contribution of the four most important O_2 destruction and production reactions at 66km and 68 km. These relations are calculated directly from the rates of the individual reactions. The biggest differences in O_2 production, between the two scenarios compared, are seen in the relative importance of Reactions 7.14 and 7.16. In the heterogeneous case, Reaction 7.16, an unimportant pathway in the gasphase scenario, becomes a significant producer of O_2 at the expense of Reaction 7.14

(see Table 7.8). The decline in rate of Reaction 7.14 is likely due to decrease in the abundance of ClOO which is formed from the destruction of O_2. Increase in abundance of SO_2 (and the increase in contribution of Reaction 7.16 towards O_2 production) will be explained in Section 7.5. Overall, there is an additional sink for O_2 (Reaction 7.13) in the heterogeneous atmosphere and efficiency of primary O_2 sink (Reaction 7.11) is reduced.

The investigation of O_2 chemistry has thus revealed interesting potential links with chlorine and sulphur compounds - trace species suspected to have significant bearing on the overall atmosphere.

7.5 Sulphur compounds' abundances

7.5.1 SO_2 abundances

SO_2 abundance shows variations between the heterogeneous and gasphase scenarios, but are not as striking as that for O_2 or CO. Figure 7.5 profiles SO_2 concentrations of different γ_{rxn} values as a factor of SO_2 concentrations of $\gamma_{rxn} = 10^{-10}$ on a linear scale.

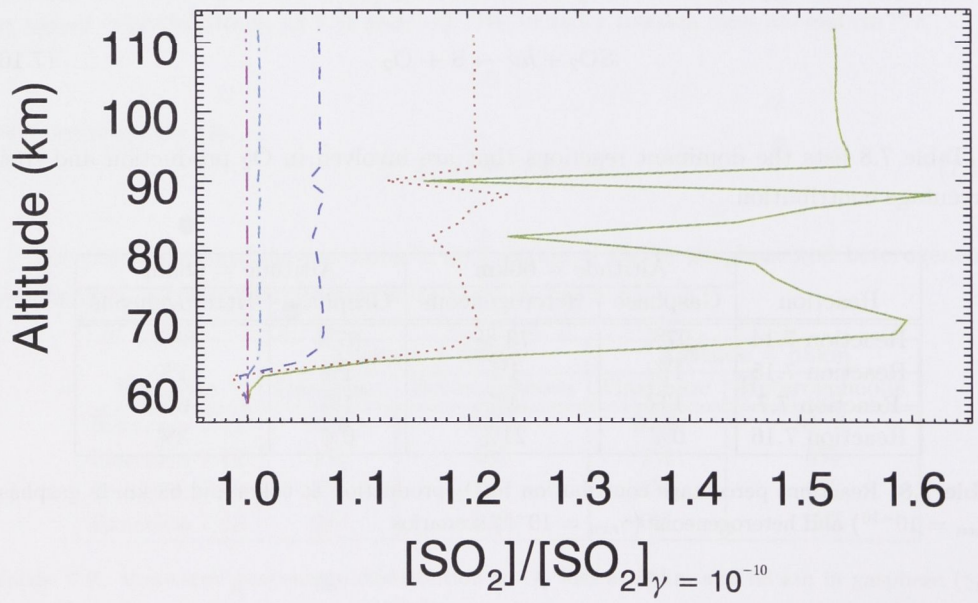

Figure 7.5: SO_2 concentration ratio profile for different γ_{rxn} values. Green solid line and red dotted line represent heterogeneous dominant cases $\gamma_{rxn} = 10^{-4}$ and $\gamma_{rxn} = 10^{-5}$, respectively. Dark blue (small dashes), light blue (dash and single dot) and magenta lines (dash and triple dots) represent gasphase dominant cases of $\gamma_{rxn} = 10^{-6}$, $\gamma_{rxn} = 10^{-7}$ and $\gamma_{rxn} = 10^{-10}$, respectively. Note: Gamma = γ_{rxn}.

SO_2 concentration shows remarkable behaviour with $\gamma_{rxn} = 10^{-4}$ atmosphere reaching maxima at three altitudes (68km, 88km and 92km). Overall, the heterogeneous atmospheres ($\gamma_{rxn} = 10^{-4}$ and $\gamma_{rxn} = 10^{-5}$) show distinct differences in SO_2 concentrations (> 20 %), from the gasphase atmosphere at all altitudes. At certain altitudes the SO_2 concentration varies by 60% or more and the currently chosen region of interest, at 66km and 68 km, is one of them. Key reactions that contribute to production and loss of SO_2 for the gasphase and heterogeneous ($\gamma_{rxn} = 10^{-4}$) atmospheres are:

$$ClSO_2 + Cl \rightarrow SO_2 + Cl_2 \tag{7.17}$$

$$SO + O + CO_2 \rightarrow SO_2 + CO_2 \tag{7.5}$$

$$SO + ClO \rightarrow SO_2 + Cl \tag{7.18}$$

$$Cl + SO_2 + M \rightarrow ClSO_2 + M \tag{7.19}$$

$$SO_2 + h\nu \rightarrow SO + O \tag{7.20}$$

Reaction	Altitude = 66km		Altitude = 68km	
	Gasphase	Heterogeneous	Gasphase	Heterogeneous
Reaction 7.17	78%	73%	65%	59%
Reaction 7.5	15%	23%	24%	36%
Reaction 7.18	4%	1%	8%	3%

Table 7.9: Reactions' percentage contribution to SO_2 production at 66km and 68 km in gasphase ($\gamma_{rxn} = 10^{-10}$) and heterogeneous ($\gamma_{rxn} = 10^{-4}$) scenarios

Reaction	Altitude = 66km		Altitude = 68km	
	Gasphase	Heterogeneous	Gasphase	Heterogeneous
Reaction 7.19	80%	74%	67%	60%
Reaction 7.20	19%	25%	33%	39%

Table 7.10: Reactions' percentage contribution to SO_2 loss at 66km and 68 km in gasphase ($\gamma_{rxn} = 10^{-10}$) and heterogeneous ($\gamma_{rxn} = 10^{-4}$) scenarios

The production of SO_2 is affected by the inclusion of heterogeneous chemistry which is apparent with Reaction 7.5 becoming faster by a factor of 2 and growing in importance as an SO_2 producing pathway. This is accompanied by three-fold decrease in rate of Reaction 7.18 at 66km and a corresponding decrease of its contribution to SO_2 production (Table 7.9). The decline in rate of Reaction 7.18 is possibly influenced by the decrease in ClO

abundances (discussed in Section 7.6.1). Increased SO_2 abundances (increase of $\sim 60\%$) in heterogeneous atmospheres cause an increase in the rate of Reaction 7.20. Decline in the proportional contribution of Reaction 7.19 is possibly due to decline in Cl concenrtations (discussed in Section 7.6.3).

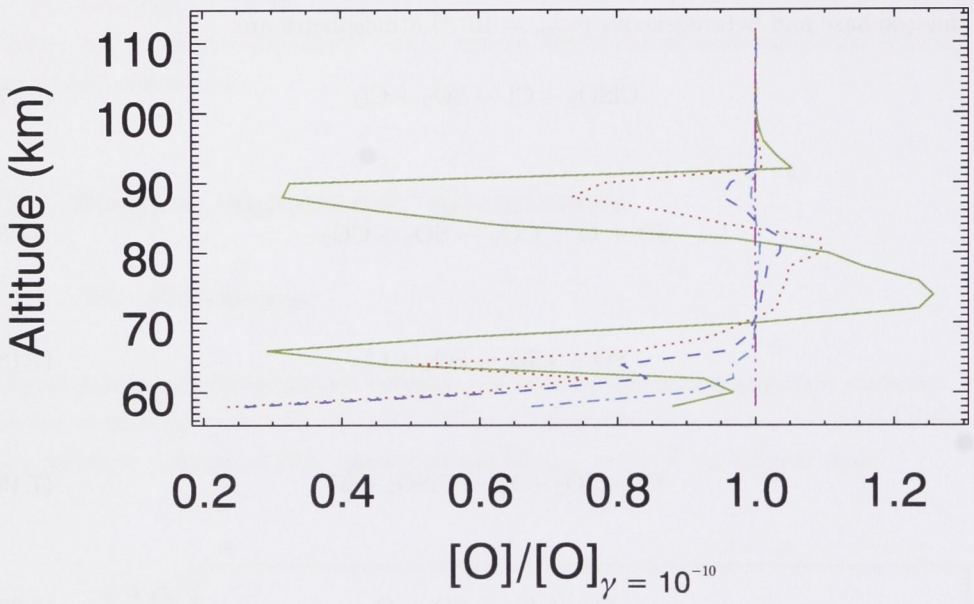

Figure 7.6: O concentration ratio profile for different γ_{rxn} values. Green solid line and red dotted line represent heterogeneous dominant cases $\gamma_{rxn} = 10^{-4}$ and $\gamma_{rxn} = 10^{-5}$, respectively. Dark blue (small dashes), light blue (dash and single dot) and magenta lines (dash and triple dots) represent gasphase dominant cases of $\gamma_{rxn} = 10^{-6}$, $\gamma_{rxn} = 10^{-7}$ and $\gamma_{rxn} = 10^{-10}$, respectively. Note: Gamma = γ_{rxn}.

Variations in SO_2 abundances for $\gamma_{rxn} = 10^{-4}$ atmosphere (Figure 7.5) show a strong correlation with corresponding O abundances seen in Figure 7.6, especially at altitudes of 68km and 88km. Inclusion of heterogeneous chemistry induces atomic oxygen to play a more important role in the production of SO_2 (Reaction 7.5), thus establishing an inverse relationship betwen the two species. The cause of this relationship is unknown and is not examined in this study. To do so, further investigation at higher altitudes is necessary, but this work is concentrated only around 66km and 68 km.

7.5.2 SO abundances

At 66km and 68km, the important production and loss reactions for SO are

$$SO_2 + h\nu \rightarrow SO + O \tag{7.20}$$

$$(SO)_2 + M \rightarrow 2SO + M \tag{7.21}$$

$$OSCl + Cl \rightarrow SO + Cl_2 \tag{7.22}$$

$$S + O_2 \rightarrow SO + O \tag{7.13}$$

$$SO + O + CO_2 \rightarrow SO_2 + CO_2 \tag{7.5}$$

$$2SO + M \rightarrow (SO)_2 + M \tag{7.23}$$

$$SO + ClO \rightarrow SO_2 + Cl \tag{7.18}$$

$$SO + Cl + M \rightarrow OSCl + M \tag{7.24}$$

$$SO + h\nu \rightarrow S + O \tag{7.25}$$

The reactions' contribution to SO production and loss, at 66km and 68km, are given in Tables 7.11 and 7.12.

Reaction	Altitude = 66km		Altitude = 68km	
	Gasphase	Heterogeneous	Gasphase	Heterogeneous
Reaction 7.20	41%	3%	60%	19%
Reaction 7.21	53%	95%	32%	75%
Reaction 7.22	3%	0%	5%	3%
Reaction 7.13	0%	0%	3%	0%

Table 7.11: Reactions' percentage contribution to SO production at 66km and 68km in gasphase ($\gamma_{rxn} = 10^{-10}$) and heterogeneous ($\gamma_{rxn} = 10^{-4}$) scenarios

Despite the decline in percentage contributions, Reactions 7.20 and 7.5 proceed at higher rates upon inclusion of heterogeneous chemistry. However, Reactions 7.21 and 7.23 increase by a factor of 10 and 20 and become most important production and loss reactions of SO for $\gamma_{rxn} = 10^{-4}$ atmosphere, respectively. This creates rapid conversion between SO and $(SO)_2$ takes place in the heterogeneous atmosphere. As a result, abundance of SO

Reaction	Altitude = 66km		Altitude = 68km	
	Gasphase	Heterogeneous	Gasphase	Heterogeneous
Reaction 7.5	31%	3%	44%	18%
Reaction 7.23	53%	95%	32%	75%
Reaction 7.18	9%	0%	14%	0%
Reaction 7.24	4%	0%	5%	1%
Reaction 7.25	0%	0%	4%	3%

Table 7.12: Reactions' percentage contribution to SO loss at 66km and 68km in gasphase ($\gamma_{rxn} = 10^{-10}$) and heterogeneous ($\gamma_{rxn} = 10^{-4}$) scenarios

in heterogeneous atmosphere is linked strongly to $(SO)_2$, and not SO_2 or atomic oxygen as in a gasphase atmosphere.

7.6 Chlorine compounds' abundances

In a gasphase atmosphere (represented in this research by $\gamma_{rxn} = 10^{-10}$), chlorine compounds such as chloroformyl (ClCO) and peroxy chloroformyl ($ClCO_3$), through a series of catalytic schemes, aid re-formation of CO_2. With heterogeneous chemistry providing an additional pathway for production of CO_2, the roles previously played by key chlorine radicals are susceptible to change. The aim of this investigation is to find whether and how the chlorine chemistry in the model may have been changed by the introduction of heterogeneous chemistry.

7.6.1 ClO abundances

ClO is significant to the production of SO_2 and loss of SO in the gasphase atmosphere at 66km and 68km (see Sections 7.5.1 and 7.5.2). Upon inclusion of heterogeneous chemistry, ClO no longer plays as significant a role in either of these functions and Reaction 7.18 decreases in importance. With an increase in the abundance of modeled SO for the heterogeneous atmosphere, a possible explanation is a strong decline in ClO abundance at this altitude. ClO abundances decrease by more than an order of magnitude at 66km and by a factor of 7 at 68km in the $\gamma_{rxn} = 10^{-4}$ atmosphere.

The dominant ClO production reactions at 66km and 68km are

$$Cl + O + M \rightarrow ClO + M \tag{7.26}$$

$$Cl + O_3 \rightarrow ClO + O_2 \tag{7.27}$$

$$ClSO_2 + O \rightarrow ClO + SO_2 \tag{7.28}$$

$$ClCO_3 + Cl \rightarrow ClO + Cl + CO_2 \tag{7.29}$$

$$ClO_3 + M \rightarrow ClO + O_2 + M \tag{7.30}$$

The percentage contribution to the production of ClO at 66km and 68km by the above reactions, for gasphase ($\gamma_{rxn} = 10^{-10}$) and heterogeneous ($\gamma_{rxn} = 10^{-4}$) atmospheres, are shown in Table 7.13

Reaction	Altitude = 66km		Altitude = 68km	
	Gasphase	Heterogeneous	Gasphase	Heterogeneous
Reaction 7.26	25%	23%	31%	46%
Reaction 7.27	12%	0%	22%	0%
Reaction 7.28	39%	74%	15%	49%
Reaction 7.29	19%	0%	13%	0%
Reaction 7.30	5%	0%	8%	0%

Table 7.13: Reactions' percentage contribution to ClO production at 66km and 68km in gasphase ($\gamma_{rxn} = 10^{-10}$) and heterogeneous ($\gamma_{rxn} = 10^{-4}$) scenarios

In the heterogeneous atmosphere, Reaction 7.28 becomes the most important ClO production reaction. As a result, ClO is dependent on $ClSO_2$, along with Cl and O (Reaction 7.26). There is no apparent change in reactions' contribution to production and loss of $ClSO_2$ from the addition of heterogeneous chemistry. The abundance of $ClSO_2$ increases by factors of ~4 and ~2 at 66km and 68km, respectively, while abundances of Cl and $ClCO_3$ decrease and account for the preference of Reaction 7.28 as leading ClO producer.

The destruction reactions and reactions' contribution (in percentage) are shown below

$$SO + ClO \rightarrow SO_2 + Cl \tag{7.18}$$

$$ClO + O \rightarrow Cl + O_2 \tag{7.7}$$

$$ClO + h\nu \rightarrow Cl + O \tag{7.31}$$

$$ClO + O_2 + M \rightarrow ClO_3 + M \tag{7.32}$$

Reaction	Altitude = 66km		Altitude = 68km	
	Gasphase	Heterogeneous	Gasphase	Heterogeneous
Reaction 7.18	72%	97%	55%	88%
Reaction 7.7	15%	1%	27%	7%
Reaction 7.31	5%	1%	8%	4%
Reaction 7.32	5%	0%	8%	0%

Table 7.14: Reactions' percentage contribution to ClO loss at 66km and 68km in gasphase ($\gamma_{rxn} = 10^{-10}$) and heterogeneous ($\gamma_{rxn} = 10^{-4}$) scenarios

Despite significant reduction in rate, Reaction 7.18 remains the pre-eminent loss mechanism for ClO. Reactions 7.7, 7.31 and 7.32 contribute less in the heterogeneous atmosphere. This is quite possibly due to decreases in the abundances of ClO, O and O_2 around 66km – 68km in the heterogeneous atmosphere (see Figures 7.2 and 7.6).

7.6.2 $ClCO_3$ abundances

Albeit drastic decrease in modeled ClCO abundance at 68 km, no apparent change is noted in the reactions' percentage contribution to the production and loss upon addition of heterogenous chemistry. Reactions 7.4 and 7.1 produce and destroy ClCO and have some of the highest reaction rates in the atmosphere model. As a result, ClCO production and loss reactions are least affected by changes to other species (Cl and CO).

$ClCO_3$ is only produced via Reaction 2.8. The loss reactions are listed below and their percentage contributions listed in Table 7.15.

$$ClCO_3 + Cl \rightarrow ClO + Cl + CO_2 \tag{7.29}$$

$$ClCO_3 + SO \rightarrow Cl + CO_2 + SO_2 \tag{7.33}$$

$$ClCO_3 + h\nu \rightarrow ClO + CO_2 \tag{7.34}$$

The drop in rates of Reactions 7.29, 7.33 and 7.34 are between three and five orders of magnitude, roughly, due to heterogeneous chemistry. The addition of heterogeneous chemistry has a dampening effect on these reactions, forcing them to progress at a much slower rate. Reaction 7.33 becomes relatively more important as a loss than Reaction 7.29.

Reaction	Gasphase	Heterogeneous
Reaction 7.29	85%	40%
Reaction 7.33	9%	56%
Reaction 7.34	3%	2%

Table 7.15: Reactions' percentage contribution to $ClCO_3$ loss at 68 km in gasphase ($\gamma_{rxn} = 10^{-10}$) and heterogeneous ($\gamma_{rxn} = 10^{-4}$) scenarios

7.6.3 Cl abundances

The decrease in the significance of Reaction 7.29 is due to declining Cl abundance at 68 km, upon addition of heterogeneous chemistry. Production and loss rates for Cl decrease by one to two orders of magnitude in the heterogeneous atmosphere. Major production and loss reactions for Cl are :

$$ClCO + CO_2 \rightarrow Cl + CO + CO_2 \tag{7.1}$$

$$Cl_2 + h\nu \rightarrow 2Cl \tag{7.35}$$

$$S + Cl_2 \rightarrow SCl + Cl \tag{7.36}$$

$$ClOO + CO_2 \rightarrow Cl + O_2 + CO_2 \tag{7.14}$$

$$Cl + CO + CO_2 \rightarrow ClCO + CO_2 \tag{7.4}$$

$$Cl + SO_2 + M \rightarrow ClSO_2 + M \tag{7.19}$$

$$ClSO_2 + Cl \rightarrow SO_2 + Cl_2 \tag{7.17}$$

$$2Cl + CO_2 \rightarrow Cl_2 + CO_2 \tag{7.37}$$

$$Cl + O_2 + CO_2 \rightarrow ClOO + CO_2 \tag{7.11}$$

Reaction	Gasphase	Heterogeneous
Reaction 7.1	74%	15%
Reaction 7.35	14%	66%
Reaction 7.36	0%	8%
Reaction 7.14	10%	0%

Table 7.16: Reactions' percentage contribution to Cl production at 68 km in gasphase ($\gamma_{rxn} = 10^{-10}$) and heterogeneous ($\gamma_{rxn} = 10^{-4}$) scenarios

Reaction	Gasphase	Heterogeneous
Reaction 7.4	74%	15%
Reaction 7.19	0%	18%
Reaction 7.17	0%	17%
Reaction 7.37	11%	42%
Reaction 7.11	10%	0%

Table 7.17: Reactions' percentage contribution to Cl loss at 68 km in gasphase ($\gamma_{rxn} = 10^{-10}$) and heterogeneous ($\gamma_{rxn} = 10^{-4}$) scenarios

The percentage contribution by the above reactions to the production and loss of Cl, for gasphase and heterogeneous atmosphere cases are given in Tables 7.16 and 7.17.

Cl is closely linked to molecular chlorine (Cl_2) in the chemical scheme via Reaction 7.35. In addition, Cl_2 production reactions involve Cl participation extensively and major loss reactions of Cl_2 return Cl back to the atmosphere, thus making these two species inter-dependent and their abundances inter-linked. As a result, Cl_2 abundances decrease like Cl and are not discussed in detail here.

7.7 Chlorosulphane abundances

In the presence of very little oxygen, chlorosulphane compounds (S_mCl_n) are likely to form and influence surrounding chemistry, according to a recent study [Mills and Allen, 2007]. The upsurge in abundances of sulphur-compounds, combined with low O_2 concentration at 68 km, seen in heterogeneous atmosphere, raise interesting possibilities for chlorosulphanes and nature of their interactions with other species. $ClSO_2$ species does not undergo changes to its production and loss pathways' contribution and its impact been discussed in conjunction with ClO abundances (Section 7.6.1). Changes to SCl are studied.

Major SCl production reactions, at 68 km, are

$$S + Cl_2 \rightarrow SCl + Cl \tag{7.36}$$

$$SCl_2 + h\nu \rightarrow SCl + Cl \tag{7.38}$$

The contributions of Reactions 7.36 and 7.38 to SCl production differ by less than 2 %, upon addition of heterogeneous chemistry. The major loss reactions for SCl, at 68 km, are

$$O + SCl \rightarrow SO + Cl \tag{7.39}$$

$$SCl + h\nu \rightarrow S + Cl \tag{7.40}$$

$$Cl + SCl + M \rightarrow SCl_2 + M \tag{7.41}$$

$$2SCl \rightarrow S_2Cl + Cl \tag{7.42}$$

Reaction	Gasphase	Heterogeneous
Reaction 7.39	53%	17%
Reaction 7.40	28%	43%
Reaction 7.41	17%	17%
Reaction 7.42	0%	16%

Table 7.18: Reactions' percentage contribution to SCl loss at 68 km in gasphase ($\gamma_{rxn} = 10^{-10}$) and heterogeneous ($\gamma_{rxn} = 10^{-4}$) scenarios

SCl loss and production reactions increase in their rates by at least two orders of magnitude. Unlike production reactions, there is a significant change in relative contribution to the loss of SCl, with photolysis (Reaction 7.40) the most significant loss pathway and indicative of rise in SCl abundance at 68 km in the heterogeneous atmosphere. Reaction 7.39 does not experience as much of an increase in its rate, limited by decrease in O abundance at 68 km. Mills and Allen [2007] propose formation of chlorosulphanes in conditions that are deficient in oxygen and abundant in chlorine compounds. This research has showed that small abundances of oxygen alone may be able to produce increased quantities of SCl.

7.8 Summary of species' abundances

The changes in the relative contribution of various, major reactions to production and loss of key species have been investigated. Venus middle atmosphere chemistry is governed by numerous chemical schemes and species. The set of species chosen is complete by no stretch of imagination, but presents a selection of those that are relevant to the CO_2 chemistry. This study focusses on CO_2 chemistry and associated chemical schemes. CO_2, being the most abundant and dominant species is connected intricately with all other constituent-species and chemical schemes. Chlorine and sulphur compounds' chemical schemes have

been identified as that of most importance to the functioning of CO_2 chemistry and overall atmospheric stability. Abundances of chlorine and sulphur compounds are good indicators of any definitive changes to the atmosphere model. Table 7.19 compares concentration of species for gasphase and heterogeneous atmosphere models at 68 km.

With introduction of heterogeneous pathway to re-form CO_2 in the middle atmosphere model, direct changes are expected to CO and O. Changes to modeled abundances of other species (Table 7.19) are strongly suggestive of "trickle-down" effect. Degree of impact on chlorine and sulphur compounds vary in accordance with 'closeness' of a species to changes to the model. The 'closeness' is parametrized by the series of reactions (kinetics) that connect different species. For convenience, species, other than CO, O and O_2, investigated in this research project may be divided in to sulphur, chlorine and chlorosulphane compounds. At 68 km, all sulphur and chlorosulphane compounds increase in abundance; and chlorine compounds decrease.

Species	Gasphase (cm^{-3})	Heterogeneous (cm^{-3})
CO_2	1.5×10^{18}	1.5×10^{18}
CO	3.1×10^{12}	1.1×10^{11}
O	7.4×10^{8}	1.6×10^{8}
O_2	3.6×10^{11}	5.0×10^{8}
SO_2	9.0×10^{10}	2.0×10^{11}
SO	2.3×10^{9}	2.0×10^{10}
S	6.6×10^{5}	1.4×10^{8}
ClO	3.7×10^{7}	8.9×10^{5}
ClCO	2.6×10^{6}	6.4×10^{4}
$ClCO_3$	3.7×10^{6}	9.0×10^{1}
Cl	2.1×10^{10}	1.4×10^{10}
Cl_2	2.3×10^{10}	1.3×10^{12}
SCl	9.1×10^{5}	1.6×10^{8}
$ClSO_2$	9.5×10^{7}	2.1×10^{8}

Table 7.19: Species' concentration at 68 km for gasphase ($\gamma_{rxn} = 10^{-10}$) and heterogeneous ($\gamma_{rxn} = 10^{-4}$) scenarios

The overall effect of heterogeneous chemistry on species' total column abundances is shown in Table 7.20. Column abundances of sulphur and chlorosulphanes increase with addition of heterogenous chemistry and column abundances of chlorine compounds decrease. These results have established that changes to species' abundances are not restricted to any particular altitude. Over the height of the middle atmosphere, abundances of chlorine, sulphur and chlorosulphane compounds are indicative of certain shift in chemistry. Aim of this study was to assess impact of heterogeneous chemistry on individual species and overall chemical schemes. Categorical changes in abundances of groups of species have been uncovered. Confirmation of the nature and degree of these changes will require further investigation into relationships between species whose abundances have displayed alterations.

Species	Gasphase (cm^{-2})	Heterogeneous (cm^{-2})
CO_2	4.9×10^{24}	4.9×10^{24}
CO	1.0×10^{19}	2.6×10^{18}
O	2.2×10^{17}	2.2×10^{17}
O_2	2.1×10^{18}	1.1×10^{18}
SO_2	2.3×10^{18}	2.5×10^{18}
SO	8.0×10^{15}	1.8×10^{16}
S	2.1×10^{12}	5.1×10^{13}
ClO	1.0×10^{14}	4.4×10^{13}
ClCO	3.2×10^{13}	2.0×10^{13}
$ClCO_3$	6.8×10^{13}	3.1×10^{13}
Cl	3.2×10^{16}	2.3×10^{16}
Cl_2	5.6×10^{16}	3.2×10^{16}
SCl	2.2×10^{13}	1.0×10^{14}
$ClSO_2$	6.3×10^{15}	6.6×10^{15}

Table 7.20: Species' column abundances for gasphase ($\gamma_{rxn} = 10^{-10}$) and heterogeneous ($\gamma_{rxn} = 10^{-4}$) scenarios

7.9 Changes to overall chemistry

Changes to species' abundances and reaction rates at 66 and 68 km altitude have been documented (Section 7.3 - 7.7). The impact of heterogeneous chemistry's inclusion to the model is manifested from changes to individual species' concentrations. Collectively, individual changes cause a paradigm shift to the overall chemical regimea and Table 7.20 indicates as much. Modeled species are in constant state of chemical activity and are converted from one to another. Processes of conversion depend on chemical (eg. rate kinetics, concentrations) and physical (eg. pressure, temperature, transport) factors. Relations between species are pre-determined by chemical reactions present in the model. Figures 7.7 and 7.8 profile loss processes which convert one species to another. Direction of arrow-head indicates reaction that contributes to 40 % or more to the conversion (ie loss process for the former) of one species to another at 66 and 68 km. 40 % is set as threshold for consideration of significant loss. Sulphur, chlorine and chlorosulphane compounds are assessed for interactions within their group and with each other.

In gasphase atmosphere (Figure 7.7), with the exceptions of ClO conversion to SO_2 (via Reaction 7.18) and SCl to Cl (Reaction 7.39), there are no significant inter-group interactions between the sulphur and chlorine family species. All other species, in the gasphase atmosphere, are converted to species within their group. This is evident from SO loss to form SO_2 (Reaction 7.18), and $ClCO_3$ conversion to ClO (Reaction 7.29).

Within the heterogeneous atmosphere (Figure 7.8), by contrast, there are evident interactions between species that belong to the chlorine and sulphur families. This is apparent from loss of S to Cl (via Reaction 7.36) and $ClCO_3$ to SO_2 (via Reaction 7.33)

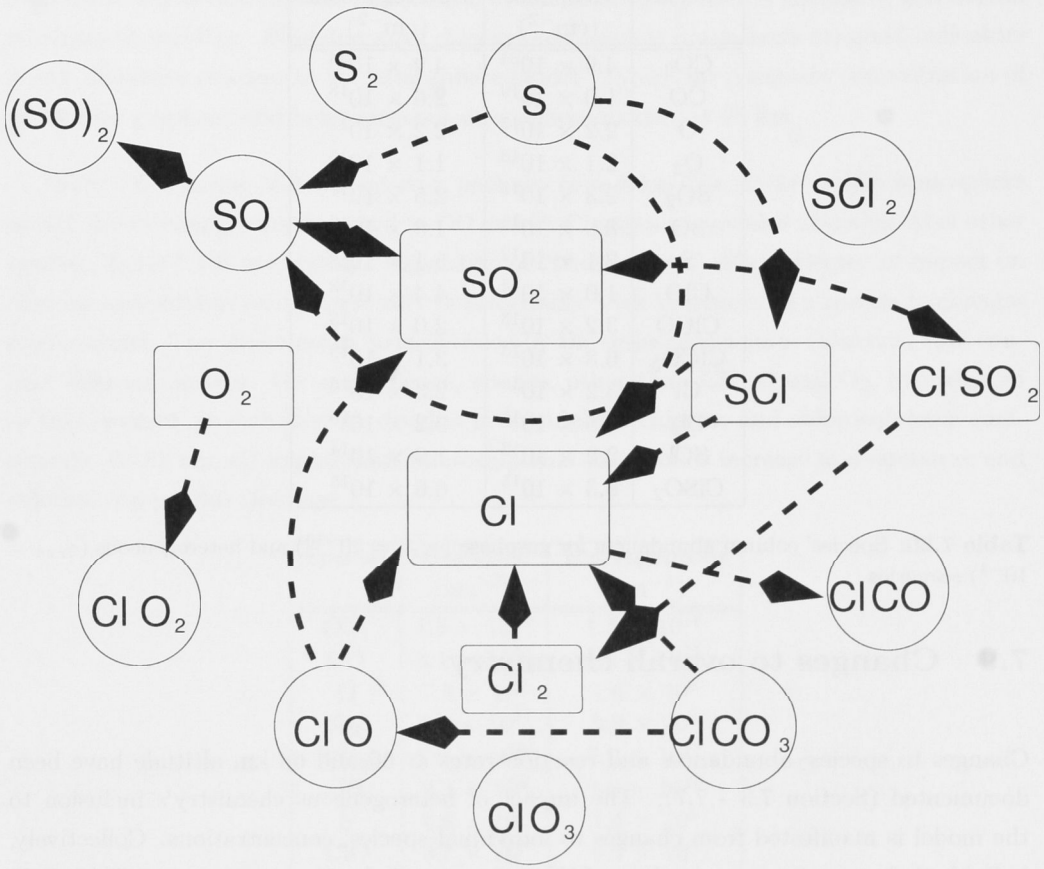

Figure 7.7: Key species' major loss reactions in gasphase atmosphere

which remain important (> 40 %) upon inclusion of heterogeneous chemistry.

Some interactions, that were previously less important (ie < 40 % contribution to loss of species) have increased in significance. These include reactions that convert S to SCl (Reaction 7.36), Cl to Cl_2 (Reaction 7.37), SO to $(SO)_2$ (Reaction 7.23) and O_2 to SO (Reaction 7.13). On the other hand, some reactions have become less important in our consideration upon introduction of heterogeneous chemistry. These are: Loss of SO to SO_2 (Reaction 7.5), S to SO (Reaction 7.13), Cl to ClCO (Reaction 7.4) and $ClCO_3$ to ClO (Reaction 7.29). Reactions that convert to Cl from ClO (Reaction 7.18) and Cl_2 (Reaction 7.35) suffer no change in their roles as major loss processes. This is the same for SO_2 and $ClSO_2$ both of which get converted to each other (via Reactions 7.19 and 7.17). Interestingly, $ClCO_3$ and SCl are both converted to Cl in both atmosphere models, but through different reactions. In the gasphase atmosphere, $ClCO_3$ reacts with Cl (via Reaction 7.29) and SCl with O (Reaction 7.39). In the dearth of O and Cl in heterogeneous atmosphere, $ClCO_3$ reacts with SO (Reaction 7.33) and SCl photolyses (Reaction

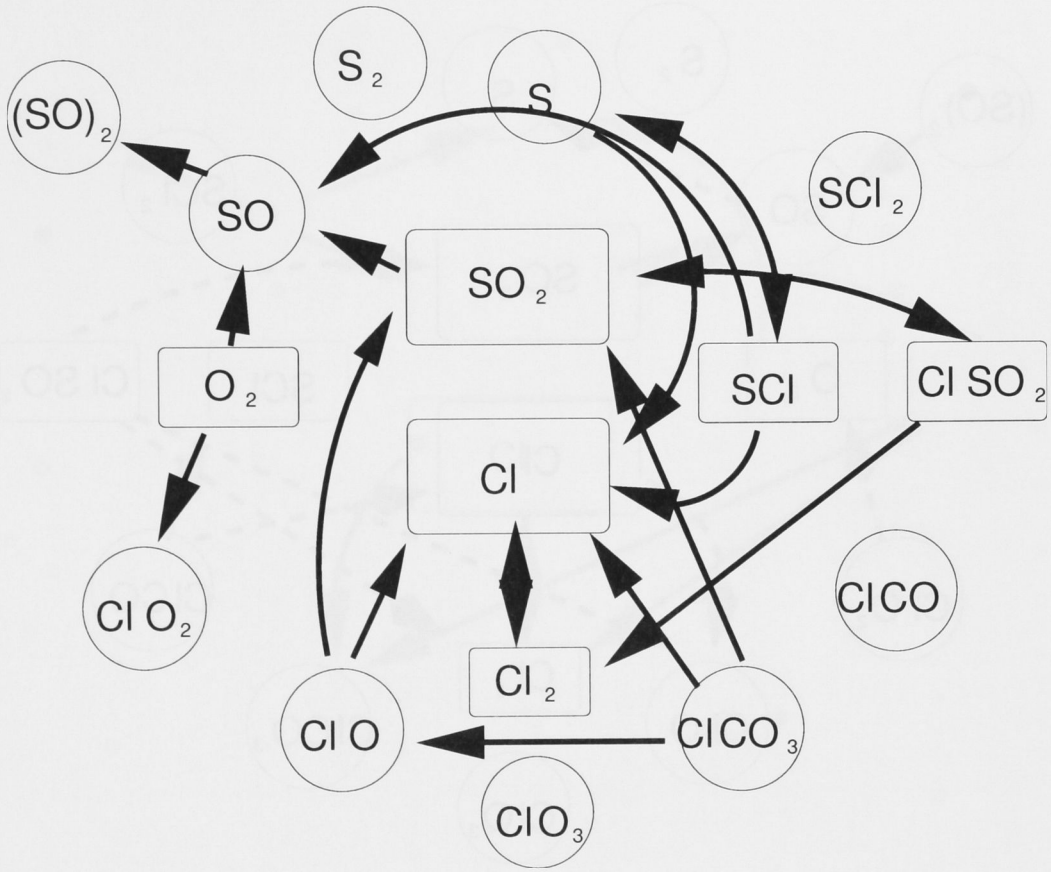

Figure 7.8: Key species' major loss reactions in heterogeneous atmosphere

7.40) to Cl. Analysis of major loss reactions has revealed a phenomena of inter-group (chlorine and sulphur species) interactions that assume significance with the introduction of heterogeneous chemistry. The most relevant change brought upon by heterogeneous chemistry is that of competition for consumption of CO and O. With introduction of heterogeneous processes (Reactions 5.16 and 5.17), chlorine species are starved of CO and O, and are thus unable to react at the same rate as before (in gasphase atmosphere). With O_2, there is a new loss mechanism to SO (Reaction 7.13), which predictably increases the abundance of SO. Greater abundance of SO augurs well for inter-group reactions such as that with $ClCO_3$.

A similar chart for production reactions of chlorine and sulphur species, at 68 km, for gasphase and heterogeneous atmospheres are shown in Figures 7.9 and 7.10. As before, species included are not a complete list but chosen from relevance to key sulphur and chlorine compounds and reactions included contribute to at least 40 % of species' production.

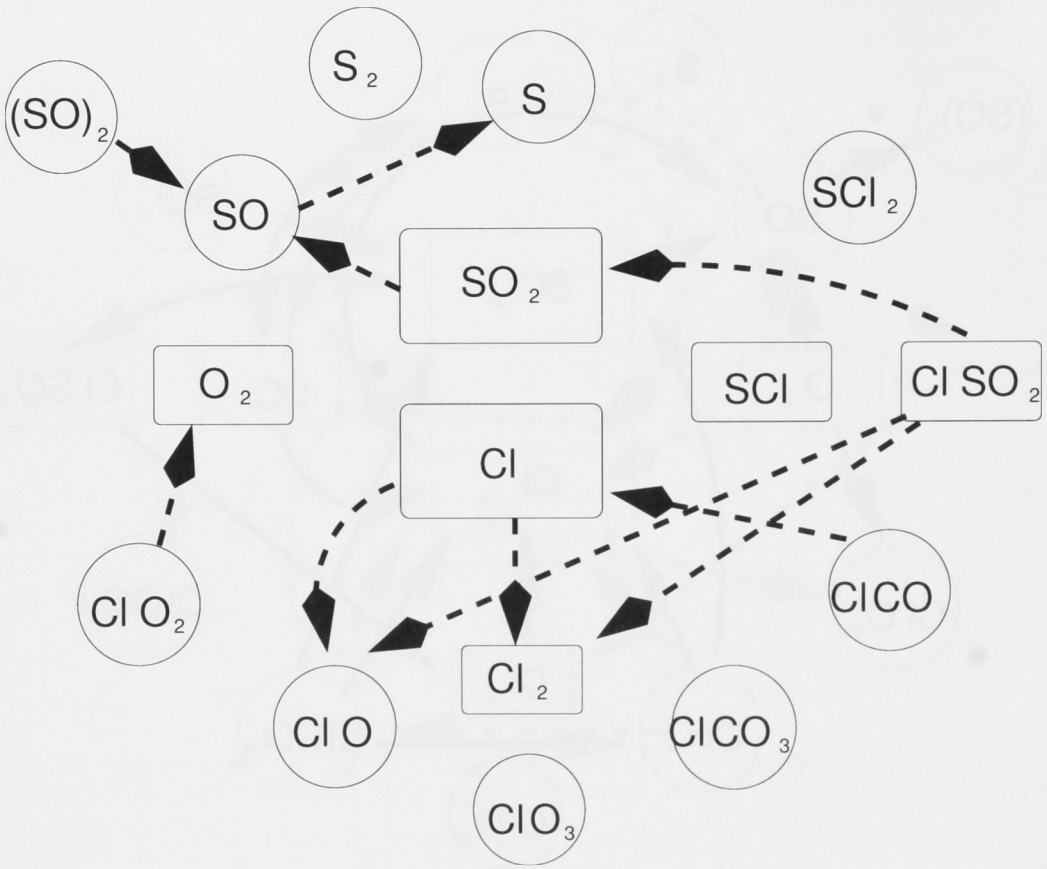

Figure 7.9: Key species' major production reactions in gasphase atmosphere

In the gasphase atmosphere (Figure 7.9), major production reactions are within the chlorine and sulphur groups. The only producer of O_2 is ClO_2. In the heterogeneous atmosphere (Figure 7.10), the crucial difference is the production of ClO (via Reaction 7.28) and Cl_2 (Reaction 7.17), along with photolysis of Cl_2 to Cl (Reaction 7.35) and SCl to S (Reaction 7.40).

7.10 Alternative chemistries - Comparison of heterogeneous cases

All results reported thus far have used the gasphase chemistry model from Pernice et al. [2004], which is based on the $1-\sigma$ model (Mills [1998]). Hereon, this model will be termed "baseline" model in subsequent discussion. While the adjustments to key rate constants and thermal stability of molecules that were made in the Pernice et al. [2004] model are

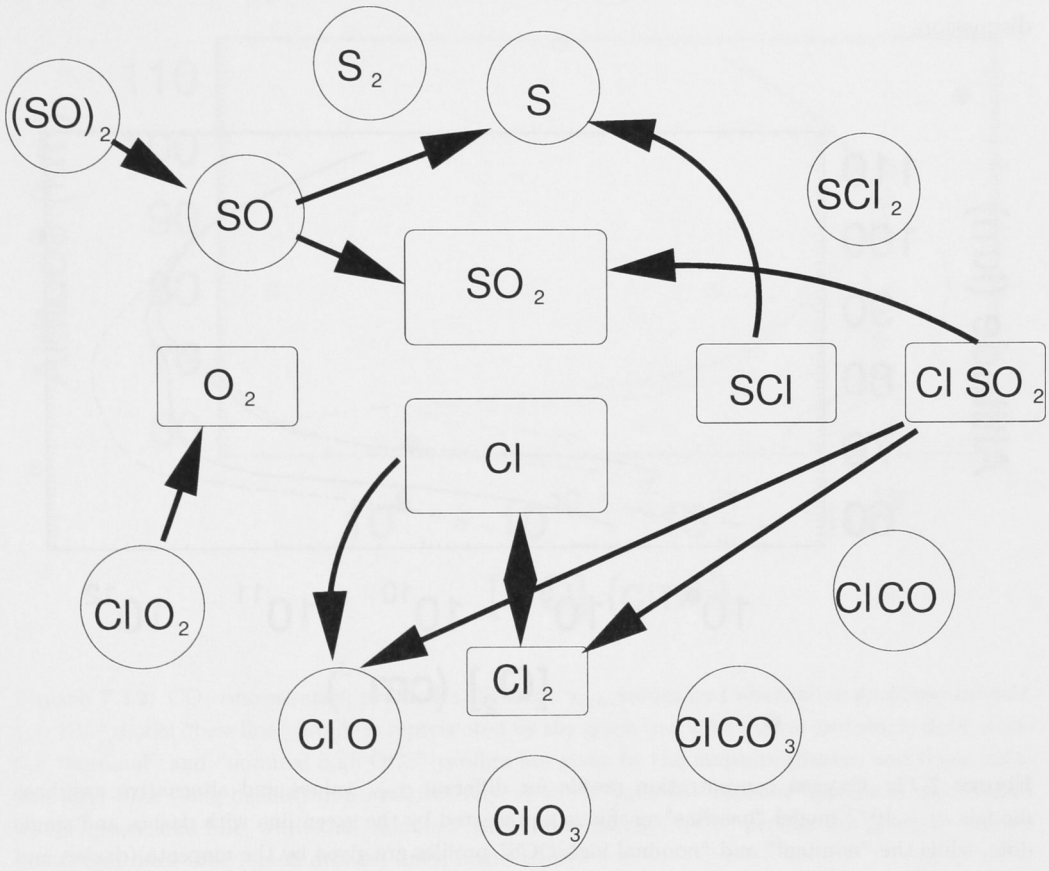

Figure 7.10: Key species' major production reactions in heterogeneous atmosphere

theoretically plausible, they have not been verified in laboratory experiments. Consequently, it is worthwhile to examine the influence of heterogeneous chemistry on a model in which the thermal stability of ClCO is set at its nominal laboratory value (detailed changes to the model are profiled in the Appendix). This model will be termed the "nominal" model in subsequent discussion. The lower boundary conditions for the model are based on observations, so there are uncertainties associated with each. The OCS mixing ratio at 58 km in our "baseline" model is 10^{-9}. However, the original interpretation of Earth-based spectra [Bézard et al., 1990] gave what may be considered an upper limit on the OCS mixing ratio above $\sim$ 65 km of 10^{-8} (*B. Bezard, personal communication, 1998*). Two factors suggest trying a larger OCS mixing ratio as our lower boundary condition. First, the modelled CO abundances below $\sim$ 85 km appear to be significantly smaller than millimeter-wavelength observations suggest [Clancy and Muhleman, 1991]. Second, the only infrared observation of CO in the cloud layers [Connes et al., 1968, Young, 1972] suggests CO may be more abundant in the upper cloud than would be implied by extrapolation downward of the millimeter-wave observations. Calculations using an OCS mixing

ratio of 10^{-8} for the lower boundary condition are denoted as "high OCS" in subsequent discussion.

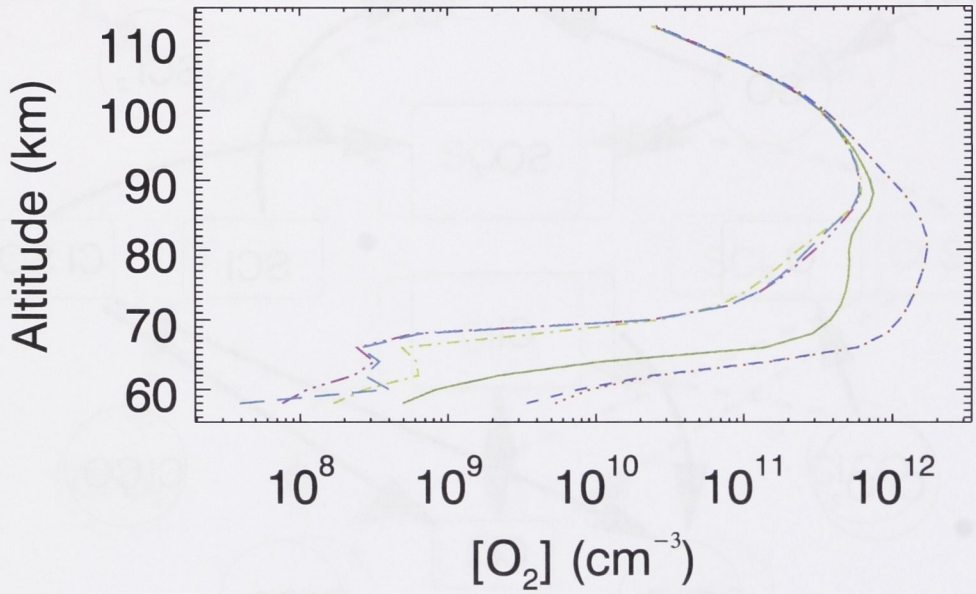

Figure 7.11: Oxygen concentration profile for different γ_{rxn} values and alternative gasphase models. $\gamma = 10^{-4}$ model "baseline" profile is represented by the green line with dashes and single dots, while the "nominal" and "nominal high OCS" profiles are given by the magenta (dashes and triple dots) and light-blue (long dashes) lines, respectively. $\gamma = 10^{-5}$ model "baseline" profile is represented by the green solid line, while the "nominal" and "nominal high OCS" profiles are given by the red (dots) and dark-blue (small dashes) lines, respectively.

Figures 7.11 and 7.12 compare the O_2 and CO profiles for six calculations: $\gamma = 10^{-4}$ and $\gamma = 10^{-5}$ for each of the "baseline," "nominal," and "nominal high OCS" models. For $\gamma = 10^{-5}$, the "nominal" and "nominal high OCS" model results are almost identical for both O_2 and CO. The "baseline" model for $\gamma = 10^{-5}$, however, gives significantly smaller O_2 and CO. For $\gamma = 10^{-4}$, all three models give similar O_2 profiles. The CO profiles for the "baseline" and "nominal" model with $\gamma = 10^{-4}$ are also similar to each other, but the calculated CO concentration for the "nominal high OCS" model is up to a factor of 10 larger at lower altitudes. This suggests the increase in OCS flux upward through the lower boundary in the "nominal high OCS" model proportionally affects the calculated CO abundance in the model but only below $\sim$ 62 km which brings this model closer to the infrared observation of CO [Connes et al., 1968, Young, 1972] than the "baseline" and "nominal" models. Further observations of CO near the lower boundary of the upper cloud, which may be provided by Venus Express, are needed to assess whether there is a significant flux of OCS upward into the upper cloud.

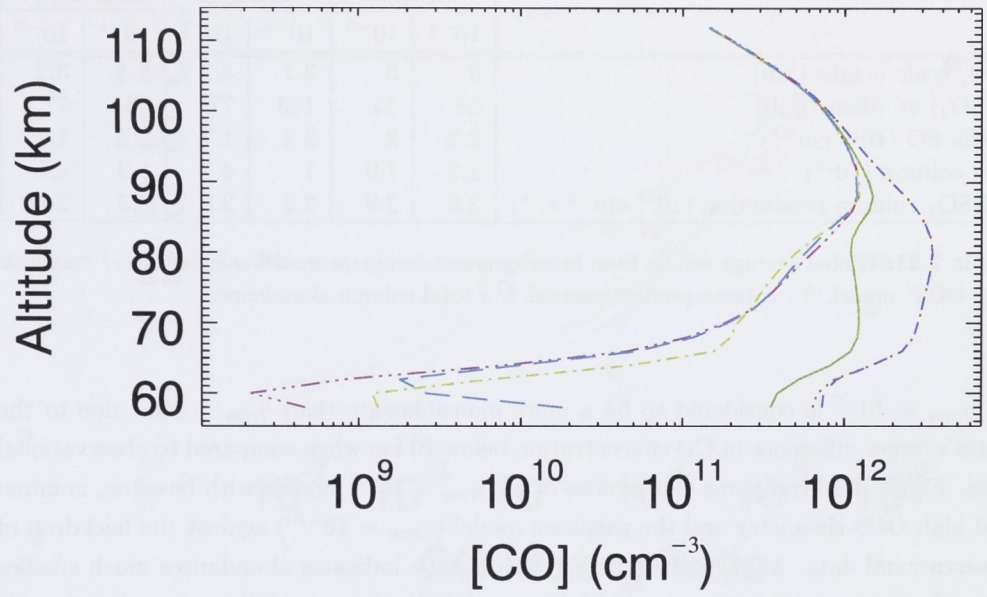

Figure 7.12: CO concentration profile for different γ_{rxn} values and alternative gasphase models. $\gamma = 10^{-4}$ model "baseline" profile is represented by the green line with dashes and single dots, while the "nominal" and "nominal high OCS" profiles are given by the magenta (dashes and triple dots) and light-blue (long dashes) lines, respectively. $\gamma = 10^{-5}$ model "baseline" profile is represented by the green solid line, while the "nominal" and "nominal high OCS" profiles are given by the red (dots) and dark-blue (small dashes) lines, respectively.

The major differences between the baseline and alternative chemistries, listed in Table 7.21, are that of mixing ratio of SO_2 and O_2 column abundance. The differences are attributed to 1-σ adjustments made to the "baseline" model, detailed discussion of which is presented elsewhere [Mills, 1998].

7.11 Comparison of models and observations

Laboratory assessments for the case of Martian atmosphere have rejected the efficiency of hetrogeneous oxidation of CO on dust and ice required to make significant differences to the overall chemistry, but concede that oxidation on photoactive aerosols are possible [Choi and Leu, 1997]. It is contended here that Venus, with a much thicker and denser population of aerosols, does indeed provide a site for heterogeneous photooxidation of CO. Laboratory work has suggested numerous possible mechanims which might be vital to heterogeneous photooxidation of CO (to CO_2) in cloud aerosol particles (discussed in Section 5.2).

Observation	Model Calculations					
	baseline		nominal		high OCS†	
$\gamma =$	10^{-4}	10^{-5}	10^{-4}	10^{-5}	10^{-4}	10^{-5}
SO_2 scale height (km)	3	3	3.1	3.2	3.1	3.2
f(SO_2) at 70km (ppb)	58	44	103	77	98	77
peak SO (10^{10} cm^{-3})	2.2	2	2.2	1.7	2.2	1.7
O_2 column (10^{18})	1.2	1.9	1	4.1	1.3	4.1
H_2SO_4 column production (10^{11} cm^{-2} s^{-1})	2.8	2.9	2.2	2.6	2.3	2.6

Table 7.21: Global average results from heterogeneous dominant model calculations. † "nominal high OCS" model. $^{\diamond}$: column production rate. $^{\square}$: total column abundance.

$\gamma_{rxn} = 10^{-5}$ is considered to be a more plausible rate than $\gamma_{rxn} = 10^{-4}$ due to the latter's larger difference in CO concentration below 70 km when compared to observational data. Figure 7.13 compares CO profiles of all $\gamma_{rxn} = 10^{-5}$ models with baseline, nominal and high OCS chemistry and the gasphase model ($\gamma_{rxn} = 10^{-10}$) against the backdrop of observational data. Modeled CO mixing ratio profile indicates abundances much smaller than that observed by Clancy and Muhleman [1991]. One possible explanation for this could be that Clancy and Muhleman [1991] observations were of the Venus night-side (close to inferior conjunction) but our one-dimensional model averages out diurnal variations. Also, variability was observed in CO over the 1982 – 1990 period. The smallest observed CO mixing ratio at 70 km was about 5×10^{-6} in 1982 [Clancy and Muhleman, 1991].

The aim of this research project is limited to assessment of impact of heterogeneous chemistry based on the posited values of γ_{rxn}. From a laboratory viewpoint, $\gamma_{rxn} = 10^{-5}$ is plausible (*L. Phillips, personal communication, 2005*). CO abundances of $\gamma_{rxn} = 10^{-5}$ nominal and high OCS atmosphere models show 3 orders of magnitude variations from observational data around 60 km [Young, 1972]. High oxygen column abundances of nominal and high OCS $\gamma = 10^{-5}$ models contribute to relinquishment of the models from further investigation. Baseline $\gamma = 10^{-5}$ atmosphere model differ by 4 orders of magnitude in comparison with CO mixing ratio observations around 60 km, but give better agreement with O_2 column abundances. Determination of γ_{rxn} from laboratory experiments is needed to establish the actual importance of heterogeneous chemistry in the Venus middle atmosphere. It is evident that increases in γ_{rxn} are accompanied by decreases in O_2 and CO abundances below 70 km. While reduced O_2 abundances are more consistent with observation [Trauger and Lunine, 1983] than previous models, decrease in CO abundances, from introduction of heterogeneous chemistry, have enhanced discrepancy between modeling and observational data.

If γ_{rxn} is as high as 3×10^{-5}, then results from this research are close to agreement with O_2 column abundance and will be of immense interest to future Venus atmospheric modeling. $\gamma_{rxn} = 3 \times 10^{-5}$ baseline model is chosen as it shows significantly reduced O_2 abundance without excessive decrease in CO abundances as that of $\gamma_{rxn} = 10^{-4}$ baseline

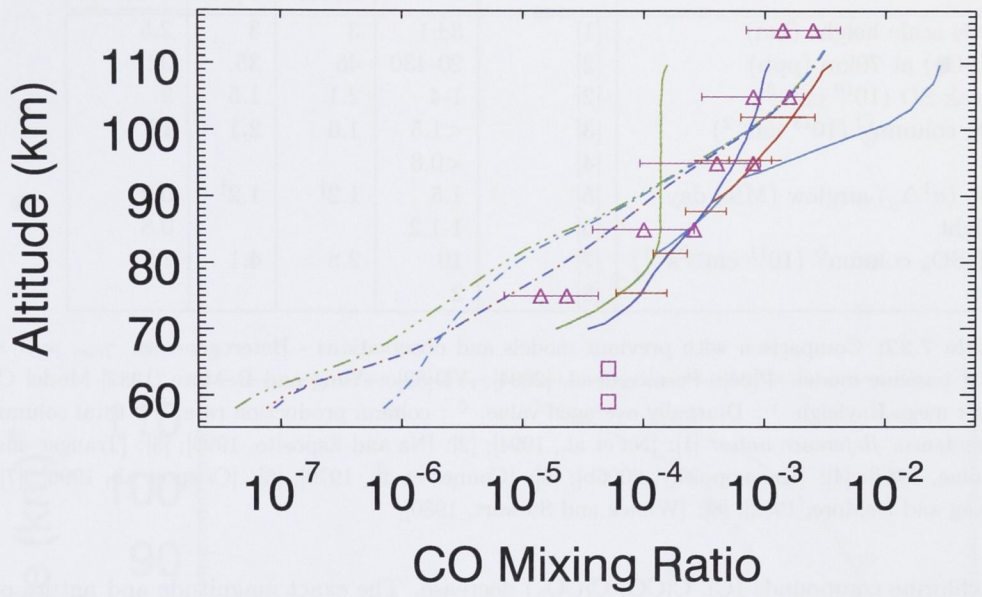

Figure 7.13: CO mixing ratio profile for γ_{rxn} values and observations. Clancy and Muhleman [1991] profiles are shown by the four solid lines - dark-blue, red, light-blue and green representing observations made at terminator, anti-solar, 3 AM and 9 AM, respectively, with indicated uncertainties shown for the 3 AM and 9 AM observations. Lellouch et al. [1994] measurements are shown as magenta coloured triangles with indicated uncertainties. The squares(magenta) represent Young [1972] interpretation of Connes et al. [1968] observations. Profiles for heterogeneous dominant chemistry ($\gamma_{rxn} = 10^{-5}$) representing the "baseline", "nominal" and "nominal high OCS" cases are the green (dashes and triple dots) line, red dots and dark-blue (small dashes) lines respectively. The gasphase dominant model is represented by the light-blue (dashes and single dots) line.

model.

Table 7.22 contextualises the research reported here by making comparisons with previous photochemical models and observations. Criteria for comparison were chosen with available observational results in mind. The primary objective of this research was to test a plausible CO_2 production pathway and study its effects on the remainder of the atmospheric chemistry. In doing so, we report that this research is able to provide a potential theoretical explanation for the observed low oxygen abundances. Heterogeneous processes (Reactions 5.16 and 5.17) are an efficient means to produce CO_2. Primary impact of the inclusion of heterogneous chemistry is felt on CO and O abundances, as CO_2 concentrations are largely unchanged by variations to the model. Large differences from previous models are seen in SO and SO_2 abundances around 70 km. The reasons underlying the behaviour of sulphur compounds are linked with that of atomic oxygen. The production and destruction rates of sulphur compounds (S, SO, SO_2) show an overall increase, while those

Observation	Reference	Value	Model Calculations		
			Heter.	P[04]	YD[82]c
SO_2 scale height (km)	[1]	3±1	3	3	2.5
f(SO_2) at 70km (ppb)	[2]	20-430	46	35	32
peak SO (10^{10} cm^{-3})	[2]	1-4	2.1	1.5	2
O_2 column$^{\square}$ (10^{18} cm^{-2})	[3]	<1.5	1.6	2.1	18
	[4]	<0.8			
O_2 ($a^1\Delta_g$) airglow (MR) day	[5]	1.5	1.2†	1.2†	0.9
night	[6]	1-1.2			0.8
H_2SO_4 column$^{\diamond}$ (10^{11} $cm^{-2}s^{-1}$)	[7]	10	2.8	4.1	14
	[8]	2			

Table 7.22: Comparison with previous models and observations - Heterogeneous: $\gamma_{rxn} = 3 \times 10^{-5}$ baseline model. P[04]: Pernice et al. [2004]. YD[82]c: Yung and DeMore [1982] Model C. MR : mega-Rayleigh. † : Diurnally averaged value. $^{\diamond}$: column production rate. $^{\square}$: total column abundance. *Reference notes:* [1]: [Na et al., 1994]; [2]: [Na and Esposito, 1995]; [3]: [Trauger and Lunine, 1983]; [4]: [Krasnopolsky, 2006b]; [5]: [Connes et al., 1979]; [6]: [Crisp et al., 1996]; [7]: [Yung and DeMore, 1982]; [8]: [Winick and Stewart, 1980];

of chlorine compounds (Cl, ClCO, $ClCO_3$) decrease. The exact magnitude and nature of the effect of species on one another is not clear from our studies. Given our knowledge of changes in the concentrations and reaction rates, it is suggested that decrease in CO abundance, from introduction of heterogeneous reaction pathways, is accompanied by a decrease in abundance of chlorine species and their reaction (production and loss) rates. Reduction of strength of reaction rates influence chlorine compounds' capabilities to react with other species, like oxygen. The sulphur compounds, are not closely related to CO like the chlorine compounds and, are unaffected. In fact, with weakening of chlorine compounds' reactions, sulphur compounds are more likely to react with oxygen. This may account for increase in abundances of sulphur compounds and decrease in chlorine compounds.

Figures 7.14 and 7.15 compare O_2 and CO concentrations of previously published photochemical models. Yung and DeMore [1982] Model C, Pernice et al. [2004] and nominal models are gasphase models whereas $\gamma_{rxn} = 3 \times 10^{-5}$ has included this research's results from heterogeneous dominant atmosphere. The differences between Yung and DeMore [1982] Model C and the nominal model are representative of laboratory advancements in the intervening time-period. Pernice et al. [2004] model contains 1-σ adjustments of ClCO stability in comparison to the nominal model [Mills, 1998].

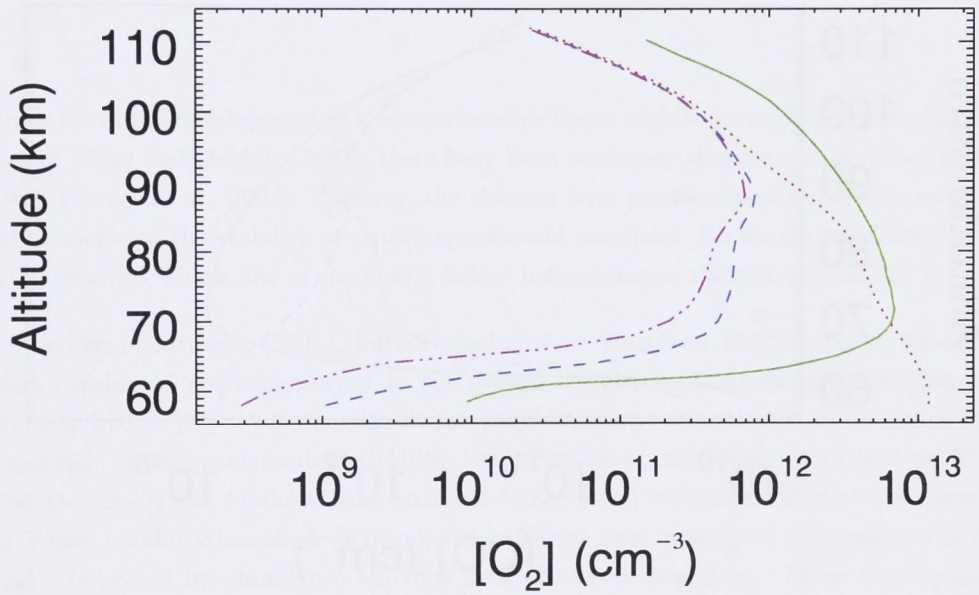

Figure 7.14: Oxygen concentration profile for different historical models. Yung and DeMore [1982] Model C model profile is given by the solid green line and the nominal model [Mills, 1998] is given by the dotted red line. The Pernice et al. [2004] model is shown by dark-blue (small dashes) line and a heterogeneous case of $\gamma_{rxn} = 3 \times 10^{-5}$, from this research, is given by the magenta (dashes and triple dots) line.

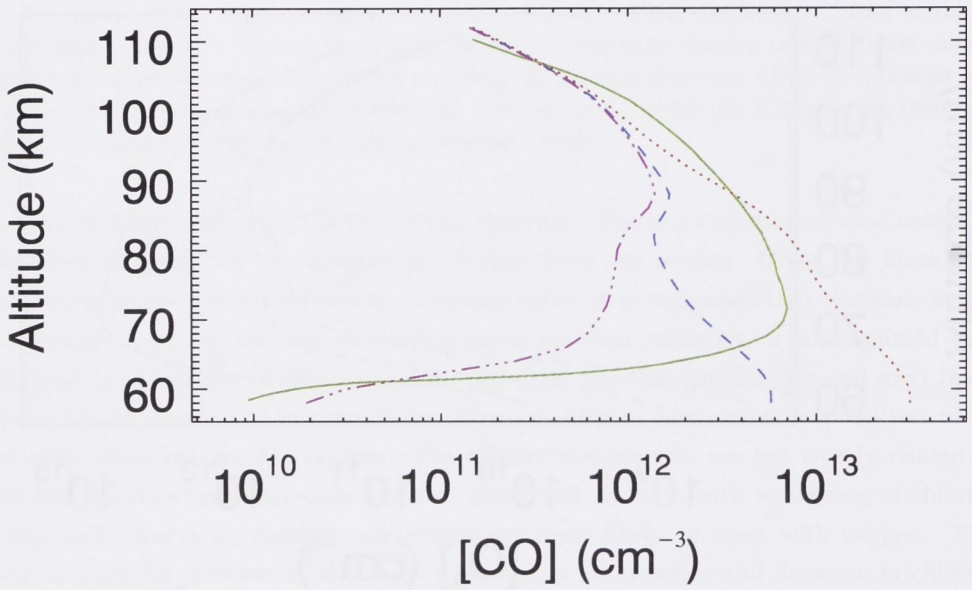

Figure 7.15: CO concentration profile for different historical models. Yung and DeMore [1982] Model C model profile is given by the solid green line and the nominal model [Mills, 1998] is given by the dotted red line. The Pernice et al. [2004] model is shown by dark-blue (small dashes) line and a heterogeneous case of $\gamma_{rxn} = 3 \times 10^{-5}$, from this research, is given by the magenta (dashes and triple dots) line.

Chapter 8

Results and Discussion - NO_x chemistry project

Since the initial development of a comprehensive Venus middle atmosphere photochemical model [Yung and DeMore, 1982], there have been numerous changes and revisions [Mills, 1998, Pernice et al., 2004]. However, the changes have predomninantly been focussed on adjustments to the stability of crucial species and reactions. No attempt has been made to incorporate a new line of chemistry, before heterogeneous chemistry (Chapter 7).

Oxides of nitrogen (NO_x), initially included in Yung and DeMore [1982] Model B, were considered not insignificant to the overall chemistry. However, the abundance of NO required to play a substantial role in overall chemistry was deemed to be higher than expected. Subsequent modeling [Mills, 1998, Pernice et al., 2004], was based on Yung and DeMore [1982] Model C and excluded NO_x-related chemistry. Recent observations of Venus middle atmosphere [Krasnopolsky, 2006a] have confirmed the presence of NO and interpreted its abundance and flux near the lower boundary. These developments are the basis for our renewed interest in NO_x chemistry and its inclusion in the current photochemical model.

The addition of the NO_x chemical scheme (discussion of methodology in Section 6.1) is expected to have an impact on existing state of chemistry in the photochemical model. It is the degree and extent of this impact that is the intended area of study. Analysis of the effect of NO_x chemistry is carried out through comparisons of species' abundances in the distinct cases of model with NO_x chemistry and those without.

8.1 Studies of nominal NO_x chemistry

With development of heterogeneous chemistry and realisation of its potential, NO_x chemistry is incorporated into the standard gas-phase and the recently developed heterogeneous atmosphere models. This way, the combined effects of heterogeneous and NO_x chemistries

1	$\gamma_{rxn} = 10^{-5}$, $\mu_{NO} = 0$	Baseline heterogeneous
2	$\gamma_{rxn} = 10^{-5}$, $\mu_{NO} = 5.5$ ppb	Heterogeneous NO_x
3	$\gamma_{rxn} = 10^{-10}$, $\mu_{NO} = 0$ ppb	Baseline gas-phase
4	$\gamma_{rxn} = 10^{-10}$, $\mu_{NO} = 5.5$ ppb	Gas-phase NO_x

Table 8.1: Different models with and without NO_x. Changes to μ_{NO} were made at 58 km.

on the overall atmosphere could be studied. The different models studied for the impact of NO_x chemistry are listed and labelled in Table 8.1.

8.1.1 O_2 abundances

The initial assessment of the impact of NO_x inclusion is carried out with an input of $\mu_{NO} = 5.5$ ppb at the lower boundary of the middle atmosphere, as suggested by recent observation [Krasnopolsky, 2006a]. Figure 8.1 compares profiles of O_2 concentrations of the baseline $\gamma_{rxn} = 10^{-10}$ (gas-phase) and $\gamma_{rxn} = 10^{-5}$ (heterogeneous) atmosphere models with those including NO_x chemistry.

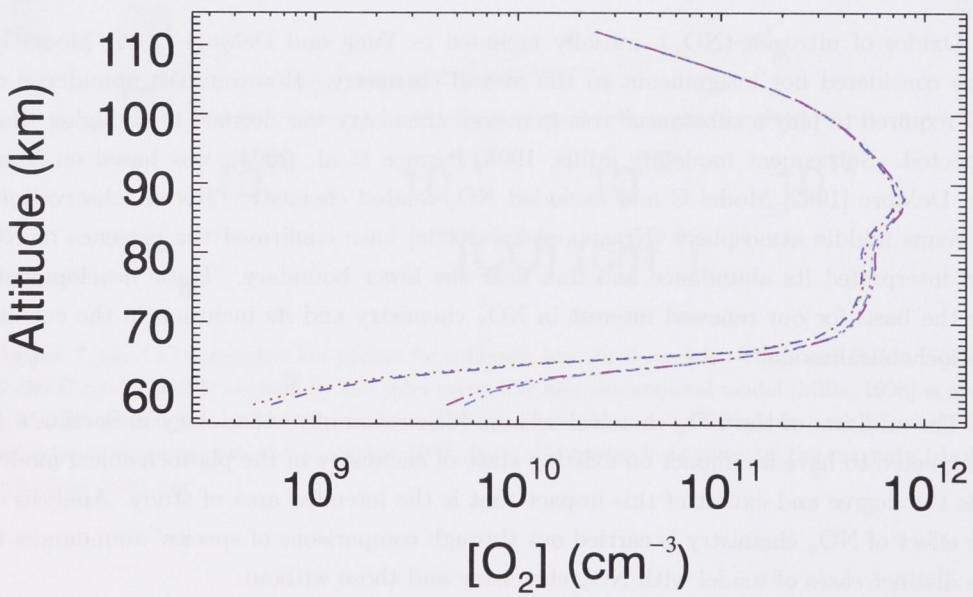

Figure 8.1: Oxygen concentration profile for baseline and nominal NO atmosphere models. Red dotted line and dark blue (small dashes) represent heterogeneous (γ_{rxn} 10^{-5}) baseline and nominal NO models, respectively. Magenta lines (dash and triple dots) and light-blue (dash and single dot) represent gasphase (γ_{rxn} 10^{-10}) baseline and nominal NO models, respectively.

The overall differences between the models, with respect to O_2 concentrations, with

and without NO_x chemistry are small. The abundance of NO_x introduced into the model (μ_{NO} = 5.5 ppb) is considered nominal. Drastic changes are not observed in the overall chemistry from introduction of this amount of NO. Table 8.2 summarises the characteristic conditions at the lower boundary region which result in the variations in modelled O_2 abundances (Figure 8.1). The addition and changes to μ_{NO} limited in the region of their potential impact to the lower boundary region. As a result, this section of the study is focussed on understanding changes to the model at 58 km.

	Heter. baseline	Heter. NO_x	Gasphase baseline	Gasphase NO_x
Production (58)	4.4×10^3	5.6×10^3	3.8×10^4	4.9×10^4
Loss (58)	4.7×10^3	6.0×10^3	4.0×10^4	5.0×10^4
Conc (58)	4.9×10^8	6.1×10^8	4.4×10^9	5.4×10^9
Column abundance	1.9×10^{18}	1.9×10^{18}	2.1×10^{18}	2.1×10^{18}

Table 8.2: O_2 concentration production and loss rates at 58 km in different atmosphere scenarios. Production and loss rates are measured in $cm^{-3}s^{-1}$, concentration in cm^{-3} and column abundance in cm^{-2}.

8.1.2 CO abundances

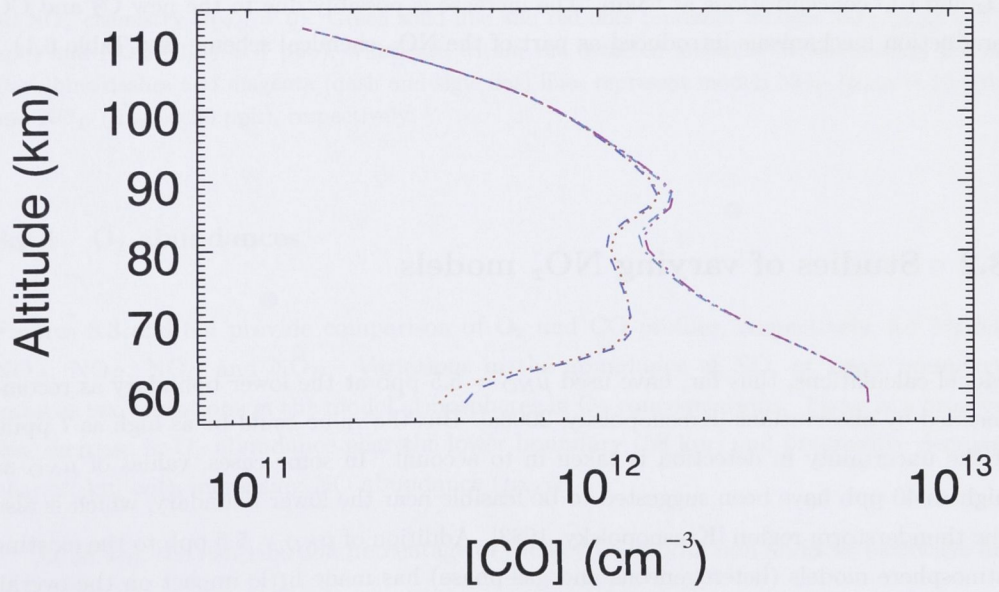

Figure 8.2: Carbon monoxide concentration profile for baseline and nominal NO atmosphere models. Red dotted line and dark blue (small dashes) represent heterogeneous (γ_{rxn} 10^{-5}) baseline and nominal NO models, respectively. Magenta lines (dash and triple dots) and light-blue (dash and single dot) represent gasphase (γ_{rxn} 10^{-10}) baseline and nominal NO models, respectively.

Figure 8.2 shows the CO concentration profiles of the heterogeneous (γ_{rxn} 10^{-5}) and

	Heter. baseline	Heter. NO_x	Gasphase baseline	Gasphase NO_x
Production (58)	1.8×10^6	2.2×10^6	2.9×10^7	3×10^7
Loss (58)	1.8×10^6	2.2×10^6	2.9×10^7	3×10^7
Conc (58)	3.0×10^{11}	4.2×10^{11}	5.9×10^{12}	5.9×10^{12}
Column abundance	5.0×10^{18}	5.0×10^{18}	1.0×10^{19}	1.0×10^{19}

Table 8.3: CO concentration production and loss rates at 58 km in different atmosphere scenarios. Production and loss rates are measured in $cm^{-3}s^{-1}$, concentration in cm^{-3} and column abundance in cm^{-2}

gasphase (γ_{rxn} 10^{-10}) atmospheres with baseline chemistry [Pernice et al., 2004] and nominal NO abundances. Table 8.3 lists the production rate, loss rate and concentration of CO at 58km along with the column abundance of CO.

Impact of NO_x chemistry is marginal and limited to below 60km. Introduction of nominal NO_x to heterogeneous and gasphase atmosphere models results in increase in the total production and loss rates of O_2 and CO, near the lower boundary. In this context, NO_x chemistry has a counter-effect to that of heterogeneous chemistry. Heterogeneous chemistry reduces the production and loss rates of CO and O_2, but NO_x chemistry has the opposite effect (see Tables 8.2 and 8.3). As a result, there is a very small increase in O_2 and CO concentrations at 58km. The increase is possibly due to the new O_2 and CO production mechanisms introduced as part of the NO_x chemical scheme (see Table 6.1).

8.2 Studies of varying NO_x models

Model calculations, thus far, have used $\mu_{NO} = 5.5$ ppb at the lower boundary as recommended by observations [Krasnopolsky, 2006a]. But the value could be as high as 7 ppm, if the uncertainty in detection is taken in to account. In some cases, values of μ_{NO} as high as 40 ppb have been suggested to be feasible near the lower boundary, which is also the thunderstorm region [Krasnopolsky, 1983]. Addition of $\mu_{NO} = 5.5$ ppb to the existing atmosphere models (heterogeneous and gas-phase) has made little impact on the overall chemistry (discussed in Section 8.1). Dedicated studies on extent of lightning are required to ascertain a value for NO_x species in the lower region of the middle atmosphere. In the meantime, key species' (O_2, CO and SO_2) abundances are profiled for a range of μ_{NO} values,in this section, to study the effect of higher NO abundances on overall chemistry. All changes are carried out on the baseline heterogeneous atmosphere model ($\gamma_{rxn} = 10^{-5}$). For convenience in future discussion, the different atmosphere scenarios modeled in this section of the research project are labelled in Table 8.4.

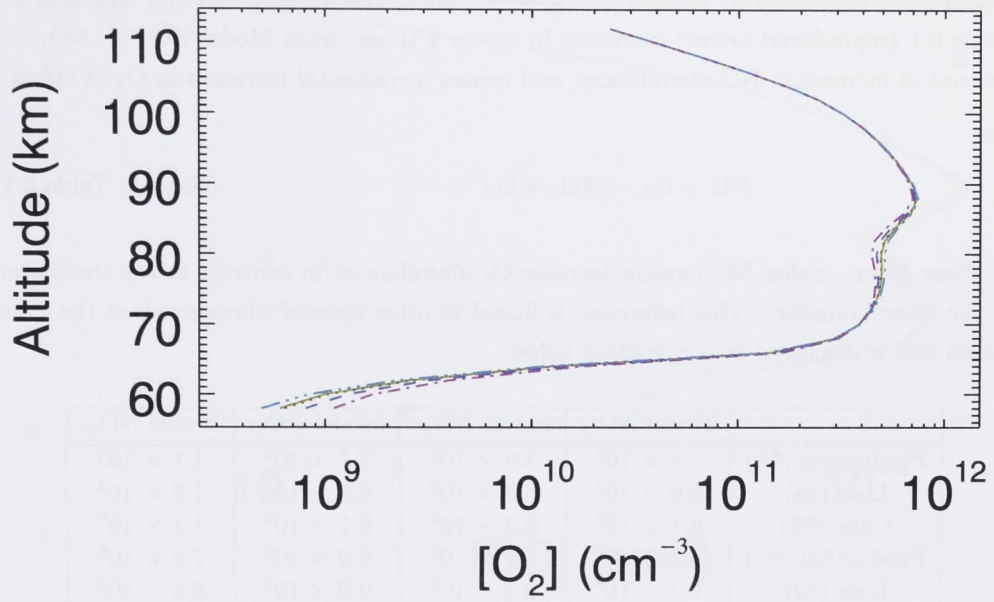

Figure 8.3: Oxygen concentration profile for baseline heterogeneous atmosphere models with different μ_{NO}. Light-blue (dash and triple dots) line is the baseline heterogeneous model with no NO_x chemistry ($\mu_{NO} = 0$). Green solid line and red dots represent models NO_A ($\mu_{NO} = 5.5$ ppb) and NO_B ($\mu_{NO} = 7$ ppb), which are within the detected amounts [Krasnopolsky, 2006a]. Dark-blue dashes and magenta (dash and sigle dot) lines represent models NO_C ($\mu_{NO} = 15$ ppb) and NO_D ($\mu_{NO} = 30$ ppb), respectively.

8.2.1 O_2 abundances

Figures 8.3 and 8.4 provide comparison of O_2 and CO profiles, respectively, for Models NO_A, NO_B, NO_C and NO_D. Variations in the abundance of NO, at lower boundary, induces two variations in the model atmospheres in O_2 concentrations. There is a progressive increase in O_2 abundance near the lower boundary (58 km) and progressive decrease near 82 km with increasing NO abundance (μ_{NO}).

At 58 km, the contribution percentage of the key O_2 production and loss pathways are

$\mu_{NO} = 0$	Baseline heterogeneous
$\mu_{NO} = 5.5$ ppb	Model NO_A
$\mu_{NO} = 7$ ppb	Model NO_B
$\mu_{NO} = 15$ ppb	Model NO_C
$\mu_{NO} = 30$ ppb	Model NO_D

Table 8.4: Labelling different NO_x models. All atmospheres are heterogeneous dominant, $\gamma_{rxn} = 10^{-5}$.

not affected by changes to NO. Rates of production and loss double from Model NO_A to Model NO_D (as shown in Table 8.5). However, one of the minor pathways, Reaction 16, Table 6.1 (reproduced below) increases by up to 4 times, from Model NO_A to NO_D on account of increase in NO abundances, and causes incremental increases in O_2 at 60km.

$$NO + O_3 \rightarrow NO_2 + O_2 \qquad \text{(Rxn 16, Table 6.1)}$$

Near 82km, higher NO models decrease O_2 abundances, in contrast to the trend seen at the lower boundary. This behaviour is linked to other species' abundances at the same region and is discussed in conjunction below.

	Model NO_A	Model NO_B	Model NO_C	Model NO_D
Production (58)	5.6×10^3	5.9×10^3	7.7×10^3	1.1×10^4
Loss (58)	6.0×10^3	6.3×10^3	8.2×10^3	1.2×10^4
Conc (58)	6.1×10^8	6.4×10^8	8.1×10^8	1.1×10^9
Production (82)	8.2×10^6	8.1×10^6	8.0×10^6	7.8×10^6
Loss (82)	9.2×10^6	9.2×10^6	9.0×10^6	8.8×10^6
Conc (82)	5.1×10^{11}	5.1×10^{11}	4.9×10^{11}	4.6×10^{11}

Table 8.5: O_2 concentration, total production and loss rates at 58 km and 82 km in different NO_x atmosphere models. Production and loss rates are measured in $cm^{-3}s^{-1}$ and concentration in cm^{-3}.

8.2.2 CO abundances

CO abundances are similar to that of O_2 with progressive increase near the lower boundary and progressive decrease around 82 km with increasing NO abundances. At the lower boundary, total production and loss rates increase by ~100 % (same as for O_2) from Model NO_A to NO_D (Table 8.6), due to increases in the major CO production and loss reactions (Reactions 7.1 and 7.4). However, heterogeneous processes (Reactions 5.16 and 5.17), which convert CO to CO_2 catalytically, increase by less than 1 %, for corresponding increase in NO abundances. The relative efficiency of heterogeneous processes, as CO sinks, decreases for the high NO_x models, which results in increase in CO abundances at the lower boundary. The differences are small as the heterogeneous processes are not the primary sinks for CO.

$$ClCO + CO_2 \rightarrow Cl + CO + CO_2 \qquad (7.1)$$

$$Cl + CO + M \rightarrow ClCO + M \qquad (7.4)$$

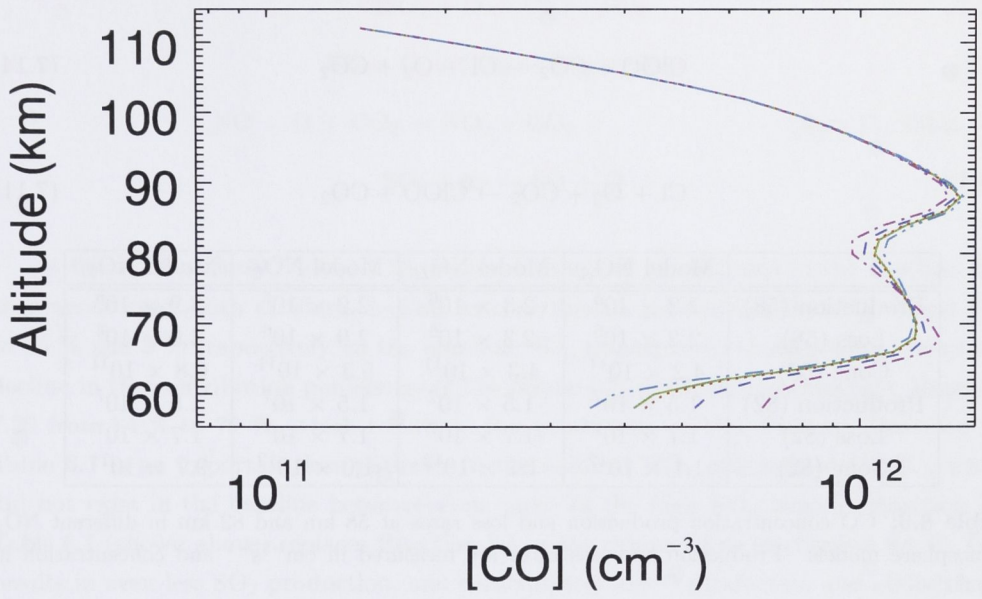

Figure 8.4: CO concentration profile for baseline heterogeneous atmosphere models with different μ_{NO}. Light-blue (dash and triple dots) line is the baseline heterogeneous model with no NO_x chemistry ($\mu_{NO} = 0$). Green solid line and red dots represent models NO_A ($\mu_{NO} = 5.5$ ppb) and NO_B ($\mu_{NO} = 7$ ppb), which within the detected amounts [Krasnopolsky, 2006a]. Dark-blue dashes and magenta (dash and sigle dot) line represent models NO_C ($\mu_{NO} = 15$ ppb) and NO_D ($\mu_{NO} = 30$ ppb), respectively.

$$CO + O + aer1 \rightarrow CO_2 + aer1 \tag{5.16}$$

$$CO + O + aer2 \rightarrow CO_2 + aer2 \tag{5.17}$$

CO abundances decrease with increasing NO abundances around 82 km (Table 8.6 and Figure 8.4), along with production and loss rates of CO which decrease by 5 %, from Model NO_A to NO_D. Rate of heteroegeneous reaction, Reaction 5.16, increases by 27 %, becoming a more efficient CO loss mechanism. Increase in the rate of Reaction 5.16 is possibly linked to variations in atomic oxygen (O) abundances at this region and is discussed in Section 8.2.3. Abundances of CO, ClCO and Cl are closely inter-related by Reactions 7.1 and 7.4. Decreases in CO abundances correspond to proportional decreases in Cl (and ClCO). Atomic chlorine (Cl) influences O_2 abundances through Reactions 7.14 and 7.11 (reproduced below for convenience), which are the primary production and loss mechanisms for O_2. Thus, changes in CO abundances at 82 km affect O_2 abundances at

the same altitude.

$$ClOO + CO_2 \rightarrow Cl + O_2 + CO_2 \tag{7.14}$$

$$Cl + O_2 + CO_2 \rightarrow ClOO + CO_2 \tag{7.11}$$

	Model NO_A	Model NO_B	Model NO_C	Model NO_D
Production (58)	2.2×10^6	2.3×10^6	2.9×10^6	3.9×10^6
Loss (58)	2.2×10^6	2.3×10^6	2.9×10^6	4.0×10^6
Conc (58)	4.2×10^{11}	4.3×10^{11}	5.3×10^{11}	6.8×10^{11}
Production (82)	1.5×10^7	1.5×10^7	1.5×10^7	1.5×10^7
Loss (82)	1.7×10^7	1.7×10^7	1.7×10^7	1.7×10^7
Conc (82)	1.1×10^{12}	1.1×10^{12}	1.0×10^{12}	9.7×10^{11}

Table 8.6: CO concentration production and loss rates at 58 km and 82 km in different NO_x atmosphere models. Production and loss rates are measured in $cm^{-3}s^{-1}$ and concentration in cm^{-3}.

8.2.3 O abundances

Variations in O abundances among the various NO_x models are small and are best studied by normalising O abundances with respect to one atmosphere, which in this case is the baseline heterogeneous model. The O abundances for high NO_x models, at different altitudes, as a factor of the baseline heterogeneous model are shown in Figure 8.5.

There are three distinct variations in O abundances from the heterogeneous baseline model - below 60km, 68km and 82km.

Production and loss rates of O increase (between 18 % to 23 % from the heterogeneous baseline atmosphere) for the NO_x atmospheres at 60 km. Atomic oxygen production mechanisms' contribution percentage are unchanged with introduction of NO_x. Heterogeneous processes (Reaction 5.16 and 5.17) accounted for 78 % of loss of atomic oxygen in the baseline heterogeneous case, as opposed to $\sim$ 25 % in the NO_x models. In the nominal NO_x case (model NO_A), Reaction 7.28 is as important (25 %) as heterogeneous processes in destruction of O. Reaction 7.5 accounts for 15 % of O loss in model NO_A, an increase from 5 % in the baseline heterogeneous atmosphere. Heterogeneous mechanisms produce CO_2 only, whereas in model NO_A there is additional production of SO_2, ClO and NO_2 from the loss of O. Photolysis of SO_2 (Reaction 7.20), in particular, is the primary source of O at this region, and this results in greater production of atomic oxygen. In Model NO_D, Reaction 15, Table 6.1 (reproduced below) is the most important loss mechanism (40 %) for O, on account of high abundance of NO. There is also an increase in the contribution percentage of Reaction 7.28, which produces more SO_2, which in turn photolyses

to produce O.

$$ClSO_2 + O \rightarrow ClO + SO_2 \quad (7.28)$$

$$SO + O + CO_2 \rightarrow SO_2 + CO_2 \quad (7.5)$$

$$NO + O + CO_2 \rightarrow NO_2 + CO_2 \quad \text{(Rxn 15, Table 6.1)}$$

$$SO_2 + h\nu \rightarrow SO + O \quad (7.20)$$

At 68km, Reactions 7.5 and 7.28 are important loss mechanisms in the baseline heterogeneous case, both of which decline, in contribution percentage, from 69 % and 6 % to 55 % and 3 % respectively, in the nominal NO_x atmosphere. Consequently, there is a decline in the contribution percentage of the primary O production mechanism, Reaction 7.20 from 84 % to 79 %, which results in less production at this altitude. Reaction 15, Table 6.1 is an important loss pathway in the nominal NO_x atmosphere (17 %), which did not exist in the baseline heterogeneous case. In the high NO_x models, Reaction 15, Table 6.1 (shown above) replaces Reaction 7.5 as the primary loss mechanism for O. This results in even less SO_2 production, and consequently less O production and abundances.

Around 82km, Reaction 7.7 is the most important loss mechanism for the baseline heterogeneous case, accounting for 44 % of total atomic oxygen loss at that altitude. Contribution of Reaction 7.7 decreases in the nominal NO_x (39 %) and high NO_x (24 %) models. There is an increase in the contributions of Reactions 5.16 and 8.1, as atomic oxygen destroyers, by a few % from the baseline heterogeneous to the NO_x models. The contribution to production of atomic oxygen by SO_2 photolysis increases from 20 % in the baseline heterogeneous case to 24 % in the high NO_x model. The absolute rate of SO_2 photodissociation increases by $\sim$ 30 %, from model NO_A to model NO_D, at this altitude. NO_2 photolysis (Reaction 2, Table 6.1) contributes 6 % of atomic oxygen in the high NO_x model, from being non-existent in the baseline heterogeneous and nominal NO_x atmosphere models, portraying an increasingly important role played by NO_x species in the high NO_x models, at this altitude. These factors combine to result in higher atomic oxygen abundance.

$$ClO + O \rightarrow O_2 + Cl \quad (7.7)$$

$$CO + O + \text{aer1} \rightarrow CO_2 + \text{aer1} \quad (5.16)$$

$$ClCO + O \rightarrow CO_2 + Cl \quad (8.1)$$

Thus, decreases in CO and O_2 abundances around 82 km are attributed to the varia-

	Heterogeneous baseline	Model NO_A	Model NO_D
Production (60)	6.1×10^5	6.2×10^5	6.4×10^5
Loss (60)	6.1×10^5	6.2×10^5	6.4×10^5
Conc (60)	1.5×10^6	1.3×10^6	7.4×10^5
Production (68)	1.4×10^7	1.7×10^7	2.4×10^7
Loss (68)	1.4×10^7	1.7×10^7	2.4×10^7
Conc (68)	7.1×10^8	6.4×10^8	4.7×10^8
Production (82)	3.7×10^6	3.8×10^6	4.5×10^6
Loss (82)	3.7×10^6	3.8×10^6	4.4×10^6
Conc (82)	9.4×10^8	1.1×10^9	1.5×10^9

Table 8.7: O concentration production and loss rates at 60 km, 68 km and 82 km in different NO_x atmosphere models. Production and loss rates are measured in $cm^{-3}s^{-1}$ and concentration in cm^{-3}.

tions in O abundances at this region. These are in turn influenced by the introduction of NO_x chemistry and closely connected with SO_2 destruction (and production).

8.2.4 SO_2 abundances

Different models studied in this research project show minute differences when SO_2 concentrations are profiled on a logarithmic scale. Ratios of SO_2 concentrations have been normalised with respect to baseline heterogeneous model and compared on a linear plot (Figure 8.6) in order to magnify the differences. Model NO_D shows greatest deviation, from the normalised atmosphere, with SO_2 concentrations increasing by 65 % at almost all altitudes while Model NO_A shows 35 % all other models, on average, show differences of $\sim$ 10 %.

Investigation of SO_2 abundances leads on from studies on atomic oxygen, and subsequently from CO and O_2. Unlike atomic oxygen, SO_2 abundances do not exhibit major deviations near the lower boundary layer. However, drastic differences are evident amongst NO_x models with respect to the baseline heterogeneous atmosphere.

Near 82 km altitude, SO_2 loss mechanims are near-identical for all NO_x and baseline heterogeneous models. There are significant differences in the production process of SO_2. Though key individual production mechanisms remain the same, there are considerable differences in the extent of each mechanism's contribution towards production of SO_2 (shown in Table 8.8). Such changes affect the overall production and abundances of SO_2 at 82 km.

Most noticable differences in SO_2 abundances are those between Models NO_A and NO_B compared with higher NO_x atmospheres (Models NO_C and NO_D), see Figure 8.6. At 82 km, model NO_D has a greater contribution of Reaction 7.5, than any other SO_2 production reaction. Reaction 7.18 is the most significant contributor towards SO_2 production in the

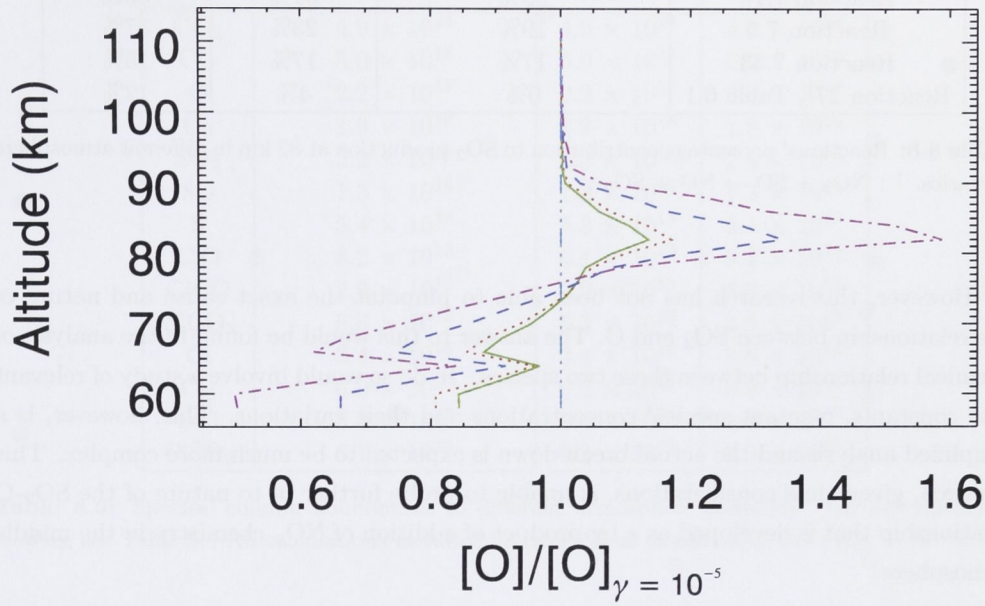

Figure 8.5: O concentration profile for different μ_{NO}. Light-blue (dash and triple dots) line is the baseline heterogeneous model with no NO_x chemistry ($\mu_{NO} = 0$). Green solid line and red dots represent models NO_A ($\mu_{NO} = 5.5$ ppb) and NO_B ($\mu_{NO} = 7$ ppb), which are within the detected amounts [Krasnopolsky, 2006a]. Dark-blue dashes and magenta (dash and sigle dot) line represent models NO_C ($\mu_{NO} = 15$ ppb) and NO_D ($\mu_{NO} = 30$ ppb), respectively. Gamma: γ_{rxn}.

low NO_x and heterogeneous baseline models at this altitude. In essence, the production (and abundance) of SO_2 is linked to that of SO and ClO in the low NO_x and heterogeneous baseline models. In high NO_x models, abundances of SO and O are the key determining factors in the production of SO_2. Thus, with increase in the NO_x chemistry, there is a correlation between O and SO_2 abundances around 82 km, which is established here. This correlation is sugested to be one of the principal causes for changes in abundances of SO_2 and O.

$$SO + ClO \rightarrow SO_2 + Cl \tag{7.18}$$

$$SO + O + CO_2 \rightarrow SO_2 + CO_2 \tag{7.5}$$

$$ClCO_3 + SO \rightarrow Cl + CO_2 + SO_2 \tag{7.33}$$

Reaction	Heterogeneous baseline	Model NO_A	Model NO_D
Reaction 7.18	60%	51%	30%
Reaction 7.5	19%	23%	37%
Reaction 7.33	17%	17%	15%
Reaction 27†, Table 6.1	0%	4%	12%

Table 8.8: Reactions' percentage contribution to SO_2 production at 82 km in different atmosphere scenarios. † : $NO_2 + SO \rightarrow NO + SO_2$;

However, this research has not been able to pinpoint the exact cause and nature of the relationship between SO_2 and O. The answer to this would be found in the analysis of chemical relationship between these two species. To do so would involve a study of relevant rate constants, reactant species' concentrations and their variations. This, however, is a simplified analysis and the actual break-down is expected to be much more complex. This research, given time considerations, is unable to probe further in to nature of the SO_2-O relationship that is developed as a by-product of addition of NO_x chemistry in the middle atmosphere.

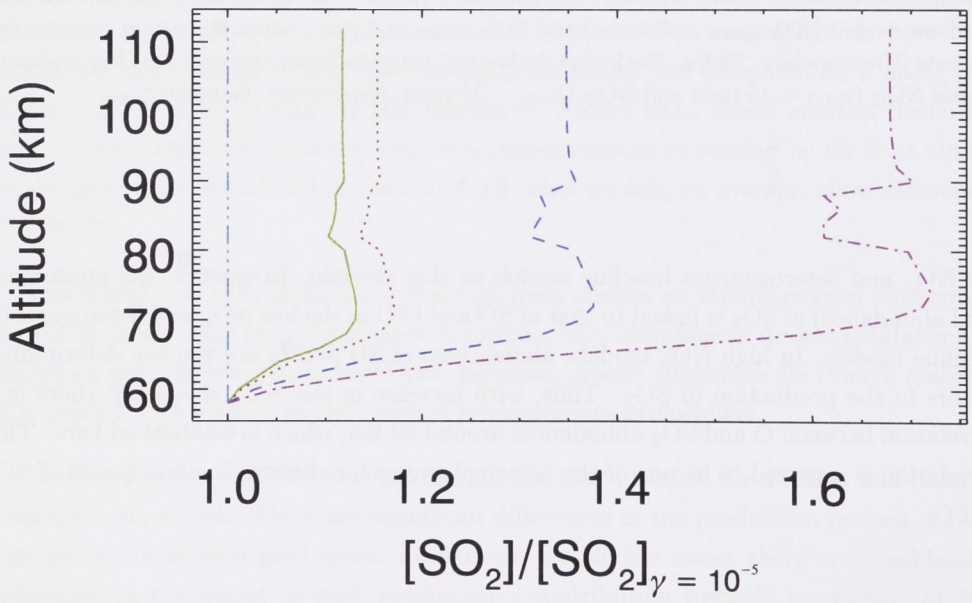

Figure 8.6: SO_2 concentration profile for different μ_{NO}. Light-blue (dash and triple dots) line is the baseline heterogeneous model with no NO_x chemistry ($\mu_{NO} = 0$). Green solid line and red dots represent models NO_A ($\mu_{NO} = 5.5$ ppb) and NO_B ($\mu_{NO} = 7$ ppb), respectively which are within the detected amounts [Krasnopolsky, 2006a]. Dark-blue dashes and magenta (dash and sigle dot) line represent models NO_C ($\mu_{NO} = 15$ ppb) and NO_D ($\mu_{NO} = 30$ ppb), respectively.

Species	Baseline heterogenous (cm^{-2})	Model NO_A (cm^{-2})	Model NO_D (cm^{-2})
CO_2	4.9×10^{24}	4.9×10^{24}	4.9×10^{24}
CO	5.0×10^{18}	5.0×10^{18}	5.2×10^{18}
O	2.2×10^{17}	2.2×10^{17}	2.2×10^{17}
O_2	1.9×10^{18}	1.9×10^{18}	1.8×10^{18}
SO_2	2.2×10^{18}	2.3×10^{18}	2.4×10^{18}
SO	1.3×10^{16}	1.3×10^{16}	1.3×10^{16}
S	5.4×10^{13}	5.3×10^{13}	5.1×10^{13}
ClO	8.2×10^{13}	6.1×10^{13}	3.2×10^{13}
ClCO	2.9×10^{13}	2.9×10^{13}	3.0×10^{13}
$ClCO_3$	5.6×10^{13}	5.3×10^{13}	4.5×10^{13}
Cl	3.4×10^{16}	3.4×10^{16}	3.5×10^{16}
Cl_2	6.0×10^{16}	6.2×10^{16}	6.8×10^{16}
SCl	5.0×10^{13}	5.0×10^{13}	4.8×10^{13}
$ClSO_2$	6.1×10^{15}	6.2×10^{15}	6.5×10^{15}

Table 8.9: Species' column abundances to different atmosphere scenarios. For description of models, see Table 8.4 All calculations included heterogeneous oxidation of CO ($\gamma_{rxn} = 10^{-5}$).

8.2.5 High NO_x models

Greatest impact to modeled atmospheric chemistry from the inclusion of NO_x is seen for high NO_x atmosphere ($\mu_{NO} = 30$ ppb). With significance of heterogeneous chemistry only established theoretically (in this research), modeled O_2 and CO abundances are profiled for baseline heterogeneous ($\gamma_{rxn} = 10^{-5}$) and gasphase atmospheres ($\gamma_{rxn} = 10^{-10}$) for nominal NO_x ($\mu_{NO} = 5.5$ ppb) and high NO_x ($\mu_{NO} = 30$ ppb) input cases (see Figures 8.7 and 8.8). The gasphase model with high NO_x conditions is an attempt to re-create Yung and DeMore [1982] Model B, albeit with revisions in photochemistry and kinetics in the last 25 years [Sander et al., 2006]. The differences between the nominal and high NO_x cases for gasphase atmosphere are nil for CO and approximately factor of 2 at the lower boundary for O_2 concentrations.

8.3 Comparison of models and observations

Most appropriate yardstick to test performance of atmosphere models examined in this research is that of comparsion with observations. Table 8.10 presents Model NO_D output results, along with plausible heterogeneous baseline model ($\gamma_{rxn} = 3 \times 10^{-5}$) from earlier research presented here and Pernice et al. [2004] (gas-phase) model which is currently the standard photochemical model. Reasons behind the choice of model NO_D as the preferred NO_x model to arise from this research project are discussed below.

Decline in O_2 column abundance of 14 % from the baseline gas-phase results suggest

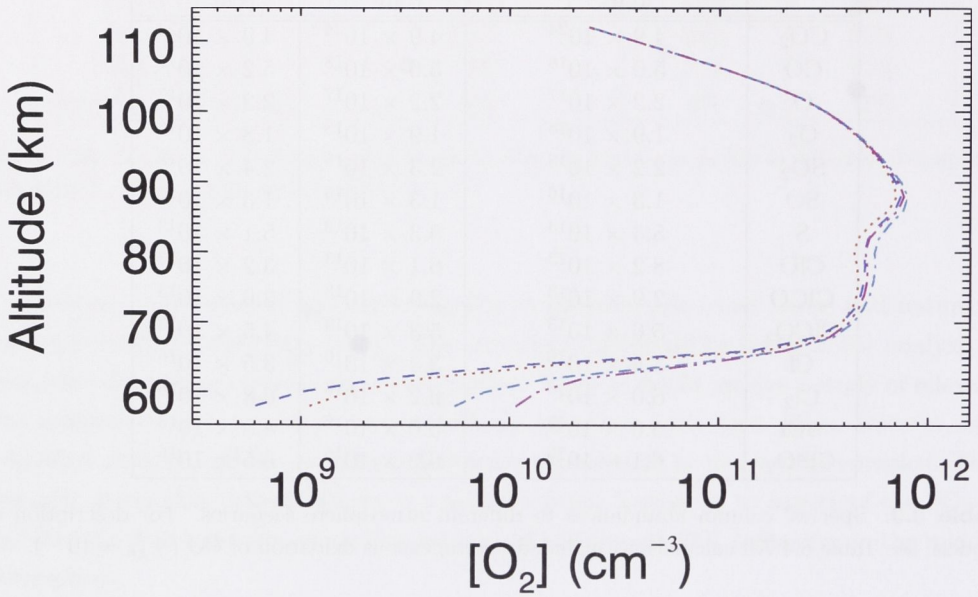

Figure 8.7: O_2 concentration profiles for heterogeneous atmosphere models with different μ_{NO}. Heterogeneous atmosphere models with nominal NO_x and high NO_x are represented by dark-blue dashes and red dots, respectively. Gas-phase atmosphere models with nominal NO_x and high NO_x are represented by light-blue (dash and single dot) and magenta (dash and triple dot) lines, respectively.

a slightly more efficient O_2 sink provided by inclusion of NO_x chemistry to the model. Peak SO concentration and H_2SO_4 column production rate of Model NO_D lie in between standard gasphase and heterogeneous baseline models. The biggest differences are seen for SO_2 species' observational parameters, but all three models lie within the range of uncertainty of temporal variability for the extant observations. Scale height and mixing ratio at 70 km for SO_2, in Model NO_D, are highest of all atmosphere models. This is due to Reaction 27, Table 6.1 (reproduced below) which produces SO_2 at an efficient rate.

$$NO_2 + SO \rightarrow NO + SO_2 \qquad \text{(Rxn 27, Table 6.1)}$$

It is conceded that amount of NO required for Model NO_D is greater than what is observed by Krasnopolsky [2006a], by a factor of 5. It is argued here that this may not be an unreasonable expectation.

Firstly, observations that recommend $\mu_{NO} = 5.5$ ppb were carried over one evening and are of the 'morning terminator' (roughly $\sim$ 6 AM) [Krasnopolsky, 2006a]. Given the heterogeneity observed for other species in the Venus atmosphere (discussed earlier, see

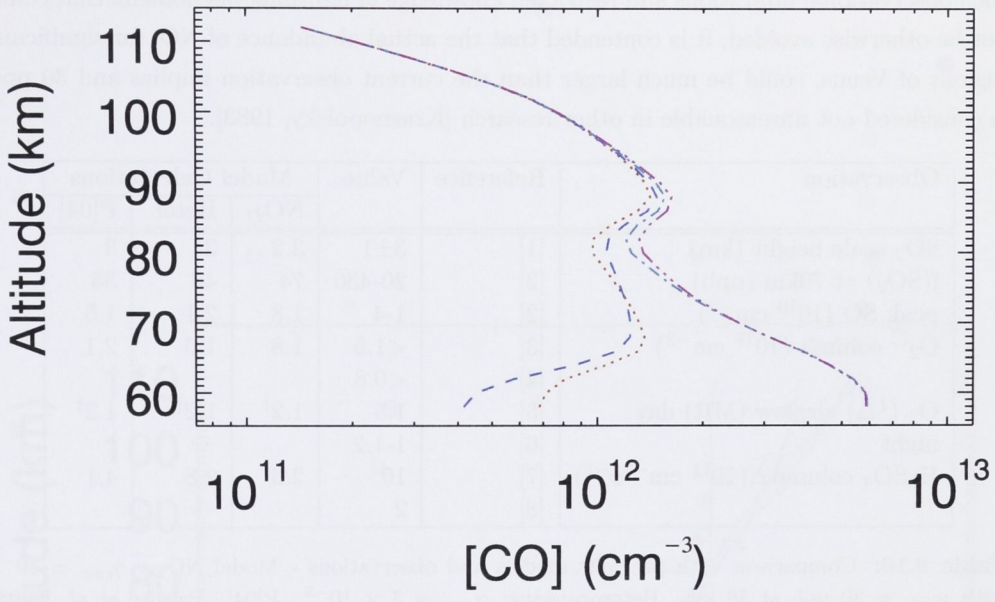

Figure 8.8: CO concentration profiles for heterogeneous atmosphere models with different μ_{NO}. Heterogeneous atmosphere models with nominal NO_x and high NO_x are represented by dark-blue dashes and red dots, respectively. Gas-phase atmosphere models with nominal NO_x and high NO_x are represented by light-blue (dash and single dot) and magenta (dash and triple dot) lines, respectively.

Chapter 4), it is expected for NO to show considerable spatial (latitudinal, longitudinal and altitudinal) variation. In the same research, it is acknowledged that lightning could be the primary source of NO in the lower atmosphere. Activation of lightning reaction in the atmosphere model presents the most accurate means of inclusion of NO_x. The lightning reaction (Reaction 34, Table 6.1, Chapter 6) was not activated in this research due to insufficient knowledge about its kinetics (see Appendix). Instead, NO_x inclusion was carried out through imposition of lower boundary condition for abundance of NO. The immediate drawback of this approach is that, unlike introduction via a reaction like that simulating lightning, NO is not distributed over all altitudes that may be affected by lightning. In fact, NO is consumed close to the lower boundary (58 km) and its impact is thus limited. To accurately model impact of this reaction, the nature of lightning on Venus needs to be investigated with greater rigour and ultimately included in to the photochemical model. The NO_x photochemical scheme utilized in interpretation of observational data consisted of four reactions. Such an over-simplified analysis could have contributed to an error in determination of NO abundance. Production of NO also takes place from the photolysis of NO_2, NO_3, HNO and HNO_2. These reactions would be possible only on the day-side of the planet and Earth-based observations have not been made over a sufficiently broad

range of Venus local times to derive a global average abundance for NO. In the context of such observational limitations and restricted knowledge of lightning phenomena that could not be otherwise avoided, it is contended that the actual abundance of NO, for significant regions of Venus, could be much larger than the current observation implies and 30 ppb is considered not unreasonable in other research [Krasnopolsky, 1983].

Observation	Reference	Value	Model Calculations		
			NO_D	Heter.	P[04]
SO_2 scale height (km)	[1]	3±1	3.2	3	3
f(SO_2) at 70km (ppb)	[2]	20-430	74	46	35
peak SO (10^{10} cm^{-3})	[2]	1-4	1.8	2.1	1.5
$O_2{}^{\square}$ column (10^{18} cm^{-2})	[3]	<1.5	1.8	1.6	2.1
	[4]	<0.8			
O_2 ($^1\Delta$) airglow (MR) day	[5]	1.5	1.2†	1.2†	1.2†
night	[6]	1-1.2			
H_2SO_4 column$^{\diamond}$ (10^{11} $cm^{-2}s^{-1}$)	[7]	10	2.6	2.8	4.1
	[8]	2			

Table 8.10: Comparison with previous models and observations - Model NO_D: $\gamma_{rxn} = 10^{-5}$ with $\mu_{NO} = 30$ ppb at 58 km. Heterogeneous: $\gamma_{rxn} = 3 \times 10^{-5}$. P[04]: Pernice et al. [2004] MR : mega-Rayleigh. † : Diurnally averaged value. $^{\diamond}$: column production rate.$^{\square}$: total column abundance. *Reference notes:* [1]: [Na et al., 1994]; [2]: [Na and Esposito, 1995]; [3]: [Trauger and Lunine, 1983]; [4]: [Krasnopolsky, 2006b]; [5]: [Connes et al., 1979]; [6]: [Crisp et al., 1996]; [7]: [Yung and DeMore, 1982]; [8]: [Winick and Stewart, 1980];

Figure 8.9 compares observations of CO mixing ratio with most plausible models to have developed from research projects presented here. Plausibility of the heterogeneous model (with $\gamma_{rxn} = 3 \times 10^{-5}$) has been discussed earlier (see Chapter 7). Model NO_D, with $\gamma_{rxn} = 10^{-5}$ baseline model with $\mu_{NO} = 30$ ppb at 58 km, is favoured of all the models that have incorporated NO_x chemical scheme. Model NO_D predicts CO abundances that show less discrepancy with the observational data below 70km than the favoured heterogeneous model ($\gamma_{rxn} = 3 \times 10^{-5}$ baseline), as seen in Figure 8.9. However, for Model NO_D to be utilized in future photochemical studies relies on heterogeneous reaction rate, γ_{rxn} to be 10^{-5} and reliable observations of $\mu_{NO} = 30$ ppb near the lower boundary.

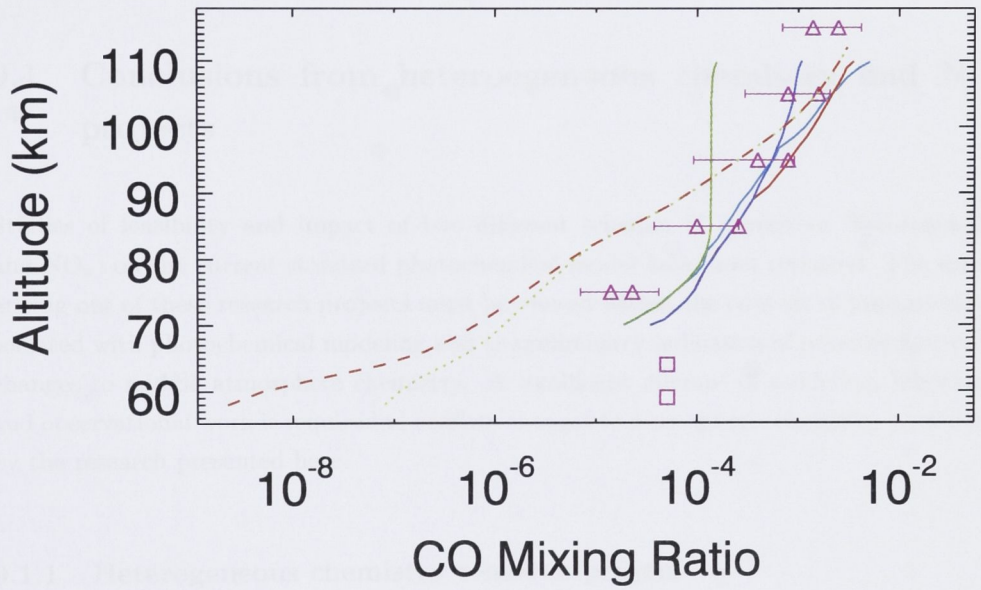

Figure 8.9: CO mixing ratio comparison of models and observations. Clancy and Muhleman [1991] profiles are shown by the four solid lines - dark-blue, red, light-blue and green representing observations made at terminator, anti-solar, 3 AM and 9 AM, respectively, with indicated uncertainties shown for the 3 AM and 9 AM observations. Lellouch et al. [1994] measurements are shown as magenta coloured triangles with indicated uncertainties. The squares (magenta) represent Young [1972] interpretation of Connes et al. [1968] observations. Dashes (red) depict the output from the most plausible heterogeneous model favored by this research ($\gamma_{rxn} = 3 \times 10^{-5}$). Dots (light-green) is the profile from Model NO_D ($\gamma_{rxn} = 10^{-5}$ with $\mu_{NO} = 30$ ppb).

Chapter 9

Conclusions and Future directions

9.1 Conclusions from heteroegeneous chemistry and NO_x projects

Studies of feasibility and impact of two different schemes of chemistry (heterogeneous and NO_x) on the current standard photochemical model have been reported. The results arising out of these research projects must be viewed within the context of limitations associated with photochemical modeling and as preliminary indicators of possible first-order changes to middle atmosphere chemistry. A significant amount of modeling, laboratory and observational work is required to confirm changes to atmospheric chemistry postulated by the research presented here.

9.1.1 Heterogeneous chemistry research project

This research project has managed to include heterogeneous chemistry into the existing middle atmosphere framework. Application of heterogeneous chemistry has been limited to CO_2 production pathways, via aerosol catalytic chemistry. Cloud aerosols, which provide reaction sites for heterogeneous chemistry, have been modeled to the best available observational information. With no existing laboratory data on kinetics governing heterogeneous chemistry for Venus middle atmospheric conditions, this project has successfully established threshold values for heterogeneous reaction rates (γ_{rxn} or reactive uptake coefficient), at altitudes 58 km to 90 km, for heterogeneous processes to be significant producers of CO_2 (ie rate of CO_2 produced by heterogeneous processes and that by gasphase processes are comparable). With adjustments to the kinetics of heterogeneous processes (ie variations to γ_{rxn}), standard (gasphase) middle atmosphere model is modified to one that is dominated by heterogeneous chemistry. $\gamma_{rxn} = 10^{-10}$, where heterogeneous chemistry is insignificant, represents a gasphase atmosphere model and is used as a representation of the current photochemical model [Pernice et al., 2004] for purposes of this study. In $\gamma_{rxn} = 10^{-4}$ and $\gamma_{rxn} = 10^{-5}$ atmosphere models, more than 30 % of total atmospheric CO_2 production is via heterogeneous pathways and both models are used to represent differing

degrees of heterogeneous dominant atmospheres.

This has been a pilot study to gauge the impact of heterogeneous mechanisms in the Venus middle atmosphere. The impact is assessed with respect to changes in species' abundances and reaction rates (production and loss). This research was limited to investigation of heterogeneous CO_2 production pathways' impact, but heterogeneous chemistry may play a much wider role in middle atmosphere chemistry through facilitation of other reactions.

Initial results for an atmosphere model with $\gamma_{rxn} = 10^{-4}$ indicates that heterogeneous mechanisms account for 45 % to 100 % of total CO_2 produced below 90km. An immediate effect from addition of heterogeneous processes (schematic reaction: CO + O + aerosol $\rightarrow$ CO_2 + aerosol) was noted in the vastly decreased ($\sim$ three orders of magnitude) modeled CO (carbon monoxide) abundances, near the lower middle atmosphere boundary. All changes caused by heterogeneous chemistry are restricted to below 90km, the altitude at which the aerosol haze terminates.

Atomic oxygen (O), another species to be directly consumed by heterogeneous processes, varies by up to 70 % of its gasphase abundances. However, the reactivity of O (via gasphase chemical processes) is high and is not affected as much by heterogenoeus processes. Previous modeling studies of the Venus middle atmosphere have not been able to reconcile efficient production of CO_2 and the O_2 column abundances to remain below the observational upper limit. $\gamma_{rxn} = 10^{-4}$ is the first reported photochemical model to successfully predict an O_2 column abundance that is in agreement with the limit suggested by Trauger and Lunine [1983]. However, a recent interpretation of Trauger and Lunine [1983] has halved this upper limit [Krasnopolsky, 2006b].

	γ value	oxygen column abundance (molecules cm^{-2})
Gasphase	10^{-10}	2.1×10^{18}
Heter.	10^{-5}	1.9×10^{18}
Heter.	10^{-4}	1.1×10^{18}
Observation	[Trauger and Lunine, 1983]	$< 1.5 \times 10^{18}$
Observation	[Krasnopolsky, 2006b]	$< 8 \times 10^{17}$

Table 9.1: Oxygen column abundances from this research (selected γ values) and observation by Trauger and Lunine [1983] and recent interpretation by Krasnopolsky [2006b].

The greatest differences in modeled O_2 abundances ($\sim$ three orders of magnitude) are seen near 68 km, where the $\gamma_{rxn} = 10^{-4}$ atmosphere model O_2 concentration profile deviates from an otherwise monotonic profile. Non-monotony in modeled O_2 abundance is due to increased roles played by atomic sulphur (S) in destruction of O_2 (via S + O_2 $\rightarrow$ SO + O) and sulphur dioxide (SO_2) in prodution of O_2 (via SO_2 + hν $\rightarrow$ S + O_2). Addition of heterogeneous chemistry leads to reduction in rates of O_2 production and loss at 68 km, which in turn enables S and SO_2 to influence O_2 production and loss. Changes

to other species' abundances and reaction rates were studied for $\gamma_{rxn} = 10^{-4}$ and $\gamma_{rxn} = 10^{-10}$ models (heterogeneous and gasphase atmospheres, respectively).

Modeled SO_2 abundances for $\gamma_{rxn} = 10^{-4}$ increase by 40 %, averaged over all altitudes, compared to standard gasphase atmosphere ($\gamma_{rxn} = 10^{-10}$). Near 68 km, the difference is around 60 %, due to an increased production of SO_2 by SO (sulphur monoxide) and O (via SO + O + CO_2 → SO_2 + CO_2), which are formed from destruction of O_2 at this region. Non-monotonic variations in SO_2 abundances are found to be complimentary to that of O and indicated a correlation between abundances of the two species. The profile of SO abundances, for $\gamma_{rxn} = 10^{-4}$, shows similar altitudinal correlation to SO_2, but with pronounced variations in abundances. Another consequence of heterogeneous chemistry was advancement of conversion rate between SO and $(SO)_2$ (SO dimer) leading to rapid exchange between the two species. Changes to production and loss of SO_2 and SO, upon inclusion of heterogeneous chemsitry, took place at the expense of reduced ClO involvement. Role of ClO in destruction of SO and production of SO_2 (via ClO + SO → SO_2 + Cl) is greatly reduced in heterogeneous dominated $\gamma_{rxn} = 10^{-4}$ atmosphere. Cumulatively, this leads to the development of an inter-dependence relationship between O_2, SO, SO_2 and O. This results in an increase in the abundances of SO and SO_2.

Mechanisms and their contributions to production and loss of ClCO are unchanged from addition of heterogeneous chemistry, despite significant changes to CO abundances. ClCO production and loss rates are higher (by few orders of magnitude, on average) than heterogeneous reaction rates and close chemical relationship between ClCO and CO is unaffected by changes to CO. However, ClCO is no longer the chief producer of Cl and Cl is no longer lost primarily to ClCO. The interchange between these two species (Cl + CO ↔ ClCO) slows down upon addition of heterogeneous pathways. This, in turn reduces the abundances of Cl and ClCO. $ClCO_3$ production (via ClCO + O_2 + M → $ClCO_3$ + CO_2) is not affected by introduction of heterogeneous chemistry. $ClCO_3$ loss via reaction with Cl ($ClCO_3$ + Cl → ClO + Cl + CO_2) and SO ($ClCO_3$ + SO → Cl + SO_2 + CO_2) changes considerably, due to increase in SO and decline in Cl abundances at 68 km. Consequently, $ClCO_3$ abundances decrease substantially at 68 km. Little or no changes to production and loss of SCl and $ClSO_2$ are caused by heterogeneous chemistry.

Amidst individual changes to species' concentrations and reaction rates, from addition of heterogeneous chemistry, investigation of selected chlorine (ClO_x) and sulphur (SO_x) species reveales consolidated growth in sulphur species and decline in chlorine species, at 68 km and in total column abundances.

In presence of an additional efficient CO oxidation scheme, middle atmosphere was likely to contain reduced abundances of O_2 and CO over all altitudes. Subsequently, changes to one or both species result in greater abundance of sulphur species and decline in chlorine species. In previous modeling, chlorine compounds are integral to CO_2 re-

formation in the gasphase atmosphere via catalytic proceses that involved ClCO and $ClCO_3$ as intermediates. With the inclusion in the model of the heterogeneous pathways that are effective in producing CO_2, chlorine-catalytic processes in the model become relatively less important, while the predicted abundances of sulphur and chlorosulphane compounds increase.

Standard, purely gasphase photochemical model has undergone changes to key reaction kinetics that are yet to be verified in the laboratory. This research utilizes this model ("baseline"). In light of the model including such experimentally unconfirmed changes to chemical kinetics, a model with kinetics set to nominal laboratory values ("nominal") is also investigated. Large differences between modeled and observed CO abundances along with significant uncertainties in OCS abundances motivated examination of model with nominal laboratory values and higher OCS abundance at the lower boundary than previously modeled ("nominal high OCS") for $\gamma_{rxn} = 10^{-4}$ and $\gamma_{rxn} = 10^{-5}$ atmospheres. Thus, nominal and nominal high OCS models serve as alternative models to assess changes caused by heterogeneous processes to O_2 and CO abundances in heterogeneous dominant atmospheres. Nominal and nominal high OCS models show negligible differences to the baseline model in the case of $\gamma_{rxn} = 10^{-4}$. For $\gamma_{rxn} = 10^{-5}$, considerable variations (between factor of 3 – 10) between nominal and baseline models emerged for CO and O_2 abundances below 90 km. Nominal high OCS model shows an marginal increase in CO abundance at the lower boundary compared to nominal model. Nominal and nominal high OCS models of $\gamma_{rxn} = 10^{-5}$ displayed best agreement with CO observations amongst all heterogeneous atmosphere models but O_2 total column abundance of the models was double that of baseline model. Large difference in modeled O_2 column abundances for nominal and nominal high OCS models contributed to their abandonment from further examination here. $\gamma_{rxn} = 3 \times 10^{-5}$ atmosphere model contained smallest O_2 abundances for least disagreement with CO observational abundances, and is recommended as the model with greatest consistency to available observational and known laboratory data by this research.

9.1.2 NO_x chemistry

Odd nitrogen compounds (NO_x) chemistry had been discarded since early photochemical models as an effective and integral chemical scheme in favour of chlorine compounds (ClO_x) when the efficiency of ClO_x was shown in re-combination schemes of CO_2 and the evidence for significant amounts of reactive NO_x in Venus remained controversial. Recent observational evidence of NO in the lower boundary of the middle atmosphere [Krasnopolsky, 2006a] along with unverified aspects of current middle atmosphere chemical kinetics motivated inclusion and studies of NO_x chemistry. This research project successfully adapted a scheme of NO_x chemistry (59 total reactions and 12 species) into the standard photochemical model. Observational studies suggested $\mu_{NO} = 5.5$ ppb at

the lower boundary (58 km). Modeling this nominal observational NO abundance with the heterogeneous chemical scheme $\gamma_{rxn} = 10^{-5}$ and $\gamma_{rxn} = 10^{-10}$ produces relatively marginal differences to modeled CO and O_2 abundances.

With the quantity of NO prescribed by observational studies failing to effect significant changes to atmospheric chemistry, this research modeled progressively higher abundances of NO – from 0 ppb (baseline heterogeneous with no NO_x) to 30 ppb for $\gamma_{rxn} = 10^{-5}$ atmosphere. $\gamma_{rxn} = 10^{-5}$ atmosphere model was used to investigate the combined effects of heterogeneous and nitrogen chemistries. On comparison, high NO_x models ($\mu_{NO} \geq$ 15 ppb) showed greater modeled O_2 and CO abundances near the lower boundary and smaller O_2 and CO abundances around 82 km.

Increase in μ_{NO} from 5.5 ppb to 30 ppb doubled O_2 production rates at 58 km. Rates for Reaction: $NO + O_3 \rightarrow NO_2 + O_2$ increase by factor of three and result in greater O_2 for high NO_x models. CO abundances increased by ~100 % at 58 km for $\mu_{NO} =$ 30 ppb, compared to low NO_x ($\mu_{NO} \leq 7$ ppb) model, due to relative decrease in rates of heterogeneous reactions. Heterogeneous processes are effective CO sinks and relative decline in their rates reduce CO loss and contribute towards an increased CO abundance. Near 82 km, rate of heterogeneous processes were found to increase with μ_{NO} which resulted in reduced CO abundances.

Atomic oxygen (O) abundances increased at 60 km and 82 km and decreased at 68 km with increase in μ_{NO}, for $\gamma_{rxn} = 10^{-5}$ atmosphere models. Near 60 km, O abundances are larger (factor of 100) for high NO_x models due to suppressed efficiency of heterogenous processes and increased SO_2 abundances. Significant amount of O was converted to SO_2 (via $ClSO_2 + O \rightarrow SO_2 + ClO$) and photolysis of SO_2 produced O ($SO_2 + h\nu \rightarrow SO +$ O). Near 68 km, O is primarily lost to NO_2 ($NO + O + CO_2 \rightarrow NO_2 + CO_2$) in the high NO_x models and NO_2 did not photodissociate efficiently to produce O. At 82 km, O is mainly lost to CO_2 and SO_2 for high NO_x models. Increased rate of SO_2 photodissociation resulted in higher O abundances at this altitude.

SO_2 abundances for high NO_x models are larger than low NO_x models. Production of SO_2 in high NO_x models is dominated by reactions of SO with O ($SO + O + CO_2 \rightarrow SO_2$ + CO_2) and not with ClO ($SO + ClO \rightarrow SO_2 + Cl$), as in the case of low NO_x models. This established strong correlation between O and SO_2 abundances in high NO_x models, examination of which was not within intended parameters of the project.

Amongst all NO_x models, $\mu_{NO} = 30$ ppb effected most significant increases to CO abundances for baseline heterogeneous $\gamma_{rxn} = 10^{-5}$ atmosphere model. Heterogeneous atmosphere models are plagued by problem of reduced CO abundances and addition of NO_x chemical scheme helped reduce disagreement with observational CO measurements to some extent. However, it remains that the acceptance of high NO_x model relies strongly on observation of high but not improbable quantities of NO at 58 km and a strong het-

erogeneous involvement ($\gamma_{rxn} = 10^{-5}$).

9.2 Proposed revisions and inclusions to current model

The results from inclusion of heterogeneous and NO_x chemical schemes have been discussed. Heterogeneous baseline ($\gamma_{rxn} = 3 \times 10^{-5}$) model and heterogeneous ($\gamma_{rxn} = 10^{-5}$) model with $\mu_{NO} = 30$ ppb, from each research project, showed best agreement with observational results. The plausibility of both models has been assessed by comparison with earlier models and known data from observations.

Heterogeneous chemistry was shown to be an effective means for CO_2 re-combination for $\gamma_{rxn} \geq 10^{-5}$. This research project used a simple schematic reaction and established potential role played by heterogeneous chemistry. In reality, this mechanism is expected to be much more complex and possibly involve photodissociated ions. Modeled heterogeneous chemistry (processes) provided sinks for O_2 and efficient oxidation mechanism for CO. It may not be unreasonable to expect sulphuric acid cloud aerosols to provide sites for heterogeneous reactions to proceed at effective rates. Follow up laboratory work is required to verify modeled chemistry and confirm proposed pathways. If $\gamma_{rxn} \geq 10^{-5}$ from laboratory studies, then heterogeneous chemistry must be included in all future modeling with respect to CO_2 production in Venus middle atmosphere.

Preliminary results of NO_x chemistry on the heterogeneous ($\gamma_{rxn} = 10^{-5}$) model were assessed for changes to species' abundances and CO_2 chemistry. Inclusion of NO_x chemical scheme was based on positive confirmation of NO near the lower boundary. Substantial observational work on NO_x abundances and lightning is necessary to accurately model the impact of NO_x chemical scheme. The observationally recommended value of NO mixing ratio at the lower boundary effected little or no change to the heterogeneous ($\gamma_{rxn} = 10^{-5}$) atmosphere model. High NO abundances, such as $\mu_{NO} = 30$ ppb, significantly altered modeled CO mixing ratio of $\gamma_{rxn} = 10^{-5}$ near the lower boundary. Inclusion of high NO abundances would depend on confirmed observational results on lightning and NO_x species.

9.3 Future work

With advancement in laboratory knowledge of chemistry and observational discovery of key species or validation of processes, the methodology from the two research projects will provide a comprehensive template for future additions and revisions to existing chemistry in the photochemical model. The standard one-dimensional photochemical model is capable of production of first-order results and analysis of overall chemistry. To achieve

greater reliability on results, Venus middle atmosphere photochemical model must include information on wind and transport of chemical species around the planet. Evolution to a two-dimensional model will add robustness to model results and provide accurate depiction of differences between sunlit and night sides of Venus.

Certain chemical species and processes that are critical to the Venus middle atmosphere are yet to be studied in laboratory environment. Laboratory studies are necessary to ascertain reactivity and stability of key species. Reactions that require imminent laboratory verification are specified elsewhere [Mills, 1998]. Formation and decomposition reactions of $ClCO_3$ and ClCO need to be assessed for kinetics and uncertainties. Heterogeneous processes' kinetics need to be reproduced under Venus middle atmospheric conditions to study chemical viability. Quantification of heterogeneous reaction rates is integral to inclusion and implementation of heterogeneous chemistry. Results from this research have indicated potential increase in influence of sulphur compounds under reduced O_2 conditions and greater inter-group interaction between sulphur and chlorine compounds. Both claims need to be investigated further to understand greater chemical interplay at work.

Observational results from Venus Express mission of aerosol properties' measurements will help constrain heterogeneous chemistry model further. Observational profiles of key species' (O_3, CO, SO_2) abundances are essential for future development of photochemical model.

Initial results from Venus Express have indicated the presence of lightning. Detailed information on frequency (rate) and extent (spatial) of lightning process along with information on NO_x species are necessary to gauge true impact of NO_x schemes. In NO_x research project, NO_x chemistry was activated by addition of NO to the middle atmosphere lower boundary. An alternative method is to include a reaction to simulate lightning and assess the rate of lightning that is required to produce postulated amount of NO. Advantage of activation of lightning reaction is the non-localization of NO_x. In comparison, introduction of NO as lower boundary condition restricts its impact to a specific region. NO_x photochemical modeling did not include temperature dependent NO_x photodissociation reactions. Instead, photolysis and branching ratios of NO_x species utilized values from the temperature closest to Venus middle atmosphere conditions. Nominal rates were assumed for HNO photolysis in the absence of laboratory data. Use of laboratory verified photodissociation information would constrain the photochemical model further.

This research has investigated interplay and impact of two distinct schemes of chemistry within the middle atmosphere model. Influences that are external to the middle atmosphere (such as surface-atmosphere interaction, species' exospheric escape) have not been considered and limit the accuracy of the model. Synchronization of middle atmosphere with the lower and upper atmospheres would alleviate such shortcomings.

Bibliography

D. A. Allen and J. W. Crawford. Cloud structure on the dark side of Venus. *Nature*, 307:222–224, January 1984.

M. A. Allen, Y. L. Yung, and J. W Waters. Vertical transport and photochemistry in the terrestrial mesosphere and lower thermospehere. *Journal of Geophysical Research*, 86:3617–3627, 1981.

J.-L. Bertaux, T. Widemann, A. Hauchecorne, V. I. Moroz, and A. P. Ekonomov. VEGA 1 and VEGA 2 entry probes: An investigation of local UV absorption (220-400 nm) in the atmosphere of Venus (SO_2, aerosols, cloud structure). *Journal of Geophysical Research*, 101:12709–12746, 1996.

B. Bézard, D. de Bergh, C.and Crisp, and J. P. Maillard. The deep atmosphere of Venus revealed by high-resolution nightside spectra. *Nature*, 345:508–510, 1990.

S. Borrmann, S. Solomon, J. E. Dye, and B. Luo. The potential of cirrus clouds for heterogeneous chlorine activation. *Geophysical Research Letters*, 23:2133–2136, 1996.

W. L. Chameides, J. C. G. Walker, and A. F. Nagy. Possible chemical impact of planetary lightning in the atmospheres of Venus and Mars. *Nature*, 280:820–822, 1979.

W. Choi and M.-T. Leu. Kinetics of the heterogeneous reaction CO+O on inorganic oxide and water ice surfaces: Implications for the Martian atmosphere. *Geophysical Research Letters*, 24:2957–2960, December 1997.

R. T. Clancy and D. O. Muhleman. Long-term changes in the thermal, dynamical, and compositional structure of the Venus mesosphere as inferred from microwave spectral line observations of ^{12}CO, ^{13}CO and $C^{18}O$. *Icarus*, 89:129–146, 1991.

P. Connes, J. Connes, L. D. Kaplan, and W. S. Benedict. Carbon monoxide in the Venus atmosphere. *Astrophysical Journal*, 152:731–743, June 1968.

P. Connes, J. F. Noxon, W. A. Traub, and N. P. Carleton. $O_2 1\ \Delta$ emission in the day and night airglow of Venus. *Astrophysical Journal*, 233:L29–L32, October 1979.

R. A. Cox, R. G. Derwent, A. E. J. Eggleton, and H. J. Reid. Kinetics of Chlorine Oxide Radicals using Modulated Photolysis. *Journal of Chemical Society Faraday Transactions*, 75:1648–1666, 1979.

D. Crisp, V. S. Meadows, B. Bézard, C. de Bergh, J. P. Maillard, and F. P. Mills. Ground-based near-infrared observations of the Venus nightside: 1.27-μm $_2(a\Delta_g)$ airglow from the upper atmosphere. *Journal of Geophysical Research*, 101:4577–4594, 1996.

A. Dalgarno, J. F. Babb, and Y. Sun. Radiative association in planetary atmospheres. *Planetary and Space Science*, 40:243–246, March 1992.

C. de Bergh, V. I. Moroz, F. W. Taylor, D. Crisp, B. Bézard, and L. V. Zasova. The composition of the atmosphere of Venus below 100 km altitude. *Planetary and Space Science*, 54:1389–1397, 2006.

W. B. DeMore, S. P. Sander, D. M. Golden, R. F. Hampson, M. J. Kurylo, C. J. Howard, A. R. Ravishankara, C. E. Kolb, and M. J. Molina. *Chemical kinetics and photochemical data for use in stratosphere modeling: Evaluation Number 12*, 1997.

W. B. DeMore and Y. L. Yung. Catalytic Processes in the Atmospheres of Earth and Venus. *Science*, 217:1209–1213, 1982.

L. W. Esposito, R. G. Knollenberg, O. B. Marov, M. Ia. Toon, and R. P. Turco. The clouds and hazes of Venus. In *Venus*, pages 484– 564. University of Arizona, 1983.

J. L. Fox. Models for aurora and airglow emissions from other planetary atmospheres. *Canadian Journal of Physics*, 64:1631–1656, December 1986.

D. M. Golden and L. R. Williams. *Heterogeneous chemistry and kinetics.* Springer-Verlag, 1994.

R. F. Hampson. *Chemical kinetic and photochemical data sheets for atmospheric reactions Report No. FAA-EE-80-17* , 1980.

R. F. Hampson and D. Garvin. *Reaction Rate and Photochemical Data for Atmospheric Chemistry - 1977* , 1978.

J. E. Hansen and J. W. Hovenier. Interpretation of the polarization of Venus. *Journal of Atmospheric Sciences*, 31:1137–1160, 1974.

J. H. Hu, Q. Shi, P. Davidovits, D. R. Worsnop, M. S. Zahniser, and C. E. Kolb. Reactive uptake of Cl_2 and Br_2 by aqueous surfaces as a function of Br^- and I^- ion concentration: The effect of chemical reaction at the interface. *Journal of Physical Chemistry*, 99:8768–8766, 1995.

J. T. Jayne, D. R. Worsnop, C. E. Kolb, E. Swartz, and P. Davidovits. Uptake of gas-phase formaldehyde by aqueous acid surfaces. *Journal of Physical Chemistry*, 100: 8015–8022, 1996.

F. Kaufman. Elementary gas reactions. *Annual Reviews of Physical Chemistry*, 20:45–90, 1969.

F. Kaufman. Kinetics of thermal gas reactions with application to stratospheric chemistry. *Annual Reviews of Physical Chemistry*, 30:411–442, 1979.

R. G. Knollenberg and D. M Hunten. Clouds of Venus : A preliminary assessment of microstructure. *Science*, 205:70–74, 1979.

R. G. Knollenberg and D. M Hunten. The microphysics of the clouds of Venus: Results of the Pioneer Venus size spectrometer experiment. *Journal of Geophysical Research*, 85: 8039–8058, 1980.

V. A. Krasnopolsky. Lightnings and nitric oxide on Venus. *Planetary and Space Science*, 31:1363–1369, 1983.

V. A. Krasnopolsky. A sensitive search for nitric oxide in the lower atmospheres of Venus and Mars: Detection on Venus and upper limit for Mars. *Icarus*, 182:80–91, May 2006a.

V. A. Krasnopolsky. Chemical composition of Venus atmosphere and clouds: Some unsolved problems. *Planetary and Space Science*, 54:1352–1359, November 2006b.

V. A. Krasnopolsky and V. A. Parshev. Chemical composition of the atmosphere of Venus. *Nature*, 292:610–613, 1981a.

V. A. Krasnopolsky and V. A. Parshev. Photochemistry of Venus' atmosphere at altitudes over 50 km. *Kosmicheskie Issledovaniya*, 19:87–104, 1981b.

S. Kumar, D. M. Hunten, and H. A. Taylor. H2 abundance in the atmosphere of Venus. *Geophysical Research Letters*, 8:237–240, March 1981.

E. Lellouch, J. J. Goldstein, J. Rosenqvist, S. W. Bougher, and G. Paubert. Global circulation, thermal structure, and carbon monoxide distribution in Venus' mesosphere in 1991. *Icarus*, 110:315–339, August 1994.

M-T. Leu and Y. L. Yung. Determination of $O_2(a^1\Delta_g)$ and $O_2(b^1\Sigma_g^+)$ yields in the reaction O + ClO $\rightarrow$ Cl + O_2: Implications for photochemistry in the atmosphere of Venus. *Geophys. Res. Lett.*, 9:949–952, 1987.

E. Marcq, B. Bézard, T. Encrenaz, and M. Birlan. Latitudinal variations of CO and OCS in the lower atmosphere of Veus from near-infrared nightside spctro-imaging. *Icarus*, 179: 375–385, December 2005.

M. B. McElroy, M. B. Prather, and J. M. Rodriguez. Escape of hydrogen from Venus. *Science*, 215:1614–1615, 1982.

M. B. McElroy, N. D. Sze, and Y. K. Yung. Photochemistry of the Venus atmosphere. *Journal of the Atmospheric Sciences*, 30:1437–1447, 1973.

M. Mendillo, A. Nagy, and J. H. Waite. *Atmospheres in the solar system: comparative aeronomy*. Atmospheres in the Solar System: Comparative Aeronomy, 2002.

C. T. Mills and L. F. Phillips. Photo-oxidation of CO in a sulphuric acid aerosol. *Journal of Photochemistry and Photobiology*, 74:7–9, 1993.

C. T. Mills, G. A. Rowland, J. Westergren, and L. F. Phillips. Quantum yields of CO_2 and SO_2 formation from 193nm photo-oxidation of CO in a sulphuric acid aerosol. *Journal of Photochemistry and Photobiology*, 93:83–87, 1996.

F. P. Mills. *I. Observations and photochemical modeling of the Venus middle atmosphere. II. Thermal infrared spectroscopy of Europa and Callisto.* PhD thesis, 1998.

F. P. Mills. A spectroscopic search for molecular oxygen in the Venus middle atmosphere. *Journal of Geophysical Research*, 104:30757–30763, 1999.

F. P. Mills and M. A. Allen. A review of selected issues concerning the chemistry in Venus' middle atmosphere. *Planetary and Space Science*, 2007.

C. Y. Na and L. W. Esposito. UV Observation of Venus with HST. In *Bulletin of the American Astronomical Society*, volume 27 of *Bulletin of the American Astronomical Society*, pages 1071–+, June 1995.

C. Y. Na, L. W. Esposito, W. E. McClintock, and C. A. Barth. Sulfur dioxide in the atmosphere of Venus. 2: Modeling results. *Icarus*, 112:389–395, December 1994.

H. Nair, M. A. Allen, A. D. Anbar, Y. L. Yung, and R. T. Clancy. Photochemical model of the Martian atmosphere. *Icarus*, 111:124–150, 1994.

H. Neckel and D. Labs. The solar radiation between 3300 and 12500 A. *Solar Physics*, 90:205–258, February 1984.

J. M. Nicovich, K. D. Kreutter, and P. H. Wine. Kinetics and thermochemistry of ClCO formation from the Cl+CO association reaction. *Journal of Chemical Physics*, 92:3539–3544, March 1990.

V. I. Oyama, G. C. Carle, F. Woeller, S. Rocklin, J. Vogrin, W. Potter, G. Rosiak, and C. Reichwein. Pioneer Venus Sounder Probe gas chromatograph. *IEEE Transactions on Geoscience and Remote Sensing*, 18:85–93, 1980.

H. Pernice, P. Garcia, H. Willner, J. S. Francisco, F. P. Mills, M. Allen, and Y. L. Yung. Laboratory evidence for a key intermediate in the Venus atmosphere: Peroxychloroformyl radical. *Proceedings of the National Academy of Science*, 101:14007–14010, September 2004.

J. B. Pollack, O. B. Toon, R. C. Whitten, R. Boese, B. Ragent, M. Tomasko, L. Eposito, L. Travis, and D. Wiedman. Distribution and source of the UV absorption in Venus' atmosphere. *Journal of Geophysical Research*, 85:8141–8150, December 1980.

R. G. Prinn. Photochemistry of HCl and other minor constituents in the atmosphere of Venus. *Journal of Atmospheric Scienes*, 28:1058–1068, 1971.

R. G. Prinn. Venus: Composition and structure of the visible clouds. *Science*, 182(4117): 1132–1135, 1973.

R. G. Prinn. Venus - Chemical and dynamical processes in the stratosphere and mesosphere. *Journal of Atmospheric Scienes*, 32:1237–1247, 1975.

R. G. Prinn. Venus - Chemistry of the lower atmosphere prior to the Pioneer Venus mission. *Geophysical Research Letters*, 5:973–976, November 1978.

O. F. Raper and W. B. DeMore. Reaction of electronically exicted O_2 with CO. *Journal of Chemical Physics*, 40:1047–1052, 1964.

R. D. Richtmyer and K. W. Morton. *Difference methods for initial value problems.* John Wiley and Sons, 1967.

P. B. Roussel and R. A. Back. Photolysis of CO at 193nm. *Journal of Photochemistry and Photobiology*, 46:159–165, 1989.

G. A. Rowland and L. F. Phillips. Cloud photochemistry and its effect on the composition of the upper atmosphere of Venus. *Geophysical Research Letters*, 27:3301–3304, 2000.

G. A. Rowland, R. van Eldik, and L. F. Phillips. Photochemistry of concentrated sulfuric acid in the presence of SO_2 and Fe(II), and implications for the cloud chemistry. *Journal of Photochemistry and Photobiology A:Chemistry*, 153:1–10, 2002.

C. T. Russell, T. L. Zhang, M. Delva, W. Magnes, R. J. Strangeway, and H. Y. Wei. Lightning on Venus inferred from whistler-mode waves in the ionosphere. *Nature*, 450: 661–662, 2007.

S. P. Sander, D. M. Golden, M. J. Kurylo, A. R. Ravishankara, C. E. Kolb, and M. J. Molina. *Chemical kinetics and photochemical data for use in stratosphere modeling: Evaluation Number 14*, 2002.

S. P. Sander, D. M. Golden, M. J. Kurylo, A. R. Ravishankara, C. E. Kolb, and M. J. Molina. *Chemical kinetics and photochemical data for use in stratosphere modeling: Evaluation Number 14*, 2006.

F. P. Schloerb, S. E. Robinson, and W. M. Irvine. Observations of CO in the stratosphere of Venus via its J = 0 - 1 rotational transition. *Icarus*, 43:121–127, August 1980.

A. Seiff. *Thermal structure of the atmosphere of Venus*, pages 215–279. Venus, 1983.

A. Seiff, D. B. Kirk, S. C. Sommer, R. E. Young, R. C. Blanchard, D. W. Juergens, J. E. Lepetich, P. F. Intrieri, and J. S. Derr. Structure of the atmosphere of Venus up to 110 kilometers - Preliminary results from the four Pioneer Venus entry probes. *Science*, 203: 787–790, February 1979.

S. Solomon, S. Borrmann, R. R. Garcia, R. W. Portmann, L. Thomason, L. R. Poole, D. Winker, and M. P. McCormick. Heterogeneous chlorine chemistry in the tropopause region. *Journal of Geophysical Research*, 102:21411–21429, 1997.

S. Solomon, R. R. Garcia, F. S. Rowland, and D. J. Wuebbles. On the depletion of Antartic ozone. *Nature*, 321:755–758, 1986.

A. I. F. Stewart, J.-C. Gerard, D. W. Rusch, and S. W. Bougher. Morphology of the Venus ultraviolet night airglow. *Journal of Geophysical Research*, 85:7861–7870, December 1980.

W. L. Taylor, F. L. Scarf, C. T. Russell, and L. H. Brace. Evidence for lightning on Venus. *Nature*, 279:614–616, 1979.

W. A. Traub and N. P. Carleton. A Search for H_2O and O_2 on Venus. *Bulletin of the American Astronomical Society*, 5:299–+, March 1973.

W. A. Traub and N. P. Carleton. Observation of O_2, H_2O, and HD in planetary atmospheres. In A. Woszczyk and C. Iwaniszewska, editors, *Exploration of the Planetary System*, pages 223–228. Reidel, Dordrecht, The Netherlands, 1974.

J. T. Trauger and J. I. Lunine. Spectroscopy of molecular oxygen in the atmospheres of Venus and Mars. *Icarus*, 55:272–281, August 1983.

U. von Zahn, S. Kumar, H. Niemann, and R. Prinn. *Composition of the Venus atmosphere*. Venus, 1983.

A. J. Watson, T. M. Donahue, D. H. Stedman, R. G. Knollenberg, B. Ragent, and J. Blamont. Oxides of nitrogen and the clouds of Venus. *Geophysical Research letters*, 6: 743–746, 1979.

W. J. Wilson, M. J. Klein, R. K. Kahar, S. Gulkis, E. T. Olsen, and P. T. P. Ho. Venus. I - Carbon monoxide distribution and molecular-line searches. *Icarus*, 45:624–637, March 1981.

J. R. Winick and A. I. F. Stewart. Photochemistry of SO2 in Venus' upper cloud layers. *Journal of Geophysical Research*, 85:7849–7860, December 1980.

T. N. Woods, D. K. Prinz, G. J. Rottman, J. London, P. C. Crane, R. P. Cebula, E. Hilsenrath, G. E. Brueckner, M. D. Andrews, O. R. White, M. E. VanHoosier, L. E. Floyd, L. C. Herring, B. G. Knapp, C. K. Pankratz, and P. A. Reiser. Validation of the UARS solar ultraviolet irradiances: Comparison with the ATLAS 1 and 2 measurements. *Journal of Geophysical Research*, 101:9541–9570, April 1996.

S. J. Wrenn, L. J. Butler, G. A Rowland, C. J. H. Knox, and L. F. Phillips. The necessity for multiphoton processes in the 193-nm photochemistry of sulphuric acid aerosols. *Journal of Photochemistry and Photobiology*, 129:101–104, 1999.

L. D. G. Young. High resolution spectra of Venus- A review. *Icarus*, 17:632–658, 1972.

Y. L. Yung and W. B. DeMore. Photochemistry of the stratosphere of Venus - Implications for atmospheric evolution. *Icarus*, 51:199–247, 1982.

Appendix for Heterogeneous and Nitrogen modeling

Altitude (km)	Temperature (K)	[CO] (cm^{-3})	CO_2 prod ($10^{12} cm^{-3} s^{-1}$)	Aer mode 1 (cm^{-3})	Aer mode 2 (cm^{-3})
58	274	5.73	5.6×10^{1}	316	340
60	263	5.69	5.7×10^{2}	975	76
62	252	5.21	5.4×10^{3}	835	70
64	244	4.47	1.2×10^{5}	338	73
66	236	3.73	8.1×10^{5}	290	26
68	237	3.03	1.0×10^{6}	200	30
70	233	2.51	1.3×10^{6}	200	30
72	228	2.14	1.4×10^{6}	500	-
74	223	1.86	1.5×10^{6}	500	-
76	217	1.67	1.6×10^{6}	500	-
78	211	1.52	1.7×10^{6}	500	-
80	201	1.40	2.6×10^{6}	500	-
82	190	1.37	4.2×10^{6}	500	-
84	178	1.46	5.5×10^{6}	500	-
86	170	1.62	4.3×10^{6}	500	-
88	165	1.66	2.5×10^{6}	500	-
90	161	1.53	1.4×10^{6}	500	-

Table A.I.1: List of parameters used to calculate the range of possible uptake coefficient values that determined the dominance of heterogeneous mechanisms.

I Heterogeneous Chemistry

I.1 Inclusion of aerosol modeling

Aerosol number densities in the current model [Pernice et al., 2004] had been derived from two data sets [Esposito et al., 1983; Knollenberg and Hunten, 1980]. This research attempts to improve on those earlier data sets by using mathematical formulations given by Knollenberg and Hunten [1980] for aerosol modes 1 and 2 (Figure A.I.1). Results from these FORTRAN programs give the range of uptake coefficient values that determined the dominance of heterogeneous mechanisms in the Venus middle atmosphere which were subsequently used to set the photochemical model to gas-phase or heterogeneous-dominant conditions. The values used in those calculations are given in Table A.I.1.

I.2 Revisions to aerosol concentrations

Aerosol mode 1 number densities are best-fit with a log-normal function [Knollenberg and Hunten,1980] and mode 2 number densities are represented by a gaussian distribution function [Knollenberg and Hunten,1979].

$$\text{Total number of particles} = \int_0^\infty n_o \mathrm{d}D \tag{A.I.1}$$

$$\text{Total surface area of particles - observed} = \int_0^\infty n_o \left(\frac{4\pi D^2}{4}\right) \mathrm{d}D \tag{A.I.2}$$

$$\text{Total surface area of particles - modeled} = n_{aer} 4\pi r_{aer}^2 \tag{A.I.3}$$

Reconciliation of observed and modeled aerosol number density expressions give:

$$n_{aer} 4\pi r_{aer}^2 = \pi \int_0^\infty n_o(D) D^2 \mathrm{d}D \tag{A.I.4}$$

$$n_{aer} = \frac{1}{4 r_{aer}^2} \int_0^\infty n_o(D) D^2 \mathrm{d}D \tag{A.I.5}$$

where n_{aer} = modeled aerosol number density (cm^{-3}); r_{aer} = modeled aerosol radius (μm); D = aerosol diameter (μm); n_o = observed aerosol number density distribution function (in cm^{-3} μm^{-1}).

Aerosol mode 1 expression (from Figure 10, Knollenberg and Hunten [1980]):

$$n_o(D) = \frac{N_T}{\sqrt{2\pi} D \ln(\sigma_g)} e^{(-1/2)\left[\frac{\ln(D/\bar{D}_g)}{\ln(\sigma_g)}\right]^2} \tag{A.I.6}$$

where n_o = observed aerosol number density distribution function (cm^{-3} μm^{-1}), N_T = total aerosol number density (cm^{-3}), D = aerosol diameter (μm), $\bar{D}_g$ = geometric mean aerosol diameter (μm), and σ_g = geometric standard deviation. Rearrangement of equations A.I.2 and A.I.5 along with substitution of calculated mode 1 aerosol number densities and integration of $n_o(D)$ (from Equation A.I.6) over aerosol diameter (D) from 0 to ∞ gives:

$$n_{aer} = \frac{N_T}{4 r_{aer}^2 \sqrt{2\pi} \ln(\sigma_g)} \int_0^\infty D e^{(-1/2)\left[\frac{\ln(D/\bar{D}_g)}{\ln(\sigma_g)}\right]^2} \mathrm{d}D \tag{A.I.7}$$

Upon simplification of integrated solution,

$$n_{aer} = N_T \left(\frac{e^{[\ln(\sigma_g)]^2} \bar{D}_g}{2 r_{aer}} \right)^2 \tag{A.I.8}$$

Aerosol mode 2 expression (from Figure 3, Knollenberg and Hunten [1979]):

$$n_o(D) = \frac{67.7}{\sqrt{2\pi}\sigma} e^{\frac{-(D-D_m)^2}{2\sigma^2}} \tag{A.I.9}$$

where n_o = observed number density distribution function (cm^{-3} μm^{-1}), D = aerosol diameter (μm), D_m = aerosol modal diameter (μm), σ = standard deviation (μm).

Substituting Equation A.I.9 into Equation A.I.5 gives:

$$n_{aer} = \frac{16.81}{\sqrt{2\pi}\sigma {r_m}^2} \int_0^\infty D^2 e^{\frac{-(D-D_m)^2}{2\sigma^2}} dD \tag{A.I.10}$$

$$n_{aer} = 6.753\left[D_m^2 \sqrt{\frac{\pi}{2}} + \sigma^2 \sqrt{\frac{\pi}{2}} + 2\sigma D_m\right] \tag{A.I.11}$$

The aerosol mode 2 number densities used in this research have been adopted from a formulation given in Figure 3, Knollenberg and Hunten [1979], but with modal diameter and standard deviation values given in Figure 10, Knollenberg and Hunten [1980]. The latter paper has a possibly more refined derivation of number densities. It is unlikely that the more recent values are much different from the values used here. However, this aspect will be investigated more closely before publication of the results in a journal.

Aerosol number model code and number density values used in this research are shown in Figure A.I.2.

II Nitrogen chemistry

In the other Research project, 'Nitrogen chemistry' is incorporated into the photochemical model. Nitrogen chemistry consists of nitrogen oxides (NO, NO_2, N_2O, HNO, HNO_2 and HNO_3) and related chemistry. In all, 12 new species and 59 reactions were added to the model. These include 32 photodissociation and 27 bimolecular and trimolecular reactions with corresponding photolytic and kinetic information taken from Sander et al. [2006]. The methodology for inclusion of nitrogen chemistry may easily be adapted to include any other form of chemistry. The steps for inclusion of new chemistry are outlined below:

II.1 Inclusion of new chemistry

- CROSS SECTION
  1. Update XSEC*.INP file with photodissociation and branching ratio information for species not previously included in the model.
  2. Run crossdiskfpm to produce .USE and .CATALOG files (CATALOG file is used to locate errors. USE file is copied over to appropriate folder for final run)
- KINETIC DATA
  1. Update KDAT*.INP file with new species (and corresponding heat of formation), photodissociation reactions, branching ratio reactions, bimolecular and termolecular reactions in that order.
  2. Run kindata2fpm to produce .PUN and .OUT files (PUN files is machine-use only and .OUT must be copied over to appropriate folder for final run)
- FORTRAN file
  1. Include new species' parameters
  2. Update numbering of parameters in order of KDAT*.OUT file, including new parameters' numbers
  3. Update photodissociation limits to activate new species' cross absorption data
- INPUT files
  1. .INP2 file sets lower and upper boundary conditions of varying species. Only change from conditions used for 'Heterogeneous Chemistry' project was mixing ratio of NO (set to 5.5 ppb for nominal case and varied for others).
  2. .INP5 files determine species' nature (varying or fixed) and convergence conditions. Introduction of new species and reactions will alter numbering of parameters in the .FOR file. This must be updated in .INP5 along with changes to NATOM, NMOL, NREACT, NPART, NFIX, NVARYF, NOVARF, NVARFM, NPHOTC and NPHOTO.
  3. .INP50 files contain information on altitude-wise concentrations of species and must be updated (new species are set to zero)
  4. .INP and .INP27 files contain information of solar irradiance and diffuse radiation parameter respectively, and are not affected by inclusion of new chemical species.
- COMMAND file
  1. Update (from template) all the changed files listed above (.FOR, .INP5, .INP50, .PUN, KDAT*.OUT and .USE)
  2. Run .COM file (.OUT is stored in SCR: disk)

Documentation of input files and associated parameters can be found elsewhere(USER:[MAA.KINETICS]KINETGEN5-MAIN-INPUT.DOC.

II.2 NO photolysis

Kinetic information for chemical species added during course of this research are tabulated in Thesis Chapter "Introduction to research project 2 - Nitrogen oxides chemistry". Corresponding cross sectional information has been included from experimental studies [Sander et al., 2006], with the exception of NO. Photolysis of NO is calculated within the photochemical model, using formulation presented in Krasnopolsky [2006].

$$J_{NO} = \frac{1.2 \times 10^{-6}}{r^2} e^{-\sigma_1 V \sec(z)} + \frac{2.4 \times 10^{-6}}{r^2} e^{-\sigma_2 V \sec(z)} \qquad \text{(A.II.12)}$$

Species	Table num	Temperature(s)	Wavelength range	Comments
NO_2	Table 4-12	220K, 294K	240nm-662nm	Absorption cross section
NO_2	Table 4-13	248K, 298K	300nm-422nm	Branching ratio
NO_3	Table 4-15	298K	403nm-691nm	Absorption cross section
NO_3	Table 4-16	198K, 230K, 298K	585nm-640nm	Branching ratio
N_2O	Table 4-18	298K	160nm-223nm	Absorption cross section
HONO	Table 4-24	298K	184nm-396nm	Absorption cross section
HNO_3	Table 4-25	298K	192nm-350nm	Absorption cross section

Table A.II.2: List of Table numbers, temperature and wavelength ranges for different NO_x species taken from Sander et al. [2006].

where $\sigma_1 = 1.7 \times 10^{-23}$ cm^2; $\sigma_2 = 3.4 \times 10^{-22}$ cm^2; r : heliocentric distance (AU); V : CO_2 vertical column abundance (cm^{-2}); z : solar zenith angle. Calculation of NO photolysis rate proceeds with calculation of CO_2 vertical optical thickness at every altitude starting from the highest (112 km) and progressing downwards up to 58 km (shown below):

$$\mathrm{V}_{112} = \mathrm{CONC}_{112} \int_z^{z+2H} dz$$

$$\mathrm{V}_{112} = \mathrm{CONC}_{112}(-H) \left. \frac{1}{e^{\frac{z}{H}}} \right|_z^{z+2H}$$

$$\mathrm{V}_{112} = \text{-}\ \mathrm{CONC}_{112}(H) \frac{1}{e^{\frac{112}{H}}} \left(\frac{1}{e^2} - 1 \right)$$

$$\mathrm{V}_{112} = \frac{\mathrm{CONC}_{112}\mathrm{H}}{e^{28}}$$

where V_{112} : CO_2 vertical optical thickness at 112 km; $CONC_{112}$: CO_2 concentration at 112 km, H : scale height; z : altitude variable. Scale height $\sim$ 4 km at 112 km. Subsequent CO_2 vertical optical thickness for each lower altitude:

$$\mathrm{V}_k = \mathrm{V}_{k+1} + MID(2 \times 10^5)$$

where V_k : CO_2 vertical optical thickness at altitude k; MID : $\frac{\mathrm{CONC}_k + \mathrm{CONC}_{k+1}}{2}$.

FORTRAN code used to implement NO photolysis in the photochemical model is shown in Figure II.2.

II.3 NO_x cross sectional data

Apart from NO, absorption cross sections and branching ratios for other NO_x species were derived from Sander et al. [2006]. Detailed information regarding the wavelength range and temperatures are documented here.

N_2O branching ratio is almost unity for

$$\mathrm{N_2O} + \mathrm{h}\nu \rightarrow \mathrm{N_2} + \mathrm{O}(^1\mathrm{D})$$

HONO branching ratios are calculated for two pathways, shown below:
Pathway 1:

$$\mathrm{HONO} + h\nu \rightarrow \mathrm{OH} + \mathrm{NO}$$

Pathway 2:

$$\mathrm{HONO} + h\nu \rightarrow \mathrm{H} + \mathrm{NO_2}$$

Energetic thresholds for the two pathways are calculated, as below: Pathway 1: Energetic threshold = - ΔH_f(HONO) + ΔH_f(H) + ΔH_f(NO_2) = 330.6 KJ/mol This corresponds to λ = 361.8nm.

Pathway 2: Energetic threshold = - ΔH_f(HONO) + ΔH_f(OH) + ΔH_f(NO) = 207 KJ/mol This corresponds to $\lambda = 577.8$nm. In the above relations, ΔH_f is the heat of formation (in KJ/mol) taken from Sander et al. [2006].

Using above calculated energetic thresholds and absorption cross section of HONO [Max Planck Institute], it is assumed that branching ratio is unity for Pathway 1 for $\lambda < 280$nm and unity for Pathway 2 for 280nm-396nm.

HNO_3 branching ratios are calcualted for three pathways, shown below:
Pathway 1:

$$HNO_3 + h\nu \rightarrow OH + NO_2$$

Pathway 2:

$$HNO_3 + h\nu \rightarrow O(^3P) + HONO$$

Pathway 3:

$$HNO_3 + h\nu \rightarrow O(^1D) + HONO$$

Energetic thresholds are: Pathway 1: 581.4nm. Pathway 2: 392.2nm. Pathway 3: 242.2nm.

Branching ratios for the three pathways are categorized according to range of wavelength. $\lambda <$ 200nm : Pathway 1 = 0.4, Pathway 2 = 0.3 and Pathway 3 = 0.3. 200nm-245nm : Pathway 1 = 0.9 and Pathway 2 = 0.06 and Pathway 3 = 0.04. 245nm-350nm : Pathway 1 = 0.97 and Pathway 2 = 0.03.

Detailed information can be found in Sander et al. [2006].

II.4 Lightning simulation

$$N_2 + O \rightarrow NO + N$$

The reaction shown above has been included to simulate the process of lightning. This reaction has not been activated in this research due to insufficient data on rate of lightning. Instead activation of nitrogen chemistry was done through changes to NO abundance at the lower boundary layer. Future studies of impact of nitrogen chemistry may be able to deduce plausible lightning rates for Venus middle atmosphere from analysis of model results for varying rates of this reaction.

III Model computational problems

Addition of new chemistry (species and/ or reactions) increases the likelihood of model experiencing computational difficulties in finding solution. If the newly introduced chemical scheme induces significant changes to existing chemistry, the convergence criteria used by the photochemical model are invariably not satisfied. The convergence criteria of the model are contained in .INP5 file. The run parameters of NTIME, DELTIM and CONVT represent number of complete model runs, time-step between each run and limit of convergence respectively. Through simultaneous adjustments of these parameters, most computational problems could be overcome.

```
      PROGRAM GAMMA
      REAL*8 M,K
      REAL GAM(28),RATECO(28),TEMP(28),CONC(28),AERHET1(28),PI,R1,R2
c     28 is the number of different altitude regions that are
present in the model (from 58-112km)
      CHARACTER*80 discard
      INTEGER ALT(28)
      OPEN (20,FILE='venus_base040114d_temp_only.txt',STATUS='OLD')
      read(20,'(A)') discard
      write(6,*) discard
      READ(20,'(A)') discard
      write(6,*) discard
      READ(20,'(A)') discard
      write(6,*) discard
      OPEN (30,FILE='venus_base040114d_co_only.txt',STATUS='OLD')
      read(30,'(A)') discard
      write(6,*) discard
      READ(30,'(A)') discard
      write(6,*) discard
      OPEN (40,FILE='venus_base040114d_aer_only.txt',STATUS='OLD')
      read(40,'(A)') discard
      write(6,*) discard
      READ(40,'(A)') discard
      write(6,*) discard
      OPEN (50,FILE='venus_base040114d_co2prod.txt',STATUS='OLD')
      read(50,'(A)') discard
      write(6,*) discard
      READ(50,'(A)') discard
      write(6,*) discard
      DO 100 I =1,28
      READ(20,*)ALT(I),TEMP(I)
      READ(30,*)ALT(I),CONC(I)
      READ(40,*)ALT(I),AERHET1(I)
      READ(50,*)ALT(I),RATECO(I)
c     all the above variable array values are read from other
files as indicated by the filenumbers
      PI = 3.14159
      M = 46.4966D-24
      R1 = 0.25E-4
      R2 = 1.0E-4
      K = 1.38D-16
      GAM(I) = (RATECO(I) * (M / (K* TEMP(I)* 3.))**(1./2.)) /(CONC(I) * AERHET1(I) *PI * R1**2)
      WRITE(6,*)'GAMMA(',I,')=',GAM(I)
 100  CONTINUE
      CLOSE(20)
      CLOSE(30)
      CLOSE(40)
      CLOSE(50)
      WRITE(6,*) ALT
      WRITE(6,*) TEMP
      WRITE(6,*) CONC
      WRITE(6,*) AERHET1
      WRITE(6,*) RATECO
      END
```

```
      PROGRAM GAMMA
      REAL*8 M,K
      REAL GAM(28),RATECO(28),TEMP(28),CONC(28),
     &AERHET1(28),AERHET2(28),PI,R1,R2
      CHARACTER*80 discard
      INTEGER ALT(28)
      OPEN (20,FILE='venus_base040114d_temp_only.txt',STATUS='OLD')
      read(20,'(A)') discard
      write(6,*) discard
      READ(20,'(A)') discard
      write(6,*) discard
      READ(20,'(A)') discard
      write(6,*) discard
      OPEN (30,FILE='venus_base040114d_co_only.txt',STATUS='OLD')
      read(30,'(A)') discard
      write(6,*) discard
      READ(30,'(A)') discard
      write(6,*) discard
      OPEN (40,FILE='venus_base040114d_aer_only.txt',STATUS='OLD')
      read(40,'(A)') discard
      write(6,*) discard
      READ(40,'(A)') discard
      write(6,*) discard
      OPEN (50,FILE='venus_base040114d_co2prod.txt',STATUS='OLD')
      read(50,'(A)') discard
      write(6,*) discard
      READ(50,'(A)') discard
      write(6,*) discard
      DO 100 I =1,28
      READ(20,*)ALT(I),TEMP(I)
      READ(30,*)ALT(I),CONC(I)
      READ(40,*)ALT(I),AERHET1(I),AERHET2(I)
      READ(50,*)ALT(I),RATECO(I)
      PI = 3.14159
      M = 46.4966D-24
      R1 = 0.25E-4
      R2 = 1.0E-4
      K = 1.38 E-16
      GAM(I) = (RATECO(I) * (M/ (K* TEMP(I)* 3.))**(1./2.)) /
     $(CONC(I) * AERHET2(I) * PI * R2**2)
      WRITE(6,*)'GAMMA(',I,')=',GAM(I)
  100 CONTINUE
      CLOSE(20)
      CLOSE(30)
      CLOSE(40)
      CLOSE(50)
      WRITE(6,*) ALT
      WRITE(6,*) TEMP
      WRITE(6,*) CONC
      WRITE(6,*) AERHET2
      WRITE(6,*) RATECO
      END
```

Figure A.I.1: FORTRAN codes to calculate γ_t (threshold γ_{rxn}) for mode 1 and mode 2 aerosols

```
c       new aerosol concentration values, for mode1, calculated by integrat.
c       expression from Figure 10 and parameters from Table 4
c       of Knollenberg & Hunten, JGR 85:8039.[MSSundaram, 23 September 2005]
c       new concn values for mode2, calculated by integrat
c       expression from Figure 3 in K&H 1979 paper [MSS, Feb 2006]
c       Typo in exponential term in Fig.3 was corrected [MSS, Aug 2007].
      If ((ALT(1,I) .GE. 57.1).AND.(ALT(1,I) .LE. 58.15)) Then
        CONC(aerhet1_conc,1,I) = 316.
        CONC(aerhet2_conc,1,I) = 69.
      Else If ((ALT(1,I) .GT. 58.15).AND.(ALT(1,I) .LE. 59.)) Then
        CONC(aerhet1_conc,1,I) = 558.
        CONC(aerhet2_conc,1,I) = 78.
      Else If ((ALT(1,I) .GT. 59.).AND.(ALT(1,I) .LE. 60.2)) Then
        CONC(aerhet1_conc,1,I) = 975.
        CONC(aerhet2_conc,1,I) = 76.
      Else If ((ALT(1,I) .GT. 60.2).AND.(ALT(1,I) .LE. 61.25)) Then
        CONC(aerhet1_conc,1,I) = 872.
        CONC(aerhet2_conc,1,I) = 71.
      Else If ((ALT(1,I) .GT. 61.25).AND.(ALT(1,I) .LE. 62.5)) Then
        CONC(aerhet1_conc,1,I) = 835.
        CONC(aerhet2_conc,1,I) = 70.
      Else If ((ALT(1,I) .GT. 62.5).AND.(ALT(1,I) .LE. 63.8)) Then
        CONC(aerhet1_conc,1,I) = 539.
        CONC(aerhet2_conc,1,I) = 65.
      Else If ((ALT(1,I) .GT. 63.8).AND.(ALT(1,I) .LE. 65.2)) Then
        CONC(aerhet1_conc,1,I) = 338.
        CONC(aerhet2_conc,1,I) = 74.
      Else If ((ALT(1,I) .GT. 65.2).AND.(ALT(1,I) .LE. 66.1)) Then
        CONC(aerhet1_conc,1,I) = 290.
        CONC(aerhet2_conc,1,I) = 26.
c       no changes made above this altitude[MSSundaram, 23 September 2005]
      Else If ((ALT(1,I) .GT. 66.1).AND.(ALT(1,I) .LE. 70.)) Then
        CONC(aerhet1_conc,1,I) = 200.
        CONC(aerhet2_conc,1,I) = 30.
      Else If ((ALT(1,I) .GT. 70.).AND.(ALT(1,I) .LE. 90.)) Then
        CONC(aerhet1_conc,1,I) = 500.
        CONC(aerhet2_conc,1,I) = 0.
      Else
        CONC(aerhet1_conc,1,I) = 0.
        CONC(aerhet2_conc,1,I) = 0.
      EndIf
    EndDo
```

Figure A.I.2: Code for specifying aerosol modes 1 and 2 concentrations in the photochemical model

```
      REAL*4 MSS_EXPO,MSS_SECZ,MSS_R
      REAL*8 MSS_SIG1,MSS_SIG2
      REAL*8 MSS_V(NALT),MSS_MID(NALT-1)
      MSS_EXPO = 2.712
      MSS_SIG1 = 1.7D-23
      MSS_SIG2 = 3.4D-22
      MSS_R = 0.7
      MSS_SECZ = 1.4
c       MSS_V(J) : vertical column abundance of CO2.
c       I : latitude variable.
c       J : altitude variable.
c       MSS_MID(J) : mean CO2 concentration of J, J+1 th altitude.
c       ZK [already in the subroutine] : photodissociation rate
c       CONC [already in the subroutine] : concentration
c       MSS_EXPO : e = 2.712
c       MSS_SIG1 : constant from formula = 1.7E-23
c       MSS_SIG2 : constant from formula = 3.4E-22
c       MSS_SECZ : secant of solar zenith angle; sec(44) = 1.4
c       MSS_R : Sun-Venus distance in AU = 0.7
c       Formulation of photolysis rate is adopted from Krasnopolsky [2006] Icarus, Vol. 182, 80-91
c       Calculate ZK(29,I,NALT) ie rate at 112 km
      DO 301 I = 1, NLAT
      MSS_V(NALT) = CONC(1,I,NALT)*4.E+5/(MSS_EXPO)**28.
      ZK(29,I,NALT) =(1.2E-6/MSS_R**2.) *(MSS_EXPO)**(-MSS_SIG1*
     $MSS_V(NALT)*MSS_SECZ) + (2.4E-6/MSS_R**2.) *(MSS_EXPO)**
     $(-MSS_SIG2*MSS_V(NALT)*MSS_SECZ)
c       Now calculate ZK(29,I,J) for altitudes lower than 112km
c       29 is the total abs cross secn rxn
      DO 302 J = NALT-1,1,-1
      MSS_MID(J) = (CONC(1,I,J) + CONC(1,I,J+1)) / 2.
      MSS_V(J) = MSS_V(J+1) + MSS_MID(J) * 2.E+5
      ZK(29,I,J) =(1.2E-6/MSS_R**2.) *(MSS_EXPO)**(-MSS_SIG1
     $*MSS_V(J)*MSS_SECZ) +(2.4E-6/MSS_R**2.) *(MSS_EXPO)**
     $(-MSS_SIG2*MSS_V(J)*MSS_SECZ)
  302 CONTINUE
  301 CONTINUE
c       116 is photodissoc cross secn rxn
c       NO = N + O + X
      DO I = 1,NLAT
      DO J = 1,NALT
      ZK(116,I,J) = ZK(29,I,J)
      END DO
      END DO
```

Figure A.II.3: FORTRAN code to calculate NO photolysis rate